COMPARISON OF TWO OBJECTIVE STRESS MEASURES FOR THE ANALYSIS OF LARGE DEFORMATION ELASTO-PLASTIC IMPACT PROBLEMS.

A Thesis Submitted

in Partial Fulfillment of the Requirements

for the Degree of

Master of Technology

by

SACHIN SINGH GAUTAM

to the

DEPARTMENT OF MECHANICAL ENGINEERING
INDIAN INSTITUTE OF TECHNOLOGY KANPUR

May, 2003

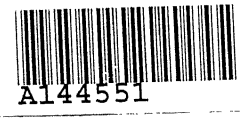

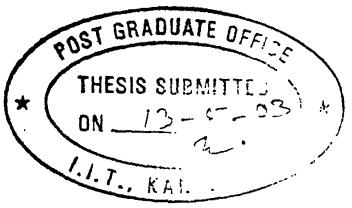

CERTIFICATE

It is certified that the work contained in the thesis entitled "***Comparison of Two Objective Stress Measures for the Analysis of Large Deformation Elasto-plastic Impact Problems.***", by **Sachin Singh Gautam**, has been carried out under my supervision and that this work has not been submitted elsewhere for a degree.

Dr. P. M. Dixit
Department of Mechanical Engineering,
I.I.T. Kanpur.

May, 2003.

Abstract

Two sets of incremental objective stress measures and incremental non-linear strain measures are compared for large deformation, dynamic, elasto-plastic, contact analysis with friction. These two sets are: (i) Jaumann stress rate tensor and incremental Green-Lagrange strain tensor, (ii) New incremental objective stress tensor and incremental logarithmic strain tensor.

A finite element computer code in FORTRAN is developed for the analysis of three dimensional, large deformation, dynamic, elasto-plastic, contact problem, including the friction at the contact interface. Elasto-plastic behaviour is modelled by an associated flow rule based on the von Mises yield criterion and power law type isotropic hardening. The material and geometric non-linearities are handled by using the updated Lagrangian method. A node-to-segment interface model is used for developing the contact stiffness matrix. Contact constraints are imposed using Lagrange multiplier method. Coulomb's friction law is used for calculating the friction forces. A finite element – finite difference scheme is used for spatial and temporal discretization respectively and Modified Newton-Raphson iteration method is used to obtain the solution of the non-linear governing equation. To improve the convergence characteristics of Newton-Raphson iterations, under-relaxation technique and line search method are used. The finite-difference scheme used for time integration is Newmark's algorithm. Unloading is incorporated to include the effects of global or local unloading during the analysis. Skyline scheme of assembly and static condensation scheme are used to reduce the computational resources required for the analysis.

Acknowledgements

First and foremost, I express my deep sense of gratitude to my thesis supervisor **Dr. P. M. Dixit**. Without his able guidance and ample support, this work would not have been materialized. His systematic approach to all matters has been a significant influence on my way of working. The lessons learned during the close interaction, which I had with him for the past twenty two months, will guide me in all my future endeavours.

I am deeply indebted to my father who encouraged me to pursue higher education and to join IIT Kanpur. I express my gratitude to my mother, sister and uncle for their support in all forms, as and when I needed, during my stay at IIT kanpur.

The fantastic atmosphere and cooperation extended by my labmates, UB, Δ(Santosh) at **FEAL** (Finite Element Analysis Lab), helped to make this thesis work a unforgettable experience.

I would like to thank all my friends@iitk for all the cherishable moments, support and help they extended to me during my stay at IIT Kanpur.The life here would not have been so memorable without my great friends, particularly, Rajat, Naik(Dhai phutiya, as I used to call him), Pawar, Manas, Chintoo, Amar, Rajit Ram(Baba Sr)and Pandit(Baba Jr).

Special mention should go for Rajiv(chicks), Vivek(bhau) and Manisha(mg) for the all the care and time they have given to me and the pains they had to take during my illness.

Last, but by no means the least, the financial support provided by **ADA** (Aeronautical Development Agency) for this work is gratefully acknowledged.

Sachin Singh Gautam,

I.I.T. Kanpur,

May , 2003.

Contents

List of Figures

List of Symbols

$a_0, \ldots, a_4$	Newmark constants
$\{a\}$	Flow vector
H	Hardening parameter
$[B_L]$	Matrix relating the incremental linear strain to the incremental displacement
$[B_N]$	Matrix relating the incremental non-linear strain to the incremental displacement
$[C^E]$, $[C^{E'}$	Two forms of matrix representation of components of $\mathbf{C^E}$
$[C^{EP}]$, $[C^{EP'}$	Two forms of matric representation of components of $\mathbf{C^{EP}}$
E	Young's Modulus
dt	Incremental time
du	Icremental displacement
de_{ij}	Green-Lagrange strain tensor
$\{f\}$	Global internal force vector
f_1^i	Normal contact force at a node for body i
f_2^i, f_3^i	Tangential contact forces at a node for body i
$\{f_t^i\}$	Resultant of tangential contact forces
$\mathbf{F}$, F_{ij}	Deformation gradient tensor,component
$[F]$	Matrix representation of $\mathbf{F}$
$\{F_1\}$	External force vector corresponding to nodes of type 1
$\{F_2\}$	External force vector corresponding to nodes of type 2
$\{F\}$	Global external force vector
$\{\widehat{F}\}$	Condensed form of global external force vector
$\{F_d\}$	Effective dynamic force vector
K	Hardening coefficient
$[K]$	Stiffness matrix
$[K_L]$	Linear part of stiffness matrix

$[K_N]$	Non-linear part of stiffness matrix
$[K_d]$	Effective stiffness matrix
$[\widehat{K}]$	Condensed form of stiffness matrix
L_e	Effective length
$[M]$	Mass matrix
n	Hardening exponent
N_i	Shape function
$\underline{N_1}$	Outward normal vector
$\underline{N_2}, \underline{N_3}$	Tangential vectors
$\{N_1\}, \ldots$	Array forms of direction vectors
P	Penetration
$[Q]$	Matrix containing the shape functions of the element
$\mathbf{R}$, R_{ij}	Rotation tensor, component
$[R]$	Matrix representation of $\mathbf{R}$
$\{R\}$	Unbalance force vector
$\{R_c\}$	Contact force vector
S_{ij}	Second Piola-Kirchoff stress tensor
$[S]$	Matrix representation of Second Piola-Kirchoff stress tensor
S_F	Surface where tractions are specified
S_D	Surface where displacements are specified
S_C	Surface where contact occurs
t	Time
t_i	Traction
tol_c	Tolerance for convergence of the numerical method
u^i	Displacement of node i specified in the X-direction
$\mathbf{U}$, U_{ij}	Right stretch tensor,component
$[U]$	Matrix representation of $\mathbf{U}$
$\mathbf{U^P}$, U^P_{ij}	Matrix representation of the components of $\mathbf{U}$ with respect to principal axes, component
$\{U_1\}$	Displacement vector corresponding to nodes of type 1
$\{U_2\}$	Displacement vector corresponding to nodes of type 2
$\{U\}$	Global displacement vector

$\{\widehat{U}\}$	Condensed form of displacement vector
$\{\dot{U}\}$	Global velocity vector
$\{\ddot{U}\}$	Global acceleration vector
v^i	Displacement of node i specified in Y-direction
V	Volume
w^i	Displacement of node i specified in Z-direction
Ω_{ij}	Spin tensor
x_i	Co-ordinate of generic particle
α, δ	Newmark parameters
δ	Variation symbol
δ_{ij}	Kronecker delta
${}_t\Delta$	Increment in quantity from t to $t + \Delta t$
ε_{ij}	Small strain tensor
$[\varepsilon]$	Matrix representation of small strain tensor
ε^p_{eq}	Equivalent plastic strain
$\epsilon^{\mathbf{pL}}$, ϵ^{pL}_{ij}	Plastic part of $[\epsilon^L]$, component
$[\epsilon^L]$, ϵ^L_{ij}	Matrix representation of the components of the logarithmic strain tensor with respect to principal axes, component
η_{ij}	Non-linear part of the Green-Lagrange strain tensor
λ, μ	Lame's constants
μ	Coefficient of friction
ν	Poisson's ratio
ρ	Density
σ_{ij}	Cauchy stress tensor
$[\sigma]$	Matrix representation of Cauchy stress tensor
$\dot{\sigma}_{ij}$	Cauchy stress rate tensor
$\mathring{\sigma}_{ij}$	Jaumann stress rate tensor
$\hat{\sigma}$, $\hat{\sigma}_{ij}$	Green-Naghdi stress rate tensor, component.
σ_y	Yield stress
σ'_{ij}	Deciatoric part of the Cauchy stress tensor
$[\sigma^M]$, σ^M_{ij}	Matrix representation of the components of stress tensor with respect to a material frame, component.

$\{\Phi_i\}$	Array of shape functions
θ	Angle between resultant tangential force $\{f_t\}$ and $\{N_2\}$

Superscripts and Subscripts

${}^{t}X$	Quantity X evaluated at time t
${}^{t+\Delta t}X$	Quantity X evaluated at time $t+\Delta t$
${}^{t+\Delta t}_{t}X$	Quantity X evaluated at time $t+\Delta t$ based on coordinates at t
X_{ij}	Row i and column j element of Matrix/Tensor X

Chapter 1

Introduction

Impact phenomenon occur in many engineering situations. The basic characteristics of an impact phenomenon are very brief duration, high force levels reached, rapid dissipation of energy and large accelerations and decelerations present. In many cases, the bodies undergo plastic deformations during impact. Sometimes frictional effects are also important during impact. A rigorous analysis of the impact problem requires the consideration of all these complex aspects. The analysis of the problems like the autmobile crashes involves the use of dynamics, elasto-plasticity and large deformation in a contact analysis scenario.

Closed form mathematical solutions are extremely difficult to develop even for simple impact problems. As the impact scenario becomes more complex, as in the case of elasto-plastic materials, arriving at a closed form solution is nearly impossible. This necessitates the use of approximate numerical tools for the analysis, of which finite element analysis is arguably the most versatile option.

1.1 Review of Literature

The classical incremental theory of elasto-plasticity [1] is generally taken to be the basis for predicting elasto-plastic response. The constitutive equation for these materials is derived by combining the stress-strain relations for elastic and plastic responses. The constitutive relation for a plastic response requires three fundamental characteristics of the material: a *yield criterion*, a *flow rule* and a *strain hardening relationship*. The yield criterion demarcates the elastic behaviour from the plastic behaviour. It specifies the state of multi-axial stress corresponding to the start of the plastic flow. Various yield

criteria have been proposed by Tresca, von Mises etc. [2], where von Mises criterion is found to be the simplest and the most accurate in terms of the predicted values. The flow rule relates the plastic strain rate to the current stress. It is represented in terms of a plastic potential, analogous to the elastic potential, and is termed as the *associated flow rule* if the potential is taken as the yield function. The hardening rule specifies how the yield condition is modified during the plastic flow. For the purpose of analysis, the non-linear hardening relationship is usually modelled in terms of a *power law.*

Unlike the case of small deformation of elastic materials, the governing equations of elasto-plastic materials, which undergo large deformation, contain two types of non-linearities: (i) *geometric non-linearity* associated with non-linear strain displacement relations and, (ii) *material non-linearity* in the form of non-linear stress-strain relations. For a contact problem, there is an additional non-linearity: *Boundary non-linearity* due to the non-linear boundary conditions at the contact interface. An incremental formulation like the *Updated Lagrangian Formulation* is the most convenient way to handle such non-linearities unlike the *Total Lagrangian Formulation.* The advantage of the former is that, if the increment size is sufficiently small, linearized incremental equations can be used. However, when the overall deformation is large, the number of increments becomes prohibitively large. In such a situation, one has to resort to one of the various iterative schemes available for solving the non-linear incremental equations. The prominent among such schemes is the *Newton-Raphson method.* In this method, the stiffness matrix is updated in each iteration of the increment. Thus, we work with the tangent modulus at that instant for each iteration. This method has two shortcomings. The first being that there is chance of divergence if the slope of force-displacement curve increases with the increment. Secondly, it takes more computational time as the stiffness matrix has to be computed afresh in each iteration [3]. Thus, the *Modified Newton-Raphson method* in which, the stiffness matrix is kept constant during the increment, is adopted.

The dynamic analysis is very basic to studying impact problems. There are various ways of performing the time discretization in this category of problems of which, the direct integration methods are prominent. These methods include the central difference method, Houbolt method, Wilson-θ method and Newmark method [4]. The first method is conditionally stable one, while the rest of them are unconditionally stable. A study of the stability of Newmark algorithm in non-linear dynamics has been done by Hughes [5]. He has studied some potential problems where the stability of the algorithm fails. He

has suggested that it can happen in a non-linear problem if the discrete internal energy is negative. Analysis of accuracy and speed of different algorithms is presented by Bathe [4]. It has been concluded that although central difference method is beneficial in terms of speed and cost, the trapezoidal method of Newmark's algorithm is best in terms of stability and accuracy.

1.1.1 Elasto-plastic Finite Element Analysis

As stated earlier, the classical theory of elasto-plasticity [1] is generally taken to be the basis for predicting the elasto-plastic response. Argyris *et al.* [6] presented one of the earliest formulations and solution techniques for elasto-plastic problems. The effect of plasticity was simulated by "initial loads" and the matrix method was used to discretize the linearized governing equations. Two approaches, the direct incremental method and the iterative incremental method, were discussed for obtaining the solution. The early applications of the iterative incremental method [3] used the initial stiffness method. However, this approach is not suited when the overall deformation is very large as it results in very slow convergence, or in many cases, even divergence.

Nagtegaal and Jong [7] dealt with the computational aspects of elastic-plastic large deformation analysis. A modified set of governing equations were formulated, which were applicable for small strain and large rotational increments. Special attention was paid to the integration of these equations in the deformation history. It is predicted that explicit methods, like the tangent modulus procedure, are conditionally stable whereas the implicit schemes, such as the mean normal method, are preferable. The main difficulty with the three dimensional analysis is the vast computational memory that it required for carrying out the analysis. But, with the advent of better machines and evolution of more efficient algorithms this problem has been solved and more and more such analyses are being acrried out.

Since the elasto-plastic constitutive relation is generally given in the differential form, the constitutive function must be integrated to obtain the incremental stress. A major research effort has been devoted in recent years to the developement and critical assessments of stress updating or integration schemes for the rate (incremental) equation of plasticity. The procedures commonly used are the simple and robust Euler forward integration technique, the implicit Euler backward integration technique and the radial return

method. The trend has lately been shifting towards the use of consistent schemes which improve the convergence characteristics of the equilibrium iterations [8]. The recent works have clearly emphasized the use of implicit integration methods [9, 10, 11] in view of their superior stability and convergence properties [12]. A one step, fully implicit method of backward Euler integration scheme for large deformation of beams has been developed by Gendy and Saleeb [13].

Bathe [4] has briefly reviewed the different approaches used for obtaining the solution of general non-linear problems. Total and updated Lagrangian descriptions of motion have been used to formulate the incremental equations of motion. It has been noticed, for the problems solved, that the two formulations give identical results, provided appropriate constitutive relations are used. One of the areas of controversy in analyzing large deformation is the choice of appropriate objective stress measures. Various objective stress measures have been discussed by Bathe [4] and Chakrabarty [14]. These measures have been discussed in detail in section 1.1.4. The classical theory of elasto-plasticity assumes that the incremental strain tensor can be additively decomposed into the elastic and plastic parts. While this may be true for small incremental deformation, this assumption is no longer valid for large incremental strains and rotations, unless appropriate strain measures are used [15, 16] .

1.1.2 Dynamic Finite Element Analysis

Bathe *et al* [17] were probably the first to propose a large deformation dynamic finite element formulation. Total and updated Lagrangian descriptions of motion were used to formulate the incremental equations of motion. A detailed finite element analysis of non-linear static and dynamic response was also carried out by Mondkar and Powell [18]. The purpose of this paper is to review the theoretical and computational techniques for non-linear structural analysis, and their applications in a general computer program. A Lagrangian frame of reference is used and a variational form of the incremental equations of motion for large displacement, finite strain deformation is incorporated in the finite element program. It is found that no specific time integration scheme is optimal for all types of non-linear behaviour. It is inferred that for large load steps it is essential to use iterations to obtain accurate results.

Direct integration methods are the most commonly used methods for solving the dis-

cretized and linearized governing equations of motion. Dynamic equilibrium including the effect of damping forces is sought at discrete time instants instead of at all times. The advantage is obvious: all solution techniques employed in static analysis can probably be used most effectively in direct integration. The selection of any one direct integration method depends upon considerations of accuracy, stability and cost. The importance of using equilibrium iterations in dynamic non-linear analysis was first realized by Bathe [4]. An extensive discussion of these and other methods can be found in Bathe [4].

More recently, Gendy and Saleeb [19] found that, for a more comprehensive perspective, work on the non-linear dynamic response of plates and shells calls for detailed studies of several important factors. These include the effect of large spatial rotations on the geometric stiffness and inertia operators, accurate updating procedures for nodal rotations and associated angular velocities and accelerations, as well as material inelasticities (especially for finite strains). Several of these issues were examined in conjunction with a newly developed mixed finite element formulation for plates and shells. To this end, and restricting the scope to the case of large overall motions but small strains, low-order displacement/strain interpolations are utilized, together with a radial return algorithm (backward Euler-integration scheme) for plasticity effects. The Newmark implicit scheme has been employed to integrate the semi-discrete equations of motion.

1.1.3 Contact Analysis

The analysis of contact has been a fascinating area since the initial days of the study of mechanics itself. A contact system may contain only one or more than one contact body, and contact-impact may occur between two bodies or within a single body. The behaviour of the contact system is governed by three main groups of equations, i.e the equation of motion, constitutive equations and initial and boundary conditions. The boundary conditions can be classified into two categories: prescribed boundary conditions and unknown boundary conditions. The prescribed boundary conditions are deformation dependent. Among other possible deformation dependent boundary conditions, contact-impact conditions are an important class. Many investigators tried to determine the stresses and displacements in two elastic bodies coming in contact. In three dimensions, the problem of two contacting elastic bodies was first formulated and solved by Hertz [20] under several restrictive assumptions. Hertz assumed that the geometry of general curved

surface in the vicinity of contact can be described by quadratic terms only. Neglecting friction and assuming that the bodies in contact deform as though they were elastic half-spaces, Hertz used the Boussinesq solution to deduce that the contact pressure distribution has to be elliptical to produce an elliptical area. For the contact between two spheres, the contact area is circular. Research work based on Hertz's theory up to 1982 has been reviewed by Johnson [21]. Although Hertz evaluated the dimensions of contact area and stresses at the contact surface, he presented only a speculative sketch of the subsurface stresses. The stresses beneath the contact surface were analyzed later. For circular contact area of radius a, it is observed that the maximum shear stress occurs at a depth of $0.57a$ [21]. Later on Muskhelishvili [22] and Gladwell [23] solved some small deformation elastic contact problems using the analytical techniques.

With the development of computers, people resorted to numerical methods. Finite element method has been the most widely used. In earlier studies, contacting bodies were assumed to consist of linearly elastic materials and hence were assumed to undergo only small deformation. The loading was assumed to be proportional. The node-to-node contact interface model was used for discretizing the contacting bodies and the contact conditions (constraints) involving nodal displacements and forces were applied by modifying the combined stiffness matrix or the flexibility matrix of the contacting bodies. The investigators who used this model are Ohte [24], Gaertner [25], Francavilla and Zienkiewicz [26], Sachdeva and Ramakrishnan [27] etc.

Kalker and Randen [28], Hung and de Saxce [29] and Mahmoud *et al.* [30] used the technique of mathematical programmming for solving the frictionless small deformation elastic contact problem. They minimised the total strain energy to find the contact area and the contact pressure distribution.

When the deformation is large, there is a possibility that a pair of nodes presently in contact, may undergo a large relative displacement. If a node-to-node interface model is used, re-meshing of the bodies becomes necessary for carrying out the subsequent analysis. To avoid frequent re-meshing, one must use the node-to-segment interface model, in which one node of a contacting body comes in contact with a segment of the other. When a node-to-segment interface model is used, the contact conditions acquire a complex form, when expressed in terms of nodal variables. To impose these conditions, an additional set of finite element equations, involving the *contact stiffness matrix*, needs to be developed using the principle of virtual work of the contact forces. The methods, which are normally

used for implementing the contact constraints are *Lagrange multiplier method, penalty funtion method* and *transformation matrix method.* Bohm [31] presented a comparison of different contact algorithms with applications. A survey of contact algorithms is given by Bourago [32].

Kikuchi and Oden [33] have provided the mathematical foundation for the Lagrange multiplier method. The work of Bathe and Chaudhary [34] seems to be the first attempt to develop an expression for contact stiffness matrix using this method. This was done for planar and axisymmetric problems assuming the contact segment to be straight. Lagrange multiplier was used to impose the contact constraints including friction forces based on *Coulomb's friction law.* Non-linear contact kinematics was used for developing a consistant contact matrix for two dimensional problems by Wriggers and Simo [35] and by Parisch [36]. They used both the Lagrange multiplier method and penalty function method. The transformation matrix method for two dimensional problems was proposed by Chen and Yeh [37]. A formulation for non-linear frictional model was proposed by Gallego and Anza [38] using perturbed Lagrangian functional. All the above formulations were used for static large deformation elastic contact problems. Some of these formulations were extended to elasto-dynamic contact problems [4, 35] and dynamic elasto-plastic problems [39]. A literature survey of contact dynamics modelling is presented by Gilardi and Sharf [40]. Sung and Kwak [41] and Bittencourt and Creus [42] have presented the analysis of dynamic, large deformation contact problem including the effects of friction. Master's thesis by Werner [43] is an attempt to compare the experimental results and the results predicted by a commercial finite element software for an elasto-plastic impact problem.

Contact-impact algorithms, which are sometimes called as *slideline algorithms*, are the computationally time-consuming parts of many explicit simulations of non-linear problems, becuase they involve so many branches, and thus are not amenáble to vectorization, which is essential for speed on supercomputers. Belytschko and Neal [44] introduced the pinball algorithm, which is a simplified slideline algorithm and is readily vectorized. Its major idea is to embed pinballs in surface elements and to enforce the impenetrability condition only to these pinballs. It can be implemented either by a Lagrange multiplier or penalty method. Malone and Johnson [45] developed a parallel contact algorithm and implemented it in a non-linear dynamic explicit finite element program to analyze the three-dimensional shell structures. The contact algorithm accounted for initial contact,

sliding and release through the use of parametric representation of motion of points located on the surface of structure combined with a contact surface representation, which approximates the actual surface by means of triangular search planes. Brown *et al.* [46] described a general strategy for parallelizing solid mechanics simulations. Such simulations often have several computationally intensive parts, including finite element integration, detection of material contacts and particle interactions if smoothed particle hydrodynamics is used to model highly deforming materials. Their strategy is to load-balance each of the significant computations independently with whatever balancing technique is most appropriate. The main advantage is that each computation can be scalably parallelized. The drawback is the data exchange between the processors and the extra coding that must be written to maintain multiple decompositions in a code.

The problems of undesirable oscillatory solutions and stability of time-integration schemes have been tackled by quite a few people. Taylor and Papadopoulos [47] address the problem of oscillatory solution along the contact interface. The standard second order implicit integrators of the Newmark family, used in earlier works, were investigated by them. In their work, control of these oscillations is attempted by introducing an artificial bulk viscosity for the compressive waves in each body. Laursen and Chawla [48] proposed an energy conserving algorithm to control the oscillations for the frictionless dynamic contact problems. It is shown that a Lagrange multiplier enforcement of an appropriate *contact rate constraint* produces these conservation properties. In particular, the ability of the formulation to produce accurate results, where more conventional integration schemes fail, is emphasized by numerical simulations. Armero and Petocz [49] presented a new dissipative time-stepping algorithm to improve the stablity of time integration scheme. They showed that although the traditional time-integration schemes were stable for most of the linear problems, instability would creep in as soon as we try to use them in nonlinear cases. Given these considerations, they developed implicit time-stepping algorithms for contact problems that posess unconditional (energy) stability in time and lead to stable enforcement of contact constraints.

Quite a few researchers have proposed new techniques. Ayari and Saouma [50] developed a new formulation for contact problems using the concept of fictitious forces. Contrary to the most existing models, this one involves very few matrix decompositions and thus is computationally inexpensive. The model was applied to fracture mechanics based analysis of a cracked dam under seismic excitation. They also showed that their model

could be applied to a vast majority of contact problems and was not only restricted to fracture phenomenon. Simo and Laursen [51] extended the augmented Lagrangian fomulation, which has certain advantages over traditional Lagrangian formulation, to problems involving frictional contact. Kane *et al* [52] proposed a nonsmooth contact algorithm, which is capable of dealing with multibody nonsmooth contact geometries for which neither the normals nor the gap functions can be defined. Farahani *et al* [53] presented a solution method for contact/impact problems, which is different from Lagrange multiplier and penalty methods. This method is based on the stiffness matrix transformation and eliminating the normal degree of freedom of contactor node. The method is absolutely general and can be used in static as well as dynamic non-linear problems. In this case, the number of unknowns does not increase and the solution scheme needs no modification as is the case with prior methods. Besides, the boundary conditions are satisfied exactly.

1.1.4 Objective Stress Measures

In large deformation elasto-plastic problem, one comes across large rotations also besides large displacements and strains. In updated Lagrangian formulation, this creates difficulty in updating of stress components. Note that the constitutive equation gives the stress increment only due to incremental straining of the material. If the Cauchy stress tensor is used as the stress measure, then one cannot simply add the incremental stress to the Cauchy stress components at time t to obtain their values at time $t+\Delta t$. This is because, the change in Cauchy stress components also occurs due to the incremental rotation. Thus, the Cauchy stress tensor is not *objective* in the sense that its components do change even when the increment consists of pure rigid rotation. The stress measures whose increment (or rate) depends only on the incremental deformation (or rate of deformation) are called as objective stress (or stress rate) measures.

The most commonly used objective stress measure in the literature as well as in finite element software on large deformation elasto-plastic problems is the Jaumann stress rate measure. It is obtained by eliminating the rate of change of Cauchy stress component due to rotation from the total rate. But it uses only the infinitesimal rotation tensor to represent the incremental rotation. Therefore, when the incremental rotation is large, it is not expected to give accurate results. Further, it is well known that the use of Jaumann stress rate measure predicts an oscillatory solution when the incremental shear

is large [54]. Other objective stress rate measures like the Green-Naghdi rate and E-rate have been proposed ([54] [55]). But they are difficult to use. A simple stress updating procedure has been proposed by Varadhan [56] which accounts for the change in Cauchy stress components due to incremental rotation. In this approach, the incremental stress is evaluated in a frame which rotates with the particle rather than in a fixed frame. While transforming the stress components from the material frame to the fixed at time $t + \Delta t$, the transformation due to incremental rotation is taken into account. This incremental stress measure has been called *New incremental objective stress measure* in this work. This stress measure, along with other objective stress measures, has been discussed in detail in section 2.3.

1.2 Objective of the Present Work

A finite element code for the analysis of 3-D, large deformation, elasto-plastic, dynamic, contact problem with friction has been developed by Jayadeep [57]. It uses the Jaumann stress rate measure and incremental Green-Lagrange strain measure. The objective of the present work is to incorporate the new incremental objective stress measure and incremental logaritmic strain measure in this code and to carry out the comparitive study of these two sets of stress and strain measures.

The salient features of the code are as follows. Since we have large deformations, including slipping at the contact interface, a node-to-segment contact model is used in contact analysis. A method outlined by Zhong [39] is used for calculating the contact stiffness matrix. Lagrange multiplier method is used for applying the contact constraints. Coulomb's friction law is used for modelling the frictional effects at the contact interface. Elastic behaviour is modelled using generalised Hooke's law and the plastic behaviour is modelled by an associated flow rule based on von Mises yield criterion and power-law type isotropic hardening. The total strain is obtained by adding the elastic and plastic components. Incremental analysis is carried out using the updated Lagrangian method [4]. Modified Newton-Raphson iterative method is used for solving the resulting finite element equation. In each Newton-Raphson iteration, contact iterations are carried out to find the contact reactions. A finite difference scheme is used for carrying out the discretization in time. Newmark's algorithm, which is found to be the best in terms of stability and accuracy among the various finite difference schemes, is used for this purpose. Unloading

scheme is incorporated to take care of the local unloading during the analysis. To reduce the computational resources required for performing the analysis, static condensation of stiffness matrix for contact and non-contact nodes and skyline scheme of assembly are used. Divergence handling techniques, viz., under relaxation and line search, are used for improving the convergence characteristics of Newton-Raphson iterations.

1.3 Structure of the Thesis

Chapter 2 deals with the mathematical formulation of the governing equations for dynamic, large deformation, elasto-plastic problem. The development of the finite element-finite difference scheme based on these governing equations and the numerical scheme used are discussed in chapter 3. Chapter 4 presents the contact formulation, where in the formulation of the contact stiffness matrix and the calculation of contact reactions are discussed. Chapter 5 is devoted to the results of the comparison between the two sets of objective stress measures for elastic, elasto-plastic, single body as well as contact problems. The last chapter summarises the work carried out and the scope for future developments.

Chapter 2

Mathematical Modeling of Dynamic Elasto-Plastic Problem

In a dynamic elasto-plastic problem, the deformations and strains in the body no longer remain small and hence the response of the body is not proportional to the load. The response of the body becomes non-linear. The non-linearities can be broadly classified into three: *Geometric non-linearity*, *material non-linearity* and *boundary non-linearity.* First two of these non-linearities occur in the analysis of large deformation of elasto-plastic materials. The most convenient formulation for such analysis is the *Updated Lagrangian Formulation* with the constitutive relations represented in an incremental manner. The third non-linearity occurs in the analysis of contact-impact problems and this is attributed to the non-linear boundary conditions at the contact surfaces.

2.1 Introduction

In the study of the deformation of a body subjected to external loading, often the original, undeformed and unstressed state of the body is used for the formulation of its governing equation. This method is known as the Lagrangian formulation. This formulation is convenient for small deformation problems, where the deformed configuration does not deviate from the original configuration significantly. Hence, the deformations are proportional to the loading and can be described by an infinitesimal or linear strain tensor, for which the strain – displacement relations are linear. On the other hand, for large deformation problems, one has to use a finite strain measure, which is expressed by a non-linear strain displacement relation. Furthermore, the equations of motion, expressed

in the original configuration, depend on the deformation. This makes the governing equations highly complex and too difficult to solve. In such cases, it is convenient to solve the problem in an incremental manner known as the *Updated Lagrangian Formulation.* In this formulation, the state of the body is updated in increments using the calculated incremental deformations and stresses. The response during Δt is calculated based on the configuration at time t, where Δt represents the increment in time, called *time step.* Hence, all the relations are to be in an incremental form rather than the total form. This methodology is particularly useful for elasto-plastic materials, since the constitutive relations for these materials depend on the state of the body and therefore they are expressed in an incremental form.

2.2 Kinematics of Finite Deformation

The relative deformation gradient tensor at time $t + \Delta t$ is defined by:

$$ {}^{t+\Delta t}_{t}F_{ij} = \frac{\partial {}^{t+\Delta t}x_i}{\partial {}^{t}x_j} = {}^{t+\Delta t}_{t}x_{i,j} \tag{2.1} $$

where ${}^{t+\Delta t}x_i$ and ${}^{t}x_j$ denote the position vectors of the particle at time t and $t + \Delta t$ respectively. When ${}^{t+\Delta t}_{t}\mathbf{F}$ is not singular, the polar decomposition theorem ([58] , [59]) allows a decomposition of the form:

$$ {}^{t+\Delta t}_{t}F_{ij} = {}^{t+\Delta t}_{t}R_{ik}\ {}^{t+\Delta t}_{t}U_{kj} \tag{2.2} $$

where ${}^{t+\Delta t}_{t}\mathbf{R_{ik}}$ is an orthogonal tensor representing the material rotation and ${}^{t+\Delta t}_{t}\mathbf{U_{kj}}$ is a positive definite symmetric tensor called the right stretch tensor. The right stretch tensor can be diagonalized by the following transformation to obtain the principle stretches ${}^{t+\Delta t}_{t}\lambda_i$:

$$ {}^{t+\Delta t}_{t}U^{P}_{ij} = {}^{t+\Delta t}_{t}Q_{ik}\ {}^{t+\Delta t}_{t}U_{kl}\ {}^{t+\Delta t}_{t}Q_{jl} \tag{2.3} $$

where ${}^{t+\Delta t}_{t}[Q]$ is orthogonal matrix and

$$ {}^{t+\Delta t}_{t}\lambda_i = {}^{t+\Delta t}_{t}U^{P}_{ii}\ (no\ sum) \tag{2.4} $$

The tensor ${}^{t+\Delta t}_{t}\mathbf{R}$ and the transformation matrix, ${}^{t+\Delta t}_{t}[Q]$ are used in the development of the stress measure while the incremental logarithmic strain tensor is obtained from the ${}^{t+\Delta t}_{t}\lambda_i$.

2.3 Stress Measures

The large deformation problems are normally associated with rigid body rotations. Hence the stress measures used in these problems should be *objective*, which means that they should vanish if the increment is a pure rigid body rotation. The most commonly used stress measure known as *Cauchy stress tensor* is not objective and hence it can not be used in a constitutive equation. There are numerous objective stress measures, of which some are discussed below.

One of the commonly used objective stress measures is the *Second Piola-Kirchoff stress tensor* ${}^{t+\Delta t}_{t}S_{ij}$ which is related to Cauchy stress tensor ${}^{t+\Delta t}\sigma_{mn}$ using the concept of equivalent work between the two configurations [4]:

$$ {}^{t+\Delta t}_{t}S_{ij} = \frac{{}^{t}\rho}{{}^{t+\Delta t}\rho} \; {}^{t}_{t+\Delta t}x_{i,m} \; {}^{t+\Delta t}\sigma_{mn} \; {}^{t}_{t+\Delta t}x_{j,n} \tag{2.5} $$

Here ${}^{t}\rho$ and ${}^{t+\Delta t}\rho$ represent the densities at time t and time $t+\Delta t$ respectively, ${}^{t}_{t+\Delta t}x_{i,m}$ is the derivative of the position vector at time t, viz., ${}^{t}x_i$ with respect to ${}^{t+\Delta t}x_m$.

Another frequently used objective stress measure is *Jaumann's stress rate tensor* $\mathring{\sigma}_{ij}$. It is related to the Cauchy rate $\dot{\sigma}_{ij}$ by the relation [4]:

$$ {}^{t}\mathring{\sigma}_{ij} \; \Delta t = \dot{\sigma}_{ij} \; \Delta t - \; {}^{t}\sigma_{ik}({}^{t}\Omega_{jk} \; \Delta t) - \; {}^{t}\sigma_{jk}({}^{t}\Omega_{ik} \; \Delta t) \tag{2.6} $$

$$ {}^{t}\Omega_{jk} \; \Delta t = \frac{1}{2}({}_{t}\Delta u_{i,j} - \; {}_{t}\Delta u_{j,i}) \tag{2.7} $$

Here, ${}^{t}\Omega_{jk} \; \Delta t$ represents the incremental spin tensor and ${}_{t}\Delta u_{i,j}$ denotes the derivative of the incremental displacement vector ${}_{t}\Delta u_i$ with respect to ${}^{t}x_j$.

Dienes [54] proposed a stress rate $\hat{\sigma}$ based upon the rotation part of the deformation gradient:

$$ \hat{\sigma}_{ij} = \dot{\sigma}_{ij} - \Omega_{ik}\sigma_{kj} + \Omega_{kj}\sigma_{ik} \tag{2.8} $$

where,

$$ \Omega_{ij} = \dot{R}_{ik} \, R_{jk} \tag{2.9} $$

is the angular velocity. The stress rate $\hat{\sigma}$ is sometimes refered to as the Green-Naghdi rate.

As pointed out by Metzer and Dubey [55], it is important that the stress measure used be compatible with the constituve equation in addtion to being objective. A new incremental objective stress measure (as against objective stress rate measures) to be used

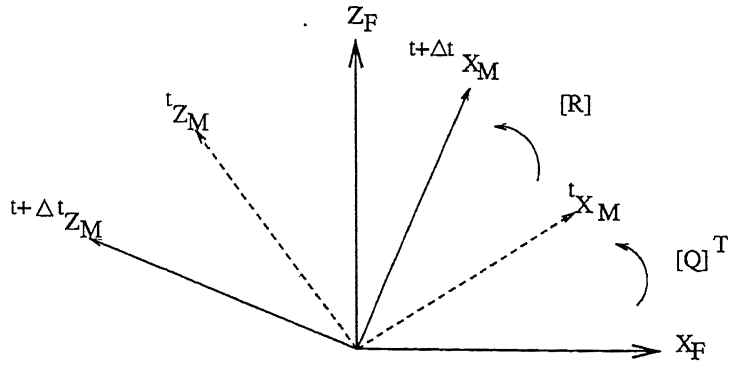

Note:

- The Fixed Frame is denoted by subscipt F.
- The Material Frame is denoted by subscript M.

Figure 2.1: Fixed and material frames

in the generalized Hooke's Law (2.16) and in the elasto-plastic constitutive equation (2.39) is developed below.

Two Cartesian referance frames (see Figure 2.1) are used:

1. The fixed frame (denoted by subscript ,F).
2. A material frame (denoted by subscript ,M) which rotates and translates along with a material particle.

The material frame is defined so as to coincide with the principal axes of the right stretch tensor at time t so that the initially orthogonal axes do not get skewed at time $t + \Delta t$.

The first step in the derivation is the transformation of the components of the Cauchy stress tensor at time t from the fixed frame to material frame:

$$ {}^t\sigma_{ij}^M = {}^{t+\Delta t}_{t}Q_{ik}\ {}^t\sigma_{kl}\ {}^{t+\Delta t}_{t}Q_{jl} \tag{2.10} $$

The increment in the components of the Cauchy stress tensor with respect to the material axes, ${}_t\Delta\sigma_{ij}^M$, is added to ${}_t\sigma_{ij}^M$ to obtain the stress components at time $t + \Delta t$ with respect to the material frame of reference:

$$ {}^{t+\Delta t}\sigma_{ij}^M = {}^t\sigma_{ij}^M + {}^t\Delta\sigma_{ij}^M \tag{2.11} $$

The final transformation from the material frame at time $t + \Delta t$ to the fixed frame gives the components of the Cauchy stress tensor at time $t + \Delta t$:

$$ {}^{t+\Delta t}\sigma_{ij} = {}^{t+\Delta t}_{t}Q_{ki}\ {}^{t+\Delta t}_{t}R_{il}\ {}^{t+\Delta t}\sigma_{lm}^M\ {}^{t+\Delta t}_{t}R_{nm}\ {}^{t+\Delta t}_{t}Q_{nj} \tag{2.12} $$

where ${}^{t+\Delta t}_{t}\mathbf{R}$ has components with respect to fixed frame.

The proposed stress and logarithmic strain measures satisfy the requirements of objectivity and lead to a physically consistent application of the usual constitutive equation.

2.4 Strain Measures

The linear or infinitesimal strain tensor, normally used in the small deformation problems, is not a valid choice for the large deformation, elasto-plastic analysis. *Green-Lagrange strain tensor* is one of the most commonly used strain measure for large deformation analysis.

The incremental Green-Lagrange strain tensor is a non-linear function of the displacement [4]:

$$ {}_{t}\Delta e_{ij} = \frac{1}{2}({}_{t}\Delta u_{i,j} + {}_{t}\Delta u_{j,i} + {}_{t}\Delta u_{k,i}\, {}_{t}\Delta u_{k,j}) \tag{2.13} $$

When the incremental deformation is small, the incremental linear strain tensor

$$ {}_{t}\Delta \varepsilon_{ij} = \frac{1}{2}({}_{t}\Delta u_{i,j} + {}_{t}\Delta u_{j,i}) \tag{2.14} $$

can be used as the measure of deformation.

These two strain measures occur in the virtual work expression at $t + \Delta t$ and its transformation to time t respectively. The components of the Green Lagrange strain tensor are invariant under rigid body rotation of the material unlike the small strain components. The following are the disadvantages one would face using one of the above strain measures in a constitutive law:

1. The solution obtained is dependent upon the size of the increment in the updated Lagrangian formulation unless the increment size is sufficiently small.

2. The components of the strain tensors do not tend to infinte values when the principal stretches tend to zero. Therefore a constitutive law which ensures that the appropriate Cauchy stress components tend to negative infinity (as is physically realistic), even though the strain components remain finite, should be used. This difficulty can be avoided by using a strain measure whose components become minus infinity when the principal stretches become zero.

The *Logarithmic strain measure* introduced by Dienes [54] is free of the above disadvantages. The components of the incremental logarithmic strain tensor, in the material

frame, are defined by:

$$ {}_t\Delta\epsilon^L_{ij} = ln({}^{t+\Delta t}_t\lambda_i)\,\delta_{ij}\ (no\ sum\ over\ i) \tag{2.15} $$

where the ${}^{t+\Delta t}_t\lambda_i$ are the principal stretches defined by equation (2.4). The components with respect to any other frame can be obtained by the usual transformation law. The logarithmic strain has the following additional advantage in elasto-plastic analysis. A loading test involving elasto-plastic deformation followed by elastic unloading reveals that the slope of the elastic unloading line is the same as that of the initial elastic loading line only when the true stress and the logarithmic strain measures are used in a constitutive law.

2.5 Elastic Constitutive Equation

The elastic constitutive equation used is the generalized Hooke's Law relating the incremental objective stress tensor and the elastic part $[\Delta\epsilon^{eL}]$ of the incremental logarithmic strain tensor:

$$ {}_t\Delta\sigma_{ij} = C^E_{ijkl}\ {}_t\Delta\epsilon^{eL}_{kl} \tag{2.16} $$

The tensor C^E_{ijkl} for isotropic case is given by:

$$ C^E_{ijkl} = \lambda\ \delta_{ij}\ \delta_{kl} + \ 2\mu\ \delta_{ik}\delta_{jl} \tag{2.17} $$

where λ and μ are Lame's constants.

The stress and strain measures used in a constitutive equation need not necessarily be energy conjugate with each other. However if it is so, the predicted response in a predictor-corrector scheme will be closer to the actual response.

2.6 Theory of Plasticity

An Elasto-plastic material model is characterized by the following:

1. Yield Criterion.
2. Strain hardening postulate.
3. Flow rule.

Baushchinger effect and the hysterisis loop are disregarded and the material is assumed to be isotropic in this work.

2.6.1 Yield Criterion

A law defining the limit of elastic behaviour under any possible combination of stress is called yield criterion. This law applies both to loading directly from the annealed state and to reloading of an element unloaded from a previous plastic state. The *von Mises yield criterion* which has been experimentally verified to predic the yield locus quite accurately is used. Yielding occurs when the equivalent stress ${}^t\sigma_{eq}$ reaches the value of the yield stress in uniaxial tension ${}^t\sigma_y$.

$$ {}^t\sigma_{eq}\,(\sigma_{ij}) = {}^t\sigma_y \tag{2.18} $$

where,

$$ {}^t\sigma_{eq} = \left(\frac{3}{2}\,{}^t\sigma'_{ij}\,{}^t\sigma'_{ij}\right)^{\frac{1}{2}} \tag{2.19} $$

and ${}^t\sigma'_{ij}$ is the deviatoric part of ${}^t\sigma_{ij}$.

2.6.2 Strain Hardening Postulate

The size and the shape of the yield surface in a strain hardening material depends upon the complete history of plastic deformation since the prevoius annealing. A convinient mathematical formulation for strain hardening is obtained by assuming that the yield surface expands uniformly without changing its shape. This is known as *isotropic hardening* and the relationship may be stated as

$$ {}^t\sigma_y \;=\; f({}^t\epsilon^p_{eq}) \tag{2.20} $$

where,

$$ {}^t\epsilon^p_{eq} = \int_{path} \sqrt{\frac{2}{3}\,d\epsilon^{pL}_{ij}\,d\epsilon^{pL}_{ij}} \tag{2.21} $$

is the equivalent plastic strain determined from the path-line integration of an invariant of ${}_td\epsilon^{pL}_{ij}$ (plastic part of the incremental logaritmic strain tensor) and the function f is determined by the relationship between the true stress and the plastic strain in uniaxial tension/compression. In this work, the following power law is chosen to represent f:

$$ {}^t\sigma_y - {}^0\sigma_y \;=\; K\,({}^t\epsilon^p_{eq})^n \tag{2.22} $$

where ${}^0\sigma_y$ denotes the initial yield stress of the material.

2.6.3 Plastic Flow Rule

The rule of plastic flow relates the current stress with the plastic strain increment. The plastic potential is a function defining the ratios of the components of the incremental plastic strain. The associated flow rule which assumes that the yield function and the plastic potential are the same is used in the present work. It states that

$$ {}_t d\epsilon_{ij}^{pL} = d\lambda \frac{\partial F}{\partial {}^t\sigma_{ij}} \qquad (2.23) $$

where $d\lambda$ is a scalar to be found from the hardening relation.

2.7 Elasto-plastic Constitutive Equation

An elasto-plastic relationship between the incremental stress and strain tensors based on the von Mises yield criterion and isotropic hardening (as discussed above) is developed below.

For an isotropically hardening material, the plastic potential is given by [60][1]:

$$ F({}^{\sigma_{ij}}, {}^p\epsilon_{eq}) = \sigma_{eq}(\sigma_{ij}) - \sigma_y({}^p\epsilon_{eq}) \qquad (2.24) $$

where,

$$ F = 0 \qquad (2.25) $$

represents the yield criterion. The plastic potential F depends on the Cauchy stress tensor through the equivalent stress, and on the variable yield stress through the hardening parameter ${}^p\epsilon_{eq}$.

The plastic part of incremental logarithmic strain tensor $d\epsilon_{ij}^{pL}$ is obtained from the plastic potential using the flow rule (equation 2.23). Differentiation of equation (2.24) with respect to σ_{ij} gives:

$$ \frac{\partial F}{\partial \sigma_{ij}} = \frac{3}{2\sigma_{eq}} \sigma'_{ij} \qquad (2.26) $$

Therefore, $d\lambda$ is determined as:

$$ d\lambda = d\epsilon_{eq}^{p} \qquad (2.27) $$

Further, the hardening relationship and the yield condition can be used to express $d\lambda$ as:

$$ d\lambda = \frac{d\sigma_y}{H} = \frac{d\sigma_{eq}}{H} \qquad (2.28) $$

[1] In this section, the superscript/subscript denoting time have been omitted for convenience.

where,

$$H = \frac{d\sigma_y}{d\epsilon^p_{eq}} = Kn(\epsilon^p_{eq})^{n-1} \tag{2.29}$$

is the slope of the hardening curve. Substitution of equations (2.26) and (2.28) in equation (2.23) leads to the following constitutive equation:

$$d\epsilon^{pL}_{ij} = \frac{3\, d\sigma_{eq}}{2H\sigma_{eq}}\sigma'_{ij} \tag{2.30}$$

This constitutive relationship between the deviatoric stress tensor and the plastic part of the incremental logarithmic strain tensor is not really convenient for the Updated Lagrangian formulation for which an incremental stress–strain relationship is needed. This can be obtained from equation (2.30) as follows:

$$d\epsilon^{pL}_{ij} = \frac{3\sigma'_{ij}}{2H\sigma_{eq}}\frac{\partial\sigma_{eq}}{\partial\sigma_{kl}}d\sigma_{kl} \tag{2.31}$$

Note that, from equations (2.24) and (2.26), we get:

$$\frac{\partial\sigma_{eq}}{\partial\sigma_{kl}} = \frac{\partial F}{\partial\sigma_{kl}} = \frac{3}{2\sigma_{eq}}\sigma'_{kl} \tag{2.32}$$

Substitution of equation (2.32) in equation (2.31) leads to the following incremental plastic stress–strain relationship:

$$d\epsilon^{pL}_{ij} = \frac{9\,\sigma'_{ij}\,\sigma'_{kl}}{4H\sigma^2_{eq}}d\sigma_{kl} \tag{2.33}$$

The incremental elastic stress–strain relationship (equations (2.16) and (2.17) in the inverted form) can be expressed as:

$$d\epsilon^{eL}_{ij} = \frac{1}{E}[-\nu\, d\sigma_{kk}\,\delta_{ij} + (1+\nu)\, d\sigma_{ij}] \tag{2.34}$$

where, $d\epsilon^{eL}_{ij}$ is the elastic part of $d\epsilon^{L}_{ij}$, E is the Young's modulus and ν is the Poisson's ratio. Adding the two relationships, we get:

$$d\epsilon^{L}_{ij} = d\epsilon^{eL}_{ij} + d\epsilon^{pL}_{ij} = \left[\frac{-\nu}{E}\delta_{ij}\,\delta_{kl} + \frac{1+\nu}{E}\delta_{ik}\,\delta_{jl} + \frac{9\,\sigma'_{ij}\,\sigma'_{kl}}{4H\sigma^2_{eq}}\right] d\sigma_{kl} \tag{2.35}$$

This is the incremental elasto-plastic stress–strain relationship needed in the updated Lagrangian formulation. However, it is the following inverse relationship which is more useful ([60] and [61]):

$$d\sigma_{ij} = C^{EP}_{ijkl}\, d\epsilon^{L}_{kl} \tag{2.36}$$

where,

$$C^{EP}_{ijkl} = 2\mu\left(\delta_{ik}\delta_{jl} + \frac{\nu}{1-2\nu}\delta_{ij}\delta_{kl} - \frac{9\mu\,\sigma'_{ij}\,\sigma'_{kl}}{2(3\mu+H)\sigma^2_{eq}}\right) \tag{2.37}$$

Here, μ is one of the Lame's constants (also called as shear modulus) and ν is Poisson's ratio. The Poisson's ratio is related to the Lame's constants λ and μ by the following relation:

$$\nu = \frac{\lambda}{2(\lambda + \mu)}. \tag{2.38}$$

Note that the stress increment appearing in equation (2.36) must be an objective stress increment in the sense that $d\sigma_{ij}$ must be a zero tensor if the increment is a pure rotation. The incremental stress measure used in the present work is the New Objective stress measure discussed in section 2.3.

The relationship (2.36) has been derived assuming the increment size to be small. When a large size increment is to be used, the relationship (2.36) takes the following form:

$${}_t\Delta\sigma_{ij} = \int_t^{t+\Delta t} {}^tC^{EP}_{ijkl}\, d({}_t\Delta\epsilon^L_{kl}) \tag{2.39}$$

where,

$${}^tC^{EP}_{ijkl} = 2\mu\left(\delta_{ik}\,\delta_{jl} + \frac{\nu}{1-2\nu}\delta_{ij}\,\delta_{kl} - \frac{9\mu\,{}^t\sigma'_{ij}\,{}^t\sigma'_{kl}}{2(3\mu + Kn({}^t\varepsilon^p_{eq})^{n-1})\,{}^t\sigma^2_{eq}}\right) \tag{2.40}$$

Here, H has been replaced by the expression (2.29) and the left subscript t has been added to make it explicit that these quantities are to be evaluated at time t.

2.8 Incremental Updated Lagrangian Formulation

The objective of the updated Lagrangian formulation is to establish dynamic equilibrium in the configuration at time $t + \Delta t$ when all the static and kinematic variables at time t are known. The principle of virtual work requires that [4]:

$$\int_{t+\Delta t V} {}^{t+\Delta t}\rho\; {}^{t+\Delta t}\ddot{u}_i\; \delta({}^{t+\Delta t}u_i)\; d^{t+\Delta t}V + \int_{t+\Delta t V} {}^{t+\Delta t}\sigma_{ij}\; \delta({}^{t+\Delta t}\varepsilon_{ij})\; d^{t+\Delta t}V = {}^{t+\Delta t}R \tag{2.41}$$

where,

${}^{t+\Delta t}\rho$ = density at time $t + \Delta t$

${}^{t+\Delta t}\ddot{u}_i$ = acceleration at time $t + \Delta t$

$\delta({}^{t+\Delta t}u_i)$ = virtual displacement at time $t + \Delta t$

${}^{t+\Delta t}V$ = volume at time $t + \Delta t$

${}^{t+\Delta t}\sigma_{ij}$ = Cauchy stress tensor at $t + \Delta t$.

The virtual linear strain tensor $\delta({}^{t+\Delta t}\varepsilon_{ij})$ is defined as:

$$\delta({}^{t+\Delta t}\varepsilon_{ij}) = \frac{1}{2}\left(\frac{\partial\,\delta^{t+\Delta t}u_i}{\partial\,{}^{t+\Delta t}x_j} + \frac{\partial\,\delta^{t+\Delta t}u_j}{\partial\,{}^{t+\Delta t}x_i}\right) \tag{2.42}$$

Further,

$$
\begin{aligned}
{}^{t+\Delta t}R \;=\; & \int_{t+\Delta t V} {}^{t+\Delta t}b_i \;\delta({}^{t+\Delta t}u_i)\; d^{t+\Delta t}V + \int_{t+\Delta t S_F} {}^{t+\Delta t}(t_i)_S \;\delta({}^{t+\Delta t}u_i) d^{t+\Delta t}S + \\
& \int_{t+\Delta t S_C} {}^{t+\Delta t}(t_i)_C \;\delta({}^{t+\Delta t}u_i) d^{t+\Delta t}S
\end{aligned} \tag{2.43}
$$

where,

${}^{t+\Delta t}b_i$ = body force per unit volume at time $t+\Delta t$

${}^{t+\Delta t}(t_i)_S$ = applied traction per unit area at time $t+\Delta t$

${}^{t+\Delta t}S_F$ = surface at time $t+\Delta t$ with traction specified

${}^{t+\Delta t}(t_i)_C$ = contact traction per unit area at time $t+\Delta t$

${}^{t+\Delta t}S_C$ = contact surface at time $t+\Delta t$

The main difficulty in applying equation (2.41) is that the configuration at time $t+\Delta t$ is unknown. Therefore, the virtual work expression at time $t+\Delta t$ is transformed to an integral over the volume at time t. It is assumed that the external load term (2.43) is deformation independent for the formulation of governing equation. The expression (2.41) after the transformation becomes [4]:

$$
\int_{{}^tV} {}^t\rho \; {}^{t+\Delta t}\ddot{u}_i \;\delta({}^{t+\Delta t}u_i)\; d\,{}^tV + \int_{{}^tV} {}^{t+\Delta t}_tS_{ij} \;\delta({}^{t+\Delta t}_te_{ij})\; d\,{}^tV = {}^{t+\Delta t}R \tag{2.44}
$$

where the virtual Green-Lagrange strain tensor $\delta({}^{t+\Delta t}_te_{ij})$ is defined by:

$$
\delta({}^{t+\Delta t}_te_{ij}) = \frac{1}{2}\left[\frac{\partial\,\delta^{t+\Delta t}u_i}{\partial\,{}^{t+\Delta t}x_j} + \frac{\partial\,\delta^{t+\Delta t}u_j}{\partial\,{}^{t+\Delta t}x_i} + \delta\left(\frac{\partial\,{}^{t+\Delta t}u_k}{\partial\,{}^{t+\Delta t}x_i}\frac{\partial\,{}^{t+\Delta t}u_k}{\partial\,{}^{t+\Delta t}x_j}\right)\right] \tag{2.45}
$$

The second Piola-Kirchoff stress tensor can be decomposed as:

$$
{}^{t+\Delta t}_tS_{ij} = {}^t_tS_{ij} + {}_t\Delta S_{ij} = {}^t\sigma_{ij} + {}_t\Delta S_{ij} \tag{2.46}
$$

Since,

$$
\delta({}^{t+\Delta t}u_i) = \delta({}^tu_i + {}_t\Delta u_i) = \delta({}_t\Delta u_i) \tag{2.47}
$$

the virtual Green-Lagrange strain tensor can be decomposed as:

$$
\delta({}^{t+\Delta t}_te_{ij}) = \delta({}_t\Delta e_{ij}) = \delta({}_t\Delta\varepsilon_{ij} + {}_t\Delta\eta_{ij}) \tag{2.48}
$$

where,

$$
{}_t\Delta\varepsilon_{ij} = \frac{1}{2}({}_t\Delta u_{i,j} + {}_t\Delta u_{j,i}) \tag{2.49}
$$

$$
{}_t\Delta\eta_{ij} = \frac{1}{2}({}_t\Delta u_{k,i}\;{}_t\Delta u_{k,j}) \tag{2.50}
$$

Therefore, equation (2.44) can be written with incremental decomposition as:

$$\int_{{}^tV} {}^t\rho\, {}^{t+\Delta t}\ddot{u}_i\, \delta({}_t\Delta u_i)\, d\,{}^tV + \int_{{}^tV} {}_t\Delta S_{ij}\, \delta({}_t\Delta\varepsilon_{ij})\, d\,{}^tV + \int_{{}^tV} {}_t\Delta S_{ij}\, \delta({}_t\Delta\eta_{ij})\, d\,{}^tV + \int_{{}^tV} {}^t\sigma_{ij}\, \delta({}_t\Delta\eta_{ij})\, d\,{}^tV + \int_{{}^tV} {}^t\sigma_{ij}\, \delta({}_t\Delta\varepsilon_{ij})\, d\,{}^tV = {}^{t+\Delta t}R \qquad (2.51)$$

The above equation is simplified by neglecting the third integral, which is a higher order term, and approximating ${}_t\Delta S_{ij}$ as ${}^tC^{EP}_{ijkl}\, {}_t\Delta\varepsilon_{kl}$:

$$\int_{{}^tV} {}^t\rho\, {}^{t+\Delta t}\ddot{u}_i\, \delta({}_t\Delta u_i)\, d\,{}^tV + \int_{{}^tV} {}^tC^{EP}_{ijkl}\, {}_t\Delta\varepsilon_{kl}\, \delta({}_t\Delta\varepsilon_{ij})\, d\,{}^tV + \int_{{}^tV} {}^t\sigma_{ij}\, \delta({}_t\Delta\eta_{ij})\, d\,{}^tV + \int_{{}^tV} {}^t\sigma_{ij}\, \delta({}_t\Delta\varepsilon_{ij})\, d\,{}^tV = {}^{t+\Delta t}R \qquad (2.52)$$

The linearized equation, when solved, will yield only approximate displacement, velocity, acceleration, strain and stress fields. The approximate quantities are denoted by a right superscript (1). The error due to the approximation involved is calculated from equation (2.41) as:

$$Error = {}^{t+\Delta t}R - \int_{{}^{t+\Delta t}V^{(1)}} {}^{t+\Delta t}\sigma^{(1)}_{ij}\, \delta({}^{t+\Delta t}\varepsilon^{(1)}_{ij})\, d\,{}^{t+\Delta t}V^{(1)} - \int_{{}^{t+\Delta t}V^{(1)}} {}^{t+\Delta t}\rho^{(1)}\, {}^{t+\Delta t}\ddot{u}^{(1)}_i\, \delta({}^{t+\Delta t}u^{(1)}_i)\, d\,{}^{t+\Delta t}V^{(1)} \qquad (2.53)$$

This error is generally minimised by a predictor – corrector scheme.

Chapter 3

Finite Element-Finite Difference Formulation

The governing equation (2.52) contains volume and surface integrals, which can not be solved analytically for most of the physical problems. In many of the cases of interest, the volume and surface may not be expressed mathematically. This necessitates the use of numerical methods for the solution of the governing equation. Since it approximates the field variable and geometry simultaneously, the *Finite Element Method* is probably the most powerful method for solving the complex boundary value problems. The integration in the time domain, which is an initial value problem, is carried out efficiently using a *Finite Difference Scheme.* This chapter presents the development of a finite element – finite difference scheme for solving the linearized governing equation of the dynamic elasto-plastic problem. A numerical iterative technique for minimizing the error term given by equation (2.53) is also presented.

3.1 Matrix Notation

Matrix notation is used in the development of finite element – finite difference equations for the convenience in computer implementation.

The components of the strain tensors ${}_t\Delta\varepsilon_{ij}$ and ${}_t\Delta\eta_{ij}$ are represented in the array form as follows:

$$ {}_t\{\Delta\epsilon\}^T = \{{}_t\Delta\epsilon_{xx}, {}_t\Delta\epsilon_{yy}, {}_t\Delta\epsilon_{zz}, 2\,{}_t\Delta\epsilon_{xy}, 2\,{}_t\Delta\epsilon_{yz}, 2\,{}_t\Delta\epsilon_{xz}\} \tag{3.1} $$

$$ {}_t\{\Delta\eta\}^T = \{{}_t\Delta u_{,x}, {}_t\Delta u_{,y}, {}_t\Delta u_{,z}, {}_t\Delta v_{,x}, \ldots\} \tag{3.2} $$

$$ {}_t\{\Delta\epsilon^L\}^T = \{{}_t\Delta\epsilon^L_{xx},\ {}_t\Delta\epsilon^L_{yy},\ {}_t\Delta\epsilon^L_{zz},\ {}_t\Delta\epsilon^L_{xy},\ {}_t\Delta\epsilon^L_{yz},\ {}_t\Delta\epsilon^L_{xz}\} \tag{3.3} $$

Note that the shear strain components in the array ${}_t\{\Delta\varepsilon\}^T$ contain a factor of 2, which is a convention followed in most finite element formulations. The components of the Cauchy stress tensor ${}^t\sigma_{ij}$ are written as:

$$ {}^t\{\sigma\}^T = \{{}^t\sigma_{xx},\ {}^t\sigma_{yy},\ {}^t\sigma_{zz},\ {}^t\sigma_{xy},\ {}^t\sigma_{yz},\ {}^t\sigma_{zx}\} \tag{3.4} $$

Two matrix forms of the tensor ${}^tC^{EP}_{ijkl}$ are needed:

1. ${}^t[C^{EP}]$ is used in the constitutive relationship ${}^t\{\Delta S\} = {}^t\,[C^{EP}]\,{}_t\{\Delta\varepsilon\}$
2. ${}^t[C^{EP'}]$ is used in the constitutive relationship ${}^t\{\Delta\sigma^M\} = {}^t\,[C^{EP'}]\,{}_t\{\Delta\varepsilon^L\}$

These matrix form are given by:

$$ {}^t[C^{EP}] = \left([C^E] - \frac{[C^E]\,{}^t\{a\}\,{}^t\{a\}^T\,[C^E]}{{}^tH + {}^t\{a\}^T\,[C^E]\,{}^t\{a\}}\right) \tag{3.5} $$

$$ {}^t[C^{EP'}] = \left([C^{E'}] - \frac{[C^{E'}]\,{}^t\{a\}\,{}^t\{a\}^T\,[C^{E'}]}{{}^tH + {}^t\{a\}^T\,[C^{E'}]\,{}^t\{a\}}\right) \tag{3.6} $$

In the above equations,

$$ {}^t\{a\} = \frac{3}{2\,{}^t\sigma_{eq}}\,{}^t\{\sigma'\} \tag{3.7} $$

$$ {}^tH = Kn\,{}^t(\varepsilon^p_{eq})^{n-1} \tag{3.8} $$

The array ${}^t\{\sigma'\}^T$ represents the deviatoric part of the Cauchy stress at time t. For an isotropic material, the matrices $[C^{E'}]$ and $[C^E]$ for the 3-D case are given by:

$$ [C^E] = \frac{E}{(1+\nu)(1-2\nu)} \begin{bmatrix} 1-\nu & \nu & \nu & 0 & 0 & 0 \\ \nu & 1-\nu & \nu & 0 & 0 & 0 \\ \nu & \nu & 1-\nu & 0 & 0 & 0 \\ 0 & 0 & 0 & \frac{1-2\nu}{2} & 0 & 0 \\ 0 & 0 & 0 & 0 & \frac{1-2\nu}{2} & 0 \\ 0 & 0 & 0 & 0 & 0 & \frac{1-2\nu}{2} \end{bmatrix} \tag{3.9} $$

$$ [C^{E'}] = \frac{E}{(1+\nu)(1-2\nu)} \begin{bmatrix} 1-\nu & \nu & \nu & 0 & 0 & 0 \\ \nu & 1-\nu & \nu & 0 & 0 & 0 \\ \nu & \nu & 1-\nu & 0 & 0 & 0 \\ 0 & 0 & 0 & 1-2\nu & 0 & 0 \\ 0 & 0 & 0 & 0 & 1-2\nu & 0 \\ 0 & 0 & 0 & 0 & 0 & 1-2\nu \end{bmatrix} \tag{3.10} $$

Equation (2.52) can be written in the following form owing to the symmetries of ${}^tC^{EP}_{ijkl}$, ${}_t\Delta\varepsilon_{ij}$, ${}_t\Delta\eta_{ij}$ and ${}^t\sigma_{ij}$:

$$\int_{{}_tV} \delta({}_t\{\Delta u\}^T)\ {}^t\rho\ {}^{t+\Delta t}\{\ddot{u}\}\ d^tV + \int_{{}_tV} \delta({}_t\{\Delta\epsilon\}^T)\ {}^t[C^{EP}]\ {}_t\{\Delta\epsilon\}\ d^tV$$
$$+ \int_{{}_tV} \delta({}_t\{\Delta\eta\}^T)\ {}^t[T]\ {}_t\{\Delta\eta\}\ d^tV + \int_{{}_tV} \delta({}_t\{\Delta\epsilon\}^T)\ {}^t\{\sigma\}\ d^tV \ = \ {}^{t+\Delta t}R \quad (3.11)$$

The matrix $[T]$ is given by:

$${}^t[T] = \begin{bmatrix} {}^t[\Sigma] & 0 & 0 \\ 0 & {}^t[\Sigma] & 0 \\ 0 & 0 & {}^t[\Sigma] \end{bmatrix} \quad (3.12)$$

where,

$${}^t[\Sigma] = \begin{bmatrix} {}^t\sigma_{xx} & {}^t\sigma_{xy} & {}^t\sigma_{xz} \\ {}^t\sigma_{xy} & {}^t\sigma_{yy} & {}^t\sigma_{yz} \\ {}^t\sigma_{xz} & {}^t\sigma_{yz} & {}^t\sigma_{zz} \end{bmatrix} \quad (3.13)$$

3.2 Finite Element Formulation

The domain is discretized into a number of elements and the incremental displacement field is approximated over each element by:

$${}_t\{\Delta u\} = \begin{Bmatrix} {}_t\Delta u \\ {}_t\Delta v \\ {}_t\Delta w \end{Bmatrix} = {}^t[\Phi]\ {}_t\{\Delta u\}^e \quad (3.14)$$

Here, the element incremental displacement vector is given by:

$${}_t\{\Delta u\}^{e^T} = \{{}_t\Delta u^1,\ {}_t\Delta v^1,\ {}_t\Delta w^1,\ {}_t\Delta u^2, \ldots\} \quad (3.15)$$

where the quantities ${}_t\Delta u^i$, ${}_t\Delta v^i$, ${}_t\Delta w^i$ stand for the unknown incremental displacements of node i in x, y and z directions respectively. The matrix ${}^t[\Phi]$ is defined by:

$${}^t[\Phi] = \begin{bmatrix} {}^t\{\Phi_1\}^T \\ {}^t\{\Phi_2\}^T \\ {}^t\{\Phi_3\}^T \end{bmatrix} \quad (3.16)$$

where,

$$\begin{aligned} {}^t\{\Phi_1\}^T &= \{{}^tN_1, 0, 0, {}^tN_2, 0, 0, \ldots\} \\ {}^t\{\Phi_2\}^T &= \{0, {}^tN_1, 0, 0, {}^tN_2, 0, \ldots\} \\ {}^t\{\Phi_3\}^T &= \{0, 0, {}^tN_1, 0, 0, {}^tN_2, \ldots\} \end{aligned} \quad (3.17)$$

The ${}^tN_i$, which are functions of (x, y, z), are called as shape functions. In the present work, 8-noded brick element with trilinear shape functions is used. The functions ${}^tN_i$ do not depend explicitly on t. However, the left superscript t is used to emphasize the fact that the shape of element (nodal coordinates) changes with time.

The acceleration can similarly be expressed as:

$$ {}^{t+\Delta t}\{\ddot{u}\} = \left\{ \begin{array}{c} {}^{t+\Delta t}\ddot{u} \\ {}^{t+\Delta t}\ddot{v} \\ {}^{t+\Delta t}\ddot{w} \end{array} \right\} = {}^t[\phi]\, {}^{t+\Delta t}\{\ddot{u}\}^e \tag{3.18} $$

The strain field is expressed in terms of the nodal displacements by diferentiating (3.14) and using the expressions (2.49) and (2.50) as:

$$ {}_t\{\Delta\varepsilon\} = {}^t[B_L]\, {}_t\{\Delta u\}^e \tag{3.19} $$

$$ {}_t\{\Delta\eta\} = {}^t[B_N]\, {}_t\{\Delta u\}^e \tag{3.20} $$

where,

$$ {}^t[B_L] = \left[\begin{array}{c} {}^t\{\Phi_1\}^T_{,x} \\ {}^t\{\Phi_2\}^T_{,y} \\ {}^t\{\Phi_3\}^T_{,z} \\ {}^t\{\Phi_2\}^T_{,x} + {}^t\{\Phi_1\}^T_{,y} \\ {}^t\{\Phi_3\}^T_{,y} + {}^t\{\Phi_2\}^T_{,z} \\ {}^t\{\Phi_1\}^T_{,z} + {}^t\{\Phi_3\}^T_{,x} \end{array} \right] \tag{3.21} $$

and

$$ {}^t[B_N]^T = \left\{ {}^t\{\Phi_1\}_{,x},\ {}^t\{\Phi_1\}_{,y},\ {}^t\{\Phi_1\}_{,z},\ {}^t\{\Phi_2\}_{,x}, \ldots \right\} \tag{3.22} $$

Using equations (3.14), (3.18), (3.19) and (3.20), the contribution to the integral (3.11) over a typical element with volume V^e is:

$$ \begin{aligned} &\delta({}_t\{\Delta u\}^{e^T}) \left(\int_{{}^tV^e} {}^t[\Phi]^T\, {}^t\rho\, {}^t[\Phi]\, d\,{}^tV^e \right) {}^{t+\Delta t}\{\ddot{u}\}^e + \\ &\delta({}_t\{\Delta u\}^{e^T}) \left(\int_{{}^tV^e} {}^t[B_L]^T\, {}^t[C^{EP}]\, {}^t[B_L]\, d\,{}^tV^e \right) {}_t\{\Delta u\}^e + \\ &\delta({}_t\{\Delta u\}^{e^T}) \left(\int_{{}^tV^e} {}^t[B_N]^T\, {}^t[T]\, {}^t[B_N]\, d\,{}^tV^e \right) {}_t\{\Delta u\}^e + \\ &\delta({}_t\{\Delta u\}^{e^T}) \left(\int_{{}^tV^e} {}^t[B_L]^T\, {}^t\{\sigma\}\, d\,{}^tV^e \right) = \delta({}_t\{\Delta u\}^{e^T})\, {}^{t+\Delta t}\{F\}^e \end{aligned} \tag{3.23} $$

The contribution to the term ${}^{t+\Delta t}R$ is expressed in terms of the elemental external force vector ${}^{t+\Delta t}\{F\}^e$ using a standard procedure [62].

Since the variation in the displacement vector is arbitrary, the above equation can be written as:

$$ {}^{t}[M]^{e}\ {}^{t+\Delta t}\{\ddot{u}\}^{e} + {}^{t}[K]^{e}\ {}_{t}\{\Delta u\}^{e} + {}^{t}\{f\}^{e} = {}^{t+\Delta t}\{F\}^{e} \tag{3.24} $$

where the element mass matrix ${}^{t}[M]^{e}$ is defined as:

$$ {}^{t}[M]^{e} = \int_{{}^{t}V^{e}} {}^{t}[\Phi]^{T}\ {}^{t}\rho\ {}^{t}[\Phi]\ d\,{}^{t}V^{e} \tag{3.25} $$

and the element stiffness matrix ${}^{t}[K]^{e}$ is expressed as:

$$ {}^{t}[K]^{e} = {}^{t}[K_{L}]^{e} + {}^{t}[K_{NL}]^{e} \tag{3.26} $$

where,

$$ {}^{t}[K_{L}]^{e} = \int_{{}^{t}V^{e}} {}^{t}[B_{L}]^{T}\ {}^{t}[C^{EP}]\ {}^{t}[B_{L}]\ d\,{}^{t}V^{e} \tag{3.27} $$

$$ {}^{t}[K_{NL}]^{e} = \int_{{}^{t}V^{e}} {}^{t}[B_{N}]^{T}\ {}^{t}[T]\ {}^{t}[B_{N}]\ d\,{}^{t}V^{e} \tag{3.28} $$

The element internal force vector is:

$$ {}^{t}\{f\}^{e} = \int_{{}^{t}V^{e}} {}^{t}[B_{L}]^{T}\ {}^{t}\{\sigma\}\ d\,{}^{t}V^{e} \tag{3.29} $$

The element mass (${}^{t}[M]^{e}$) and stiffness (${}^{t}[K]^{e}$) matrices along with the element force vectors ${}^{t}\{f\}^{e}$ and ${}^{t+\Delta t}\{F\}^{e}$ are assembled to obtain the global equation:

$$ {}^{t}[M]\ {}^{t+\Delta t}\{\ddot{U}\} + {}^{t}[K]\ {}_{t}\{\Delta U\} + {}^{t}\{f\} = {}^{t+\Delta t}\{F\} \tag{3.30} $$

where,

${}^{t}[M]$ = global mass matrix,

${}^{t}[K]$ = global stiffness matrix,

${}^{t}\{f\}$ = global internal force vector at time t,

${}^{t+\Delta t}\{F\}$ = global external force vector at $t + \Delta t$.

The equation (3.30) represents a system of ordinary coupled second order linear differential equations. The next section describes the technique to convert it into a system of algebraic equations.

3.3 Finite Difference Scheme

The number of efficient methods for the solution of a large system of coupled ordinary differential equations such as those arising from a finite element formulation is limited. A

popular technique is the direct integration of equation (3.30), where the dynamic equilibrium is sought only at discrete time intervals instead of at all times t. The assumptions on the variations of displacement, velocity and acceleration within each time interval determine the accuracy, stability and cost of the solution procedure.

Two broad classifications exist in the direct integration methods: *Explicit* and *Implicit integration methods.* Explicit integration methods are based upon the equilibrium conditions at time t for obtaining the solution at time $t + \Delta t$, resulting in such procedures being only conditionally stable. One main advantage of explicit schemes is that factorization of the effective stiffness matrix is not necessary. Implicit integration methods use the dynamic equilibrium conditions at both time t and $t + \Delta t$ for obtaining the solution at time $t + \Delta t$. Since the implicit time integration methods are unconditionally stable, the time step used can be several orders of magnitudes larger, but the factorization of effective stiffness matrix is necessary for obtaining the solution. In this work, an implicit method called *Newmark method* is used for integration.

The Newmark method makes use of the following assumptions [4]:

$$\begin{aligned} {}^{t+\Delta t}\{\dot{U}\} &= {}^{t}\{\dot{U}\} + \left[(1-\delta)\,{}^{t}\{\ddot{U}\} + \delta\,{}^{t+\Delta t}\{\ddot{U}\}\right]\Delta t \\ {}^{t+\Delta t}\{U\} &= {}^{t}\{U\} + {}^{t}\{\dot{U}\}\,\Delta t + \left[(\frac{1}{2} - \alpha)\,{}^{t}\{\ddot{U}\} + \alpha\,{}^{t+\Delta t}\{\ddot{U}\}\right](\Delta t)^2 \end{aligned} \tag{3.31}$$

The parameters α and δ can be determined so as to obtain desired accuracy and stability. The constant average acceleration method corresponding to $\alpha = \frac{1}{4}$ and $\delta = \frac{1}{2}$ is used in this work, which results in an implicit unconditionally stable integration scheme. The Newmark constants are defined below:

$$\begin{aligned} a_0 &= \frac{1}{\alpha(\Delta t)^2} \\ a_1 &= \frac{1}{\alpha(\Delta t)} \\ a_2 &= \frac{1}{2\alpha} - 1 \\ a_3 &= \Delta t(1-\delta) \\ a_4 &= \delta\,\Delta t \end{aligned} \tag{3.32}$$

Substituting for ${}^{t+\Delta t}\{\ddot{U}\}$ from equation (3.30) and splitting ${}^{t+\Delta t}\{U\}$ as:

$${}^{t+\Delta t}\{U\} = {}^{t}\{U\} + {}_{t}\{\Delta U\} \tag{3.33}$$

the expression (3.30) becomes:

$${}^{t}[K_d]\,{}_{t}\{\Delta U\} + (a_0\,{}^{t}[M]\,{}^{t}\{U\} + {}^{t}\{f\}) = {}^{t+\Delta t}\{F_d\} \tag{3.34}$$

where the effective stiffness matrix ${}^{t}[K_d]$ and the effective force vector ${}^{t+\Delta t}\{F_d\}$ are given by:

$$ {}^{t}[K_d] = a_0\,{}^{t}[M] + {}^{t}[K] \tag{3.35} $$

$$ {}^{t+\Delta t}\{F_d\} = {}^{t+\Delta t}\{F\} + {}^{t}[M](a_0\,{}^{t}\{U\} + a_1\,{}^{t}\{\dot{U}\} + a_2\,{}^{t}\{\ddot{U}\}) \tag{3.36} $$

Since the dynamic equilibrium is satisfied at time t and assuming that change in mass matrix in an increment is not very significant, the following equation must hold, which can be obtained from the finite element discretization of the integral (2.41) written at time t:

$$ {}^{t}[M]\,{}^{t}\{\ddot{U}\} + {}^{t}\{f\} = {}^{t}\{F\} \tag{3.37} $$

Using equation (3.31), this can be expressed as:

$$ a_0\,{}^{t}[M]\,{}^{t}\{U\} + {}^{t}\{f\} = {}^{t}\{F_d\} \tag{3.38} $$

Decomposing the effective force vector as:

$$ {}^{t+\Delta t}\{F_d\} = {}^{t}\{F_d\} + {}_{t}\{\Delta F_d\} \tag{3.39} $$

and using the expression (3.38) for ${}^{t}\{F_d\}$, the following equation in ${}_{t}\{\Delta U\}$ is obtained from equation (3.34):

$$ {}^{t}[K_d]\,{}_{t}\{\Delta U\} = {}_{t}\{\Delta F_d\} \tag{3.40} $$

Using equations (3.36) and (3.38) we get:

$$ {}_{t}\{\Delta F_d\} = {}^{t+\Delta t}\{F_d\} - {}^{t}\{F_d\} = {}^{t+\Delta t}\{F\} - {}^{t}\{f\} + {}^{t}[M](a_1\,{}^{t}\{\dot{U}\} + a_2\,{}^{t}\{\ddot{U}\}) \tag{3.41} $$

This algebraic system (equation (3.40)) is solved to obtain the incremental displacement vector ${}_{t}\{\Delta U\}$.

Once the incremental displacement is obtained by solving equation (3.40), the velocity and acceleration at time $t + \Delta t$ are obtained using the following expressions:

$$ {}^{t+\Delta t}\{\ddot{U}\} = a_0({}^{t+\Delta t}\{U\} - {}^{t}\{U\}) - a_1\,{}^{t}\{\dot{U}\} - a_2\,{}^{t}\{\ddot{U}\} \tag{3.42} $$

$$ {}^{t+\Delta t}\{\dot{U}\} = {}^{t}\{\dot{U}\} + a_3\,{}^{t}\{\ddot{U}\} + a_4\,{}^{t+\Delta t}\{\ddot{U}\} \tag{3.43} $$

3.4 Determination of Stress

The evaluation of stress components (at the Gauss points of the elements) is done by the following stepwise procedure:

1. Calculate the relative deformation gradient ${}^{t+\Delta t}_{t}[F]$:

$$ {}^{t+\Delta t}_{t}F_{ij} = \delta_{ij} + \frac{\partial({}_t(\Delta u_i)}{\partial {}^t x_j} \tag{3.44} $$

It should be noted that the position vector $\mathbf{x}$ corresponds to the equilibrium position, though ${}_t\{\Delta u\}$ may be incremental or iterative displacement (See section 3.9.3). If the reference position vector corresponds to a non-equilibrium position, say the configuration at $t^{(i)}$, there exists a possibility of divergence of the numerical method.

2. Decompose ${}^{t+\Delta t}_{t}[F] = {}^{t+\Delta t}_{t}[R]{}^{t+\Delta t}_{t}[U]$ and determine ${}^{t+\Delta t}_{t}[Q]$ and ${}^{t+\Delta t}_{t}[U^P]$ using equation (2.3).

3. Determine the principal incremental logaritmic strain ${}_t\Delta\epsilon^L$ using equation (2.15).

4. Calculate ${}_t\{\Delta\sigma^M\}$ using equation (2.39). The integration of the constitutive equation is performed using the Euler forward technique described below.

5. Use equation (2.12) to calculate the Cauchy stress components at time $t + \Delta t$

3.4.1 Integration of the Constitutive Equation

Various techniques exist for the integration of the constitutive equation. A simple and robust technique is the *Euler forward integration* scheme discussed below.

Assume that the principal incremental strain components have been calculated and the state of the Gauss point at time t (*elastic or plastic*) is known.

- If the state at time t is *elastic*,

  1. Calculate the stress increment assuming elastic behaviour.

$$ {}_t\{\Delta\sigma^M\} = [C^{E'}]\,{}_t\{\Delta\varepsilon^L\} \tag{3.45} $$

  2. Calculate ${}^{t+\Delta t}\{\sigma\}$ using (2.12).

  3. Determine ${}^t\sigma_{eq}$ and ${}^{t+\Delta t}\sigma_{eq}$ using equation (2.19).

  4. If ${}^{t+\Delta t}\sigma_{eq} \leq {}^t\sigma_y$, then the Gauss point is still in elastic state, or if ${}^{t+\Delta t}\sigma_{eq} = {}^t\sigma_{eq}$ the Gauss point is neutrally loaded. RETURN.

     Else, a transition from elastic to plastic has ocurred. Calculate:

$$ Ratio = \frac{{}^{t+\Delta t}\sigma_y - {}^t\sigma_{eq}}{{}^{t+\Delta t}\sigma_{eq} - {}^t\sigma_{eq}} \tag{3.46} $$

and change the state to *plastic*. The sub-incrementation method is followed and the stress components with respect to the material frame are updated after each subincrement by the increment in stress components corresponding to the elasto-plastic strain sub-increment. The $[C^{EP'}]$ corresponding to last updated state is used :

$$^{t+\Delta t}\{\sigma^M\}^{(i)} = ^{t+\Delta t}\{\sigma^M\}^{(i-1)} + ^{t+\Delta t}[C^{EP'}]^{(i-1)}\, d_t\{\Delta\epsilon^L\} \;\; for\; i = 1, n \quad (3.47)$$

where,

$$d_t\{\Delta\epsilon^L\} = \frac{(1 - Ratio)_t\{\Delta\epsilon^L\}}{n} \quad (3.48)$$

$$^{t+\Delta t}\{\sigma^M\}^{(0)} = ^t\{\sigma^M\} + Ratio\,[C^{E'}]_t\{\Delta\epsilon^L\} \quad (3.49)$$

$$^{t+\Delta t}[C^{EP}]^{(0)} = ^t[C^{EP}]\; evaluated\; at\; ^{t+\Delta t}\{\sigma^M\}^{(0)} \quad (3.50)$$

Use equation (2.12) to find $^{t+\Delta t}\sigma_{ij}$. RETURN.

- If the state at time t is *plastic*, check for unloading as described in section (3.4.2). If there is no unloading, the sub-incrementation method described in (4) above is applied with *Ratio* set to zero.

This describes the Euler forward integration scheme for the elasto-plastic model described in section (2.7)

3.4.2 Unloading Scheme

The phenomenon of local unloading is to be incorporated to reproduce more closely the elasto-plastic response of a structure. The unloading criterion defined by Chakrabarty [14]:

$$^t\{n\}^T\,{}_t\{\Delta\varepsilon^T\} < 0 \quad (3.51)$$

where, ${}_t\{\Delta\epsilon\}^L$ is the incremental strain and $^t\{n\}^T$ represents the unit outward normal to the yield surface at the current stress point $\{^t\sigma\}$ in a 9-D stress space, is implemented in this work. Neutral loading and postive loading are represented by replacing the "<"symbol in(3.51) by "=" and ">" symbols respectively.

When unloading is detected, the yield stress at that Gauss point is changed to the equivalent stress at the Gauss point at time t ($^t\sigma_y = {}^t\sigma_{eq}$), the state tag of the Gauss point is changed from plastic to elastic and the elastic constitutive equation is applied to calculate the incremental stress, $^t[\Delta\sigma^M]$.

3.5 Skyline Scheme of Global Assembly

The three-dimensional dynamic elasto-plastic contact problem is computationally intensive one and therefore every effort should be made to reduce the storage and the computational time required for solving the problem. Skyline assembly scheme [4] is one such technique, which significantly reduces the storage required for the global stiffness matrix ${}^t[K]$. In this storage scheme, only the elements below the skyline of the matrix ${}^t[K]$ are stored in a one-dimensional array ${}^t\{A\}$. However, along with the storage scheme, a specific procedure for addressing the elements of ${}^t[K]$ in ${}^t\{A\}$ is needed. Thus, before proceeding with the assembly of the element stiffness matrices, it is necessary to establish the address of the global stiffness matrix elements in one-dimensional array ${}^t\{A\}$.

The element pattern of a typical global stiffness matrix is shown below:

$$ {}^t[K] = \begin{bmatrix} k_{11} & k_{12} & 0 & k_{14} & 0 \\ k_{12} & k_{22} & k_{23} & 0 & 0 \\ 0 & k_{23} & k_{33} & k_{34} & 0 \\ k_{14} & 0 & k_{34} & k_{44} & k_{45} \\ 0 & 0 & 0 & k_{45} & k_{55} \end{bmatrix} $$

Since the matrix ${}^t[K]$ is symmetric, only the elements above the diagonal and the diagonal elements need to be stored. Defining by m_i the row number of the first non-zero element in column i, the variables $m_i = 1, \ldots, n$ represent the skyline of the matrix, and the value $(m_{i+1} - m_i)$ represents the column height. (The zero elements below the skyline are stored, since they may become non-zero during the solution process). The column heights are determined from the connectivity arrays of the elements. Once the column heights of the global stiffness matrix are known, we can store all the elements below the skyline of ${}^t[K]$ as a one-dimensional array in ${}^t\{A\}$; i.e., the *active elements* (elements below the skyline) of ${}^t[K]$ are stored consecutively in ${}^t\{A\}$:

$$ {}^t\{A\}^T = \{k_{11}, k_{22}, k_{12}, k_{33}, k_{23}, k_{44}, k_{34}, 0, k_{14}, k_{55}, k_{45}\} $$

In addition to ${}^t\{A\}$, we also define an array $\{MAXA\}$, which stores the addresses of diagonal elements of ${}^t[K]$ in ${}^t\{A\}$; i.e., the address of the i^{th} diagonal element of ${}^t[K]$, k_{ii}, in array ${}^t\{A\}$ is given by $MAXA_i$. Thus,

$$ \{MAXA\}^T = \{1, 2, 4, 6, 10, 12\} $$

Note that, $MAXA_i$ is equal to the sum of column heights upto the $(i-1)^{th}$ column plus 1. Hence the number of active elements in the i^{th} column of ${}^t[K]$ is equal to $MAXA_{i+1} - MAXA_i$, and the element addresses are $MAXA_i$, $(MAXA_i + 1)$, ..., $(MAXA_{i+1} - 1)$. It follows that using the above storage scheme of ${}^t[K]$ in ${}^t\{A\}$, together with the address array $\{MAXA\}$ as defined above, each element of ${}^t[K]$ in ${}^t\{A\}$ can be addressed uniquely.

3.6 Static Condensation Scheme

The contact analysis is done in an iterative manner to determine the nodes which are out of contact, in sticking contact or in slipping contact. Solving the complete system of equations in each iteration is highly inefficient in terms of time and computer resources, especially when the contact region is small compared to the whole system. In order to reduce the solution time, it is desirable to condense the effective stiffness matrix and the effective force vector to the size of the degrees of freedom to which the contact boundary conditions are to be applied.

The condensation procedure starts by dividing the nodes into two categories: the nodes at which the contact boundary conditions are to be applied (referred to as the nodes of *type 1*) and the remaining nodes (referred to as the nodes of *type 2*). To facilitate the condensation, the nodes are renumbered so that the nodes of type 1 are numbered first (called *internal node numbers*, while the original node numbers are called *external node numbers*). Then the essential boundary conditions (i.e., the displacement boundary conditions) are applied to equation (3.40).

Then these equations are partitioned as follows:[1]

$$\begin{bmatrix} [K_{11}] & [K_{12}] \\ [K_{21}] & [K_{22}] \end{bmatrix} \begin{Bmatrix} \{\Delta U_1\} \\ \{\Delta U_2\} \end{Bmatrix} = \begin{Bmatrix} \{\Delta F_1\} \\ \{\Delta F_2\} \end{Bmatrix} \tag{3.52}$$

where $\{\Delta U_1\}$ denotes the incremental displacement vector corresponding to the nodes of type 1 and $\{\Delta U_2\}$ denotes the incremental displacement vector corresponding to the nodes of type 2. Equation (3.52) can be seperated as follows:

$$[K_{11}]\{\Delta U_1\} + [K_{12}]\{\Delta U_2\} = \{\Delta F_1\} \tag{3.53}$$

$$[K_{21}]\{\Delta U_1\} + [K_{22}]\{\Delta U_2\} = \{\Delta F_2\} \tag{3.54}$$

[1] In this section, the superscript/subscript denoting time have been omitted for the sake of convenience

Solving for $\{\Delta U_2\}$ from equation (3.54), we get:

$$\{\Delta U_2\} = [K_{22}]^{-1} (\{\Delta F_2\} - [K_{21}] \{\Delta U_1\}) \tag{3.55}$$

Substitution of this expression for $\{\Delta U_2\}$ in equation (3.53) and rearrangement of the resulting equation leads to the following condensed set of dynamic equilibrium equations:

$$[\widehat{K}]\{\Delta \hat{U}\} = \{\Delta \hat{F}\} \tag{3.56}$$

where,

$$[\widehat{K}] = [K_{11}] - [K_{12}] [A] \tag{3.57}$$

$$\{\Delta \hat{U}\} = \{\Delta U_1\} \tag{3.58}$$

$$\{\Delta \hat{F}\} = \{\Delta F_1\} - [K_{12}] \{B\} \tag{3.59}$$

$$[A] = [K_{22}]^{-1} [K_{21}] \tag{3.60}$$

$$\{B\} = [K_{22}]^{-1} \{\Delta F_2\} \tag{3.61}$$

The number of equations in the condensed set (3.56) is equal to the number of degrees of freedom of type 1. The coefficient matrix $[\widehat{K}]$ and the right side vector $\{\Delta \hat{F}\}$ are evaluated from equations (3.57 – 3.61) using the partitioned matrices and vectors of equation (3.52). Note that while evaluating $[A]$ and $\{B\}$, it is not necessary to invert the matrix $[K_{22}]^{-1}$. Instead one can solve the following equations by the Gauss elimination method:

$$[K_{22}] [A] = [K_{21}] \tag{3.62}$$

$$[K_{22}] \{B\} = \{\Delta F_2\} \tag{3.63}$$

To reduce the time further, one can store the upper triangular form of $[K_{22}]$. In this way, one can solve for the columns of $[A]$ by performing Gauss elimination and back substitution operations on the corresponding columns of $[K_{21}]$. The vector $\{B\}$ is obtained in similar fashion by performing the Gauss elimination and back substitution on the vector $\{\Delta F_2\}$.

3.7 Modified Newton-Raphson Scheme

The solution to equation (3.40) represents only an approximate solution to the governing equation (2.44), because of the linearization and simplifications employed in deriving the

equation (2.52). The error obtained should to be minmized and there are various iterative techniques for this. One of the simplest and very effective technique is the *Modified Newton-Raphson algorithm*, which offers fast convergence with less computation [4].

This technique can elegantly be represented as follows:

Solve:

$$ {}^{t}[K_d]\ {}_{t}\{\Delta U\}^{(i)} = {}_{t}\{\Delta F_u\}^{(i-1)} \tag{3.64} $$

where,

$$ {}_{t}\{\Delta F_u\}^{(i-1)} = {}^{t+\Delta t}\{F\}^{(i-1)} - {}^{t+\Delta t}\{f\}^{(i-1)} - {}^{t+\Delta t}[M]\ {}^{t+\Delta t}\{\ddot{U}\}^{(i-1)} \tag{3.65} $$

$$ {}_{t}\{\Delta F_u\}^{(0)} = {}_{t}\{\Delta F_d\} \tag{3.66} $$

till the convergence criterion:

$$ \frac{\|{}_{t}\{\Delta F_u\}^{(i)}\|}{\|{}^{t+\Delta t}\{F\}^{(i)}\|} \leq tol_c \tag{3.67} $$

is satisfied. The vector ${}_{t}\{\Delta F_u\}$ is called the *unbalance force vector.*

3.8 Divergence Handling Procedures

The modified Newton Raphson method diverges in some cases; i.e., the ratio of unbalance force to the external force, instead of reducing, increases in each iteration. Also, in some other cases, the rate of convergence is not fast enough, requiring a large number of iterations for reducing the unbalance force to acceptable limits. Two of the methods, which are simple and fairly effective for handling divergence or accelerating the rate of convergence are *Under-relaxation method* and *Line search method* [8] . These methods are generally applied by modifying the displacement vector ${}_{t}\{\Delta u\}^{(i)}$. However, in the contact analysis scenario, it is not acceptable, since the contact status may get changed due to modification in the displacement vector. Therefore, in this work, these methods are applied by modifying the unbalance force vector ${}_{t}\{\Delta F_u\}^{(i-1)}$ and repeating the solution process when divergence is detected.

In this work, the Newton Raphson iterations are said to be diverging when:

$$ \frac{\|{}_{t}\{\Delta F_u\}^{(i)}\|}{\|{}^{t+\Delta t}\{F\}^{(i)}\|} > \beta \frac{\|{}_{t}\{\Delta F_u\}^{(i-1)}\|}{\|{}^{t+\Delta t}\{F\}^{(i-1)}\|} \tag{3.68} $$

is satisfied. The value of the factor β is taken as 0.9.

The under-relaxation and line search methods are discussed below:

Under-relaxation method: If divergence is detected in the i^{th} iteration, the unbalance force vector ${}_t\{\Delta F_u\}^{(i-1)}$ is scaled by a factor α repeatedly, till the above criterion is not satisfied:

$$ {}_t\{\Delta F_u\}^{(i-1)} = \alpha \, {}_t\{\Delta F_u\}^{(i-1)} \tag{3.69} $$

If the under-relaxation is not able to find a value of unbalance force for which the above criterion is not satisfied, the solution run is terminated with a warning message.

Line search method: In this method, the basic aim is to search for the point, which corresponds to minimum unbalance, along a direction specified by the unbalance force vector ${}_t\{\Delta F_u\}^{(i-1)}$. However, it is not very efficient to perform a full line search, since, in that case the number of solution runs required may become prohibitively high. The approach used is to repeat the solutions for a fixed number of values of factor α_j (defined below), within a preselected range.

$$ {}_t\{\Delta F_u\}^{(i-1)} = \alpha_j \, {}_t\{\Delta F_u\}^{(i-1)} \tag{3.70} $$

$$ \text{where, } \alpha_{min} \leq \alpha_j \leq \alpha_{max} $$

The value of α_j corresponding to the minimum unbalance force is chosen as the best point and the solution corresponding to this α_j is accepted as the result of line search method.

Since in both the above methods, the complete iteration is repeated, including a number of contact iterations, it is very costly to do either under-relaxation or line search, in terms of both computational time and resources. Therefore, it is preferable to use these methods only when some difficulties in convergence are observed. Under-relaxation is cheaper compared to line search, while line search is more efficient.

3.9 Numerical Aspects

The selection of parameters controlling the numerical scheme in dynamic non-linear analysis is of importance not only for efficiently obtaining the solution, but also for the accuracy of the solution. The following sections discuss various aspects related to the numerical scheme used.

3.9.1 Choice of Time-step

A procedure for the selection of time step is given in Bathe [4], which may be used to select an initial time step and mesh. A time step and mesh convergence study should then be performed to arrive at the proper values. It is important to note that an unconditionally stable method *does not* provide a solution close to the exact solution for an arbitrary time step. Phenomena such as amplitude reduction and period elongation may occur due to an improper choice of time step. Hence the proper way to perform a dynamic non-linear analysis is to study the effect of time step and mesh size on the solution and to search appropriate values.

The choice of a time step is based on the type of problem considered. In general, dynamic problems can be categorized as: 1. *Strucural dynamics problems* and 2. *Wave propagation problems.*

Structural Dynamics Problem: The step by step procedure for modeling a strucutural dynamics problem is given below.

1. Identify the frequencies involved in loading, using a Fourier analysis if necessary. These frequencies may change with time. Let the highest significant frequency contained in the loading be w_u.
2. Choose a finite element mesh that can accurately represent the static response and accurately represent all frequencies upto about $w_{co} = 4w_u$, where w_{co} is called as the *optimum critical frequency.*
3. Perform the direct integration analysis. The time step Δt for this solution should be equal to about $\frac{1}{20}T_{co}$, where $T_{co} = \frac{2\pi}{w_{co}}$.

Wave Propagation Problems: Assuming that the critical wavelength to be calculated correctly is L_w, then the time taken by the wave to travel past a point is given by:

$$t_w = \frac{L_w}{c} \tag{3.71}$$

where c is the wave speed. Assuming that n time steps are necessary to represent the travel of the wave, the time step should be:

$$\Delta t = \frac{t_w}{n} \tag{3.72}$$

and the *effective length*[2] of a finite element should be:

$$L_e = c\Delta t \tag{3.73}$$

The above choice of time step and corresponding effective length represents the complete wave travel accurately. But, care has to be taken to ensure that $\Delta t \leq \frac{T_n}{\pi}$, where T_n is the smallest time period of the problem.

It is found that the most accurate solution is obtained by integrating with a time step equal to the above limits (denoted by Δt_{cr}) and the solution is less accurate, when a smaller time step is employed. This deterioration in the accuracy of the predicted solution when Δt is smaller than Δt_{cr} is more pronounced, when a relatively coarse spatial discretization is used.

3.9.2 Deformation Dependent Loading

Deformation dependent loading is taken care of by evaluating the consistent force vector ${}^{t+\Delta t}\{F\}$ at time $t + \Delta t$ for the calculation of the unbalance force vector (3.65). An alternate procedure given by Bathe *et al.* [17] incorporates deformation dependency into the formulation of the governing equation, but this results in an asymmetric stiffness matrix, the solution of which is computationally expensive. The method used in this work may take a slightly more number of iterations for convergence, but this loss is offset by the gains acquired by retaining a symmetic stiffness matrix.

3.9.3 Stress Updation

There exist two methods for updating the stress at a Gauss point: 1. *Iterative updation* and 2. *Incremental updation* (Crisfield [8]).

Iterative Updation: The iterative displacement is used to compute the iterative strain, which is then used in the constitutive equation to update the stress at iteration $(i-1)$ to stress at iteration (i).

Incremental Updation: All the iterative displacements upto iteration (i) are added to find the cumulative incremental displacement of the current increment. This is used to compute the incremental strain, which is used in the constitutive equation to

[2]Effective length is the smallest distance between any two nodes in the mesh used

update the stress from last equilibrium point (end of the previous increment) to the state after iteration (i).

The first method may lead to spurious unloading, since the unbalance force vector calculated in some iterations may be in different directions compared to that of the initial force vector. This can be avoided by using the incremental updation procedure. The examples solved in this work employ the incremental updation method. Iterative updation may be used if the convergence is monotonic.

Chapter 4

Contact Formulation

The dynamic, large deformation, elasto-plastic, updated Lagrangian finite element formulation developed in the previous two chapters, can be used for contact analysis with appropriate modifications. The most important modification is the development of an additional set of finite element equations (involving the contact stiffness matrix) relating the unknown contact forces and displacements. These equations, which consist of the kinematic constraints and the contact force expressions based on the discretization of the contact boundary, are developed using the *Lagrange multiplier method.* These developments are described in the following sections. Finally the algorithm for the analysis of dynamic, large deformation, elasto-plastic contact problem including the effects of friction, is described.

4.1 Contact Constraints

A typical two body contact system is shown in Figure (4.1). The bodies occupy the domains ${}^{t+\Delta t}\overline{V}^1$ and ${}^{t+\Delta t}\overline{V}^2$ at time $t+\Delta t$. The boundaries of ${}^{t+\Delta t}\overline{V}^1$ and ${}^{t+\Delta t}\overline{V}^2$ are denoted by ${}^{t+\Delta t}S^1$ and ${}^{t+\Delta t}S^2$ and their interior volumes by ${}^{t+\Delta t}V^1$ and ${}^{t+\Delta t}V^2$ respectively. At any time $t+\Delta t$, the boundary of contact body n (n = 1,2) can be partitioned as:

$$ {}^{t+\Delta t}S^n = {}^{t+\Delta t}S^n_D \bigcup {}^{t+\Delta t}S^n_F \bigcup {}^{t+\Delta t}S^n_C \tag{4.1} $$

where,

${}^{t+\Delta t}S^n_D$ = surface on which displacements are specified,

${}^{t+\Delta t}S^n_F$ = surface on which tractions are specified,

${}^{t+\Delta t}S^n_C$ = surface on which contact occurs.

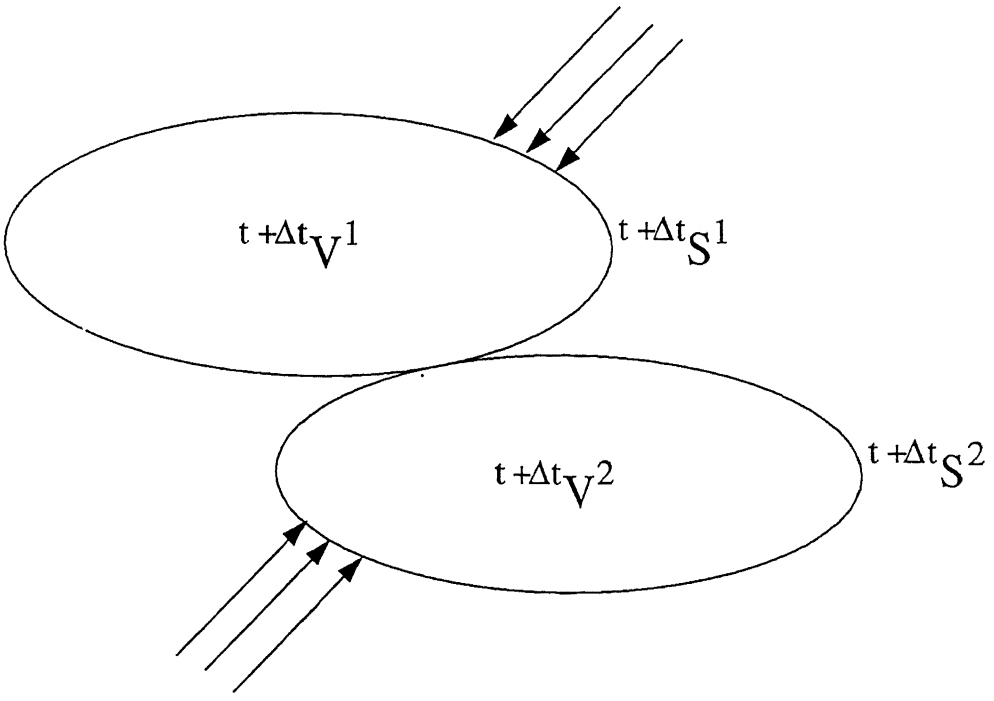

Figure 4.1: Two body contact system

Assuming the boundary ${}^{t+\Delta t}S^n$ to be smooth, outward unit normal vector at point[1] ${}^{t+\Delta t}\underline{x}^n$ on the boundary ${}^{t+\Delta t}S^n$ is denoted by ${}^{t+\Delta t}\underline{N}_1^n$. Other two orthonormal boundary vectors (in tangential directions) are ${}^{t+\Delta t}\underline{N}_2^n$ and ${}^{t+\Delta t}\underline{N}_3^n$ (see Figure (4.2)).

Suppose that two boundary points ${}^{t+\Delta t}\underline{x}^1$ and ${}^{t+\Delta t}\underline{x}^2$ are in contact with each other at time $t + \Delta t$ and the contact traction at ${}^{t+\Delta t}\underline{x}^n$ is denoted as ${}^{t+\Delta t}\underline{T}_c^n$. Then by Newton's third law of motion, we have:

$$ {}^{t+\Delta t}\underline{T}_c^1 = -{}^{t+\Delta t}\underline{T}_c^2 \tag{4.2} $$

where ${}^{t+\Delta t}\underline{T}_c^n$ can be expressed as:

$$ {}^{t+\Delta t}\underline{T}_c^n = \sum_{i=1}^{3} {}^{t+\Delta t}t_i^n \, {}^{t+\Delta t}\underline{N}_i^n \tag{4.3} $$

where, ${}^{t+\Delta t}t_i^n$ denotes the component of ${}^{t+\Delta t}\underline{T}_c^n$ along ${}^{t+\Delta t}\underline{N}_i^n$.

If the two contact bodies are not welded together, then the normal component of traction can not be tensile. Thus we have:

$$ {}^{t+\Delta t}t_1^n \leq 0 \tag{4.4} $$

Further, from the Coulomb friction law we have:

$$ \sqrt{({}^{t+\Delta t}t_2^n)^2 + ({}^{t+\Delta t}t_3^n)^2} \leq \mu |{}^{t+\Delta t}t_1^n| \tag{4.5} $$

[1]Vectors are denoted by a letter with underbar

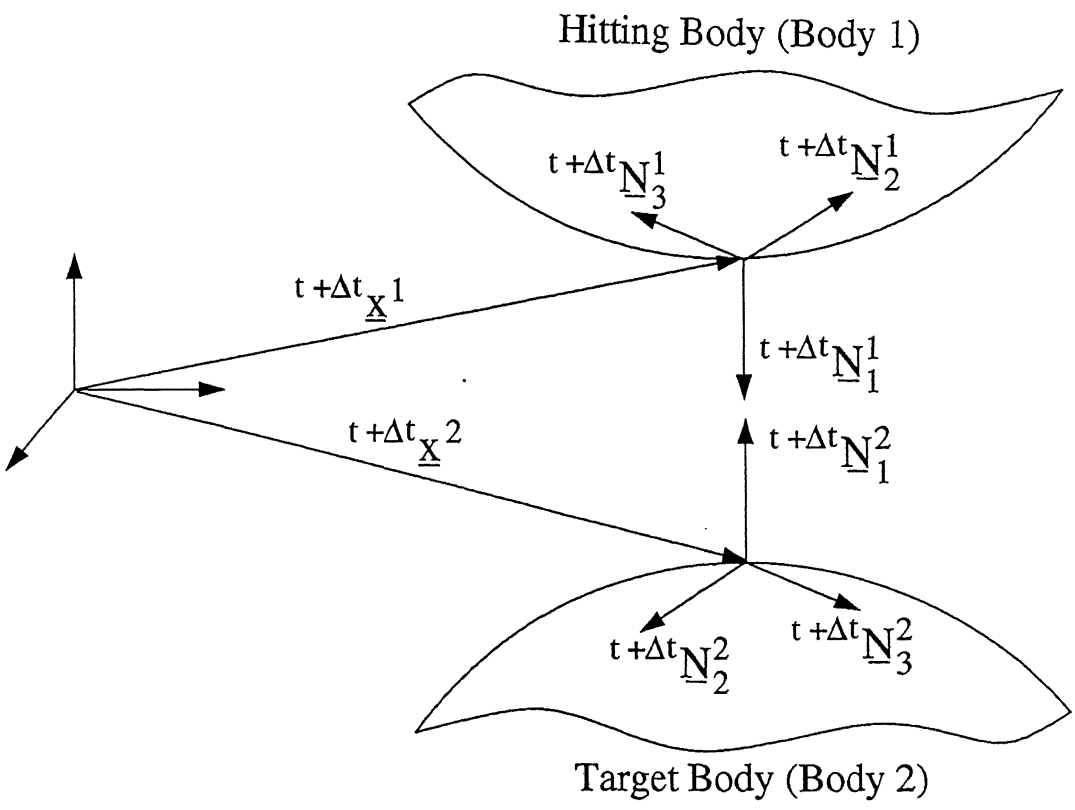

Figure 4.2: Points in contact and associated normal and tangent vectors

In equation (4.5), the "<" symbol represents the *sticking friction condition* and "=" represents the *slipping condition.* Further, the resultant tangential (friction) force is in the direction opposite to the relative velocity of slipping. The equations (4.4) and (4.5) represent *traction constraints.*

Physical considerations require that one body can not penetrate the other. Thus, for the points in contact, *pentration* must be zero. This condition can be mathematically stated as:

$$^{t+\Delta t}p_1 = (^{t+\Delta t}\underline{x}^2 - {}^{t+\Delta t}\underline{x}^1).\ ^{t+\Delta t}\underline{N}_1^2 = 0 \tag{4.6}$$

where $^{t+\Delta t}p_1$ represents the penetration between the two points in contact. In addition to (4.6), we need to have two more conditions to enforce the sticking friction condition, which ensure that there are no relative displacements (slip) between the contacting points in the tangential directions. These conditions can be stated as:

$$^{t+\Delta t}p_2 = (^{t+\Delta t}\underline{x}^2 - {}^{t+\Delta t}\underline{x}^1).\ ^{t+\Delta t}\underline{N}_2^2 = 0 \tag{4.7}$$

$$^{t+\Delta t}p_3 = (^{t+\Delta t}\underline{x}^2 - {}^{t+\Delta t}\underline{x}^1).\ ^{t+\Delta t}\underline{N}_3^2 = 0 \tag{4.8}$$

The conditions (4.6), (4.7) and (4.8) are called as the *kinematic constraints.*

4.2 Contact Force Expressions

As the contacting bodies are discretized for the purpose of developing finite element equations, the contact boundary gets automatically divided into surface elements, called as *contact segments.* The contact force formulation in this work employs a node-to-surface interface model, since this work deals with a large deformation problem including slipping at the contact interface. Normally in a contact formulation, contact is considered only at discrete nodes. Here, it is assumed that a node of the *hitting body* (body 1) comes into contact with a segment of the *target body* (body 2). The first step in the development of the contact force expression is the determination of the unit normal and tangent vectors at a point on the target segment. This is described in the next paragraph.

Geometry of a target segment can be described using 2-D shape functions. Thus,

$$^{t+\Delta t}\underline{x}^2(\xi,\eta) = \sum_{j=1}^{N} \Phi_j(\xi,\eta)\, {}^{t+\Delta t}\underline{x}_j^2 \tag{4.9}$$

where, $\Phi_j(\xi,\eta)$ $j = 1,n$ are the shape functions, $^{t+\Delta t}\underline{x}_j^2$ denotes the position vector of node j and N is the number of nodes per target segment. The side of a segment on which contact can occur is referred to as the positive side of the segment and the other side as the negative side of the segment. The local numbering of the nodes on a contact segment should be counter clockwise when we face the positive side of the segment. This is to get the correct sense for the outward normal vector at a given point. A normal vector at point $^{t+\Delta t}\underline{x}^2(\xi,\eta)$ on the positive side of the segment is defined as:

$$^{t+\Delta t}\underline{N}_1^2 = {}^{t+\Delta t}\underline{N}_\xi^2 \times {}^{t+\Delta t}\underline{N}_\eta^2 \tag{4.10}$$

where, $^{t+\Delta t}\underline{N}_\xi^2$ and $^{t+\Delta t}\underline{N}_\eta^2$ are the two tangent vectors at $^{t+\Delta t}\underline{x}^2(\xi,\eta)$ given by:

$$^{t+\Delta t}\underline{N}_\xi^2 = {}^{t+\Delta t}\underline{x}^2(\xi,\eta)_{,\xi} \tag{4.11}$$

$$^{t+\Delta t}\underline{N}_\eta^2 = {}^{t+\Delta t}\underline{x}^2(\xi,\eta)_{,\eta} \tag{4.12}$$

The unit normal and tangent vectors are defined as:

$$^{t+\Delta t}\underline{N}_1^2 = {}^{t+\Delta t}\underline{N}_1^2 / |^{t+\Delta t}\underline{N}_1^2| \tag{4.13}$$

$$^{t+\Delta t}\underline{N}_2^2 = {}^{t+\Delta t}\underline{N}_\xi^2 / |^{t+\Delta t}\underline{N}_\xi^2| \tag{4.14}$$

$$^{t+\Delta t}\underline{N}_3^2 = {}^{t+\Delta t}\underline{N}_\eta^2 / |^{t+\Delta t}\underline{N}_\eta^2| \tag{4.15}$$

Since the contact is considered only at discrete hitting nodes, we can deal only with point forces at hitting nodes rather than with contact tractions. At time $t + \Delta t$, let

${}^{t+\Delta t}\{F^2\}$ be an array of Cartesian components of point force vector ${}^{t+\Delta t}\underline{F}^2$ at a point of the target segment at which the hitting node makes contact. By Newton's third law, the force vector on the hitting node will be $-{}^{t+\Delta t}\{F^2\}$.

Let ${}^{t+\Delta t}\{\delta u^2\}$ and ${}^{t+\Delta t}\{\delta u^1\}$ be the virtual displacement vectors at time $t+\Delta t$ at these points (on the target and hitting bodies respectively), when they come in contact. Then, the virtual work at hitting node can be expressed as:[2]

$$\delta w_c = {}^{t+\Delta t}\{\delta u^2 - \delta u^1\}^T {}^{t+\Delta t}\{F^2\} \tag{4.16}$$

Note that the elements of ${}^{t+\Delta t}\{\delta u^1\}$, namely $\delta\,{}^{t+\Delta t}u^1$, $\delta\,{}^{t+\Delta t}v^1$, $\delta\,{}^{t+\Delta t}w^1$ are the virtual nodal displacements of the hitting node. The elements of ${}^{t+\Delta t}\{\delta u^2\}$ can be expressed in terms of the virtual nodal displacements of the target segment ($\delta\,{}^{t+\Delta t}u_i^2$, $\delta\,{}^{t+\Delta t}v_i^2$, $\delta\,{}^{t+\Delta t}w_i^2$, $i=1,\,N$) using the 2-D shape unctions (Φ_i, $i=1,\,N$). Thus:

$${}^{t+\Delta t}\{\delta u^2 - \delta u^1\} = [Q_c]\,{}^{t+\Delta t}\{\delta u_c\} \tag{4.17}$$

where,

$$[Q_c] = \begin{bmatrix} -1 & 0 & 0 & \Phi_1 & 0 & 0 & \Phi_2 & 0 & 0 & \ldots & \Phi_N & 0 & 0 \\ 0 & -1 & 0 & 0 & \Phi_1 & 0 & 0 & \Phi_2 & 0 & \ldots & 0 & \Phi_N & 0 \\ 0 & 0 & -1 & 0 & 0 & \Phi_1 & 0 & 0 & \Phi_2 & \ldots & 0 & 0 & \Phi_N \end{bmatrix} \tag{4.18}$$

and

$${}^{t+\Delta t}\{\delta u_c\}^T = \{\delta\,{}^{t+\Delta t}u^1, \delta\,{}^{t+\Delta t}v^1, \delta\,{}^{t+\Delta t}w^1, \delta\,{}^{t+\Delta t}u_1^2, \delta\,{}^{t+\Delta t}v_1^2, \delta\,{}^{t+\Delta t}w_1^2, \ldots, \delta\,{}^{t+\Delta t}w_N^2\} \tag{4.19}$$

4.2.1 Sticking Friction Condition

For the sticking friction, the vector ${}^{t+\Delta t}\{F^2\}$ can be expressed as:

$${}^{t+\Delta t}\{F^2\} = \begin{bmatrix} {}^{t+\Delta t}N_{11}^2 & {}^{t+\Delta t}N_{21}^2 & {}^{t+\Delta t}N_{31}^2 \\ {}^{t+\Delta t}N_{12}^2 & {}^{t+\Delta t}N_{22}^2 & {}^{t+\Delta t}N_{32}^2 \\ {}^{t+\Delta t}N_{13}^2 & {}^{t+\Delta t}N_{23}^2 & {}^{t+\Delta t}N_{33}^2 \end{bmatrix} \begin{Bmatrix} {}^{t+\Delta t}f_1^2 \\ {}^{t+\Delta t}f_2^2 \\ {}^{t+\Delta t}f_3^2 \end{Bmatrix} \tag{4.20}$$

or,

$${}^{t+\Delta t}\{F^2\} = {}^{t+\Delta t}\left[N^2\right]\,{}^{t+\Delta t}\{f^2\} \tag{4.21}$$

where, ${}^{t+\Delta t}N_{ij}^2$ represents the j^{th} Cartesian component of the unit vector ${}^{t+\Delta t}\underline{N}_i^2$ and ${}^{t+\Delta t}f_i^2$ is the component, with respect to ${}^{t+\Delta t}\underline{N}_i^2$, of the contact force vector ${}^{t+\Delta t}\underline{F}^2$. Combining

[2] In this section, the right superscript denoting the iteration number has been omitted for convenience

equations (4.16), (4.17) and (4.21), we get the following expression for the virtual work at the hitting node:

$$\delta w_c = {}^{t+\Delta t}\{\delta u_c\}^T \, {}^{t+\Delta t}\{r_c\} \tag{4.22}$$

where the vector ${}^{t+\Delta t}\{r_c\}$ is given by:

$${}^{t+\Delta t}\{r_c\} = [Q_c]^T \, {}^{t+\Delta t}\left[N^2\right] \, {}^{t+\Delta t}\{f^2\} \tag{4.23}$$

This is the contact force expression at a *sticking node* (hitting node, which is under sticking friction condition).

4.2.2 Slipping Condition

The contact force expression for a *slipping node* (hitting node, which is slipping on the target segment) is developed below:

The vector ${}^{t+\Delta t}\{r_c\}$ in equation (4.23) can be split as a contribution from the normal contact forces and tangential contact forces. Thus,

$${}^{t+\Delta t}\{r_c\} = {}^{t+\Delta t}\{r_n\} + {}^{t+\Delta t}\{r_t\} \tag{4.24}$$

where,

$${}^{t+\Delta t}\{r_n\} = [Q_c]^T \, {}^{t+\Delta t}\left\{N_1^2\right\} \, {}^{t+\Delta t}f_1^2 \tag{4.25}$$

and

$${}^{t+\Delta t}\{r_t\} = [Q_c]^T \left({}^{t+\Delta t}\left\{N_2^2\right\} \, {}^{t+\Delta t}f_2^2 + {}^{t+\Delta t}\left\{N_3^2\right\} \, {}^{t+\Delta t}f_3^2 \right) \tag{4.26}$$

Here, the arrays ${}^{t+\Delta t}\{N_i^2\}$, $i = 1, 2, 3$ contain the Cartesian components of the vectors ${}^{t+\Delta t}\underline{N}_i^2$.

The three components of a contact force are not independent at a slipping node. From Coulomb's friction law, we have the relation:

$$\sqrt{({}^{t+\Delta t}f_2^2)^2 + ({}^{t+\Delta t}f_3^2)^2} = \mu |{}^{t+\Delta t}f_1^2| \tag{4.27}$$

where μ is the coefficient of friction at a slipping node. Therefore, the tangential components of the contact force can be written as:

$${}^{t+\Delta t}f_2^2 = -{}^{t+\Delta t}f_1^2 \, \mu \cos\theta \tag{4.28}$$

$${}^{t+\Delta t}f_3^2 = -{}^{t+\Delta t}f_1^2 \, \mu \sin\theta \tag{4.29}$$

where, θ is the angle between the resultant tangential (friction) force and the vector ${}^{t+\Delta t}\underline{N}_2^2$ and since the normal contact force is always compressive, "$-$" sign is used in the right hand side of both the above equations.

Calculation of the angle θ:

The friction force in the case of slipping is in a direction opposite to the relative velocity of slipping, which is same as the difference in incremental displacement of the target point and the hitting node. Therefore, the direction of the friction force on the target body is given by: $-\{{}_t\Delta u^2 - {}_t\Delta u^1\}_t = -\left([Q_c]\ {}_t\{\Delta u_c\}\right)_t$, where the right subscript t indicates the tangential component. Define:

$$ {}_t\Delta\overline{u}_2 = -\ {}^{t+\Delta t}\{N_2^2\}^T\,[Q_c]\ {}_t\{\Delta u_c\} \tag{4.30} $$

$$ {}_t\Delta\overline{u}_3 = -\ {}^{t+\Delta t}\{N_3^2\}^T\,[Q_c]\ {}_t\{\Delta u_c\} \tag{4.31} $$

Thus, the angle θ is given by:

$$ \theta = \tan^{-1}\left(\frac{{}_t\Delta\overline{u}_3}{{}_t\Delta\overline{u}_2}\right) \tag{4.32} $$

However, to avoid the difficulty in handling *infinity*, the computer implementation uses *cosine* function instead of *tangent* function for calculating θ.

Substituting equations (4.28) and (4.29) in equation (4.26) and then combining equations (4.25) and (4.26) with equation (4.24) we get:

$$ {}^{t+\Delta t}\{r_c\} = [Q_c]^T\left({}^{t+\Delta t}\{N_1^2\} - {}^{t+\Delta t}\{N_2^2\}\,\mu\cos\theta - {}^{t+\Delta t}\{N_3^2\}\,\mu\sin\theta\right)\,{}^{t+\Delta t}f_1^2 \tag{4.33} $$

4.3 Kinematic Constraints in Nodal Form

The kinematic constraints should be written separately for the sticking nodes and for slipping nodes.

4.3.1 Sticking Friction Condition

To express the kinematic constraints in terms of the nodal displacements, equations (4.6), (4.7) and (4.8) are combined in matrix form for the i^{th} Newton-Raphson iteration as:

$$ {}^{t+\Delta t}\{p\}^{(i)} = {}^{t+\Delta t}\left[N^2\right]^T\,{}^{t+\Delta t}\{x^2 - x^1\}^{(i)} \tag{4.34} $$

where,

$$ {}^{t+\Delta t}\{p\}^{(i)T} = \{{}^{t+\Delta t}p_1^{(i)},\ {}^{t+\Delta t}p_2^{(i)},\ {}^{t+\Delta t}p_3^{(i)}\} \tag{4.35} $$

We have,

$$^{t+\Delta t}\{x^2 - x^1\}^{(i)} = {}^{t+\Delta t}\{x^2 - x^1\}^{(i-1)} + {}_t\{\Delta u^2 - \Delta u^1\}^{(i)} \tag{4.36}$$

where, the second term on the right hand side is an array of Cartesian components of the difference of the displacement vectors of the target and hitting bodies at the contact node, for the current iteration. For the first iteration:

$$^{t+\Delta t}\{x^2 - x^1\}^{(i-1)} = {}^{t+\Delta t}\{x^2 - x^1\}^{(0)} = {}^{t}\{x^2 - x^1\} \tag{4.37}$$

Analogus to equation (4.17), the second term of the right side of equation (4.36) can be written as:

$${}_t\{\Delta u^2 - \Delta u^1\}^{(i)} = [Q_c]\ {}_t\{\Delta u_c\}^{(i)} \tag{4.38}$$

where, the vector:

$${}_t\{\Delta u_c\}^{(i)^T} = \{{}_t\Delta u^{1(i)}, {}_t\Delta v^{1(i)}, {}_t\Delta w^{1(i)}, {}_t\Delta u_1^{2(i)}, {}_t\Delta v_1^{2(i)}, {}_t\Delta w_1^{2(i)}, \ldots, {}_t\Delta w_N^{2\,(i)}\} \tag{4.39}$$

contains the nodal values of displacement at the hitting node and the nodes of the target segment for the current iteration. Recognizing the first term of the right hand side of equation (4.36) as corresponding to $^{t+\Delta t}\{p\}^{(i-1)}$ (penetration for the previous iteration), equation (4.34) can be written as:

$$^{t+\Delta t}\{p\}^{(i)} = {}^{t+\Delta t}\{p\}^{(i-1)} + {}^{t+\Delta t}\left[N^2\right]^T [Q_c]\ {}_t\{\Delta u_c\}^{(i)} \tag{4.40}$$

where for the first iteration,

$$^{t+\Delta t}\{p\}^{(i-1)} = {}^{t+\Delta t}\{p\}^{(0)} = {}^{t}\{p\} \tag{4.41}$$

Since $^{t+\Delta t}\{p\}^{(i)}$ is zero, the kinematic constraint at a sticking node is:

$$^{t+\Delta t}\{p\}^{(i-1)} + {}^{t+\Delta t}\left[N^2\right]^T [Q_c]\ {}_t\{\Delta u_c\}^{(i)} = \{0\} \tag{4.42}$$

The first term of the right hand side of equation (4.36), on similar development, gives:

$$^{t+\Delta t}\{p\}^{(i-1)} = {}^{t+\Delta t}\left[N^2\right]^T [Q_c]\ {}^{t+\Delta t}\{x_c\}^{(i-1)} \tag{4.43}$$

where, $^{t+\Delta t}\{x_c\}^{(i-1)}$ is the array of coordinates of the hitting node and the nodes of the target segment updated upto the previous iteration. Expression (4.43) is used to calculate $^{t+\Delta t}\{p\}^{(i-1)}$.

4.3.2 Slipping Condition

Development of the nodal constraints for the slipping nodes is similar to the sticking nodes, except that we have only one kinematic constraint, viz., equation (4.6).

We can write the matrix form of the kinematic constraints for the i^{th} Newton-Raphson iteration as:

$$ {}^{t+\Delta t}p_1^{(i)} = {}^{t+\Delta t}\{N_1^2\}^T \, {}^{t+\Delta t}\{x^2 - x^1\}^{(i)} \tag{4.44} $$

Substituting equations (4.36) and (4.38) in equation (4.44) we get:

$$ {}^{t+\Delta t}p_1^{(i)} = {}^{t+\Delta t}p_1^{(i-1)} + {}^{t+\Delta t}\{N_1^2\}^T \, [Q_c] \, {}_t\{\Delta u_c\}^{(i)} \tag{4.45} $$

where for the first iteration,

$$ {}^{t+\Delta t}p_1^{(i-1)} = {}^{t+\Delta t}p_1^{(0)} = {}^{t}p_1 \tag{4.46} $$

Since ${}^{t+\Delta t}p_1^{(i)}$ is zero, the kinematic constraint at a slipping node is:

$$ {}^{t+\Delta t}p_1^{(i-1)} + {}^{t+\Delta t}\{N_1^2\}^T \, [Q_c] \, {}_t\{\Delta u_c\}^{(i)} = 0 \tag{4.47} $$

Similar to the sticking condition, we have:

$$ {}^{t+\Delta t}p_1^{(i-1)} = {}^{t+\Delta t}\{N_1^2\}^T \, [Q_c] \, {}^{t+\Delta t}\{x_c\}^{(i-1)} \tag{4.48} $$

where, ${}^{t+\Delta t}\{x_c\}^{(i-1)}$ contains the coordinates of the hitting node and the nodes of target segment updated upto the previous iteration. Expression (4.48) is used to calculate ${}^{t+\Delta t}p_1^{(i-1)}$.

4.4 Lagrange Multiplier Method

In Lagrange Multiplier Method, the contact forces are considered as primary unknowns and the kinematic constraints are enforced exactly. We have the contact force expression for a sticking node given by equation (4.23) and for a slipping node by equation (4.33). The kinematic constraint for a sticking node is given by equation (4.42):

$$ {}^{t+\Delta t}\left[N^2\right]^T \, [Q_c] \, {}_t\{\Delta u_c\}^{(i)} = -{}^{t+\Delta t}\{p\}^{(i-1)} \tag{4.49} $$

and for a slipping node is given by equation (4.47):

$$ {}^{t+\Delta t}\{N_1^2\}^T \, [Q_c] \, {}_t\{\Delta u_c\}^{(i)} = - {}^{t+\Delta t}p_1^{(i-1)} \tag{4.50} $$

Combining equations (4.23) and (4.49) for a sticking node, we get

$$\begin{bmatrix} 0 & -{}^{t+\Delta t}[q_1]^T \\ -{}^{t+\Delta t}[q_1] & 0 \end{bmatrix} \begin{Bmatrix} {}^{t+\Delta t}\{f^2\}^{(i)} \\ {}_t\{\Delta u_c\}^{(i)} \end{Bmatrix} = \begin{Bmatrix} {}^{t+\Delta t}\{p\}^{(i-1)} \\ -{}^{t+\Delta t}\{r_c\}^{(i-1)} \end{Bmatrix} \tag{4.51}$$

where,

$${}^{t+\Delta t}[q_1]^T = {}^{t+\Delta t}\left[N^2\right]^T [Q_c] \tag{4.52}$$

Similarly, combining the equations (4.33 and 4.50) for a slipping node, we get

$$\begin{bmatrix} 0 & -{}^{t+\Delta t}\{q_3\}^T \\ -{}^{t+\Delta t}\{q_2\} & 0 \end{bmatrix} \begin{Bmatrix} {}^{t+\Delta t}f_1^{2(i)} \\ {}_t\{\Delta u_c\}^{(i)} \end{Bmatrix} = \begin{Bmatrix} {}^{t+\Delta t}p_1{}^{(i-1)} \\ -{}^{t+\Delta t}\{r_c\}^{(i-1)} \end{Bmatrix} \tag{4.53}$$

where,

$${}^{t+\Delta t}\{q_3\}^T = {}^{t+\Delta t}\left\{N_1^2\right\}^T [Q_c] \tag{4.54}$$

$${}^{t+\Delta t}\{q_2\} = [Q_c]^T \left({}^{t+\Delta t}\{N_1^2\} - {}^{t+\Delta t}\{N_2^2\}\,\mu\cos\theta - {}^{t+\Delta t}\{N_3^2\}\,\mu\sin\theta\right) \tag{4.55}$$

Assembling these equations (4.51) and (4.53) over all the potential contact nodes, we get the following global equation:

$$\begin{bmatrix} 0 & -{}^{t+\Delta t}[Q_1]^T \\ -{}^{t+\Delta t}[Q_2] & 0 \end{bmatrix} \begin{Bmatrix} {}^{t+\Delta t}\{F^2\}^{(i)} \\ {}_t\{\Delta U_c\}^{(i)} \end{Bmatrix} = \begin{Bmatrix} {}^{t+\Delta t}\{P\}^{(i-1)} \\ -{}^{t+\Delta t}\{R_c\}^{(i-1)} \end{Bmatrix} \tag{4.56}$$

Here, the vectors ${}_t\{\Delta U_c\}^{(i)}$ and ${}^{t+\Delta t}\{R_c\}^{(i-1)}$ are the assembled versions of ${}_t\{\Delta u_c\}^{(i)}$ and ${}^{t+\Delta t}\{r_c\}^{(i-1)}$ respectively. Further, the vectors ${}^{t+\Delta t}\{F^2\}^{(i)}$ and ${}^{t+\Delta t}\{P\}^{(i-1)}$ are the assembled versions of ${}^{t+\Delta t}\{f^2\}^{(i)}$ and ${}^{t+\Delta t}\{p\}^{(i-1)}$ respectively for the sticking nodes and ${}^{t+\Delta t}f_1^{2(i)}$ and ${}^{t+\Delta t}p_1^{(i-1)}$ for the slipping nodes. Similarly, the matrices ${}^{t+\Delta t}[Q_1]^T$ and ${}^{t+\Delta t}[Q_2]$ are global versions of ${}^{t+\Delta t}\{q_1\}^T$ and ${}^{t+\Delta t}\{q_1\}$ respectively for the sticking nodes and ${}^{t+\Delta t}\{q_3\}^T$ and ${}^{t+\Delta t}\{q_2\}$ for the slipping nodes.

Note that, while the whole global coefficient matrix is known from the geometry, only a part of the right side vector, namely ${}^{t+\Delta t}\{P\}^{(i-1)}$ is known from the geometry. The other part, ${}^{t+\Delta t}\{R_c\}^{(i-1)}$, is unknown. This vector is eliminated by combining this equation with equation (3.64) of chapter 3. Before this, the set of equation (3.64) is condensed to retain only those degrees of freedoms, which are associated with the contact nodes. This condensed and combined set is solved to find the nodal displacements of the contact nodes and the contact forces. Then equation (3.55) is used to find displacements of the nodes of type 2.

4.5 Algorithm used for Dynamic Large Deformation Elasto-plastic Contact Problem

For solving a typical dynamic, large deformation, elasto-plastic, contact problem, the following steps are used:

1. Finding the potential contact nodes for which the hitting and target nodes are closer than a prescribed length.

2. Renumbering the nodes: Nodes of the hitting and target bodies are renumbered such that the contact nodes are numbered first. This is carried out to facilitate the static condensation of the stiffness matrix which helps in reducing the computational time.

3. Forming the coefficient matrix and right side vector: Based on the current geometry and state of stress, condensed form of effective stiffness matrix and force vector are formed.

4. Beginning the Newton-Raphson iteration.

5. Contact search: Search for the target segment corresponding to each hitting node. Master-slave algorithm is used here.

6. Contact iterations:

   - Initially all the potential nodes are assumed to be in sticking friction condition. Then, the contact stiffness matrix and right side vector are formed and combined with the condensed form of the effective stiffness matrix and the effective force vector. This system of equations is solved.
   - Then, the "out of contact" nodes, for which the normal component of the contact reaction is tensile (refer to equation (4.4)) are found. The contact reactions at these nodes are set to zero during the subsequent contact iterations.
   - After removing all the "out of contact" nodes, the nodes which are slipping are determined. We know that a node slips, if the contact reactions at that node violate equation (4.5), expressed in a nodal form.

- The contact iterations are repeated till the correct direction of friction force is obtained for all the slipping nodes and the status of all the contact nodes does not change.

7. Finding the displacements of the non-contact nodes (type 2 nodes) from the displacements of type 1 nodes.

8. Euler forward integration scheme: Depending on the choice of Stress measure (i.e Jaumann or New objective) and type of updation (i.e iterative or incremental), the Euler forward integration is performed.

   - Jaumann Stress Measure: From the iterative or incremental displacement, first the strain is found. Then, the change of state (i.e elastic to elastic , elastic to plastic, plastic to plastic or plastic to elastic) is determined. Finally, depending on the change of state, Euler forward integration is performed.
   - New Objective Stress Measure: Using the iterative or incremental displacement, first deformation gradient matrix is found out and then using the polar decomposition theorem, the logarithmic strain is found. The initial stress is transformed to the material coordinate system. The change of state at the Gauss point is found. Depending on the change of state at the Gauss point, the Euler forward integration scheme is implemented. Finally, the updated stress is transformed back to the fixed frame.

9. Updating: The stresses, strains and contact forces are updated.

10. Convergence: The unbalance force is found and convergence is checked. If the Newton-Raphson iterations converge, the results at the end of the increment are stored and the next time increment is started. If the convergence criterion is not satisfied, the Newton-Raphson iterations are continued till convergence.

Chapter 5

Results and Discussion

A finite element code for the analysis of 3-D, dynamic, large deformation, elasto-plastic contact problem with friction is developed based on the formulations developed in the chapters 2, 3 and 4. The stiffness matrix, mass matrix and force vectors are evaluated using numerical integration, while Newmark's scheme is used to update the velocity and acceleration after each time-step. The code is developed for 8-noded brick element and 2-point Gauss-Legendre numerical integration is used in each direction.

The code with Jaumann stress rate and incremental Green-Lagrange strain measures was developed and validated by Jayadeep [57] for large deformation, dynamic, elasto-plastic analysis (for both the single-body as well as contact problems). Now, an additional set of objective stress and non-linear strain measures, namely new incremental objective stress tensor and incremental logarithmic strain tensor, is added. The objective of the thesis is to carry out the comparitive study of these two sets of stress and strain measures. This is done for the following four cases:

1. Large Deformation, Dynamic, Elastic, Single Body Analysis.

2. Large Deformation, Elastic, Contact-Impact Analysis.

3. Large Deformation, Dynamic, Elasto-plastic, Single Body Analysis.

4. Large Deformation, Elasto-plastic, Contact Analysis.

5.1 Large Deformation Dynamic Elastic Single Body Analysis

5.1.1 Dynamic Response of a Cantilever

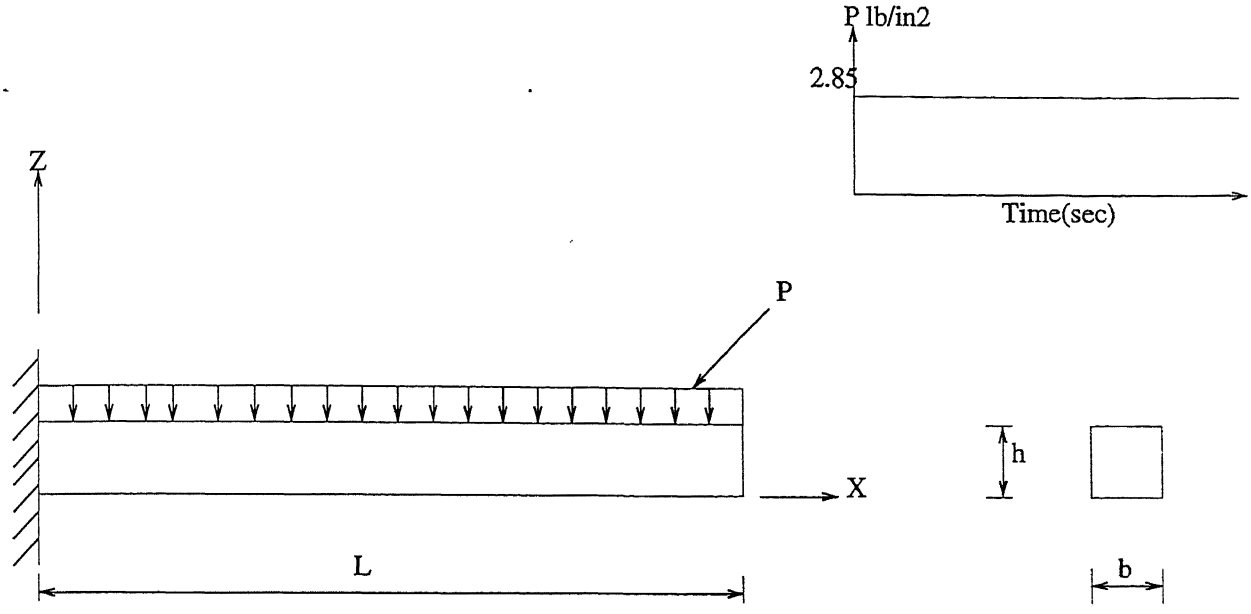

Figure 5.1: Cantilever : geometry and boundary conditions

A benchmark problem solved by Bathe *et al.* [17] has been chosen for the large deformation dynamic elastic single body analysis. Figure (5.1) shows the geometry and boundary conditions of the cantilever analyzed. The geometric and material parameters used are:

- Length of cantilever L = 10 inches
- Height h = 1.0 inch
- Width b = 1.0 inch
- Young's modulus E = 1.2×10^4 lb/in^2
- Poisson's ratio $\nu = 0.2$
- Density $\rho = 1.0 \times 10^{-4}$ lb-sec^2/in^4

Mesh and Time – step Convergence Studies

A mesh and time-step convergence study is essential to ascertain that a proper mesh and time step are selected so that a correct solution is obtained with proper utilization of computational resources. First a mesh convergence study is carried out to select an appropriate mesh. As the problem is a dynamic one, so the time step convergence study is carried out next to select a proper time step.

1. **Mesh Convergence:** Following are the discretizations used for the mesh convergence study. The time step used is 1.35×10^{-04} sec and the convergence tolerance of 1% is used.

   - Discretization No. 1:
     - Number of elements: 80 $(20 \times 2 \times 2)$
     - Degrees of freedom: 567
   - Discretization No. 2:
     - Number of elements: 640 $(40 \times 4 \times 4)$
     - Degrees of freedom: 3075

   From the mesh convergence study, it is found that the second discretization gives more accurate result. So, for the final study it is selected.

2. **Time – step Convergence:** Following are the time-steps considered for the time-step convergence study. The discretization used is $(40 \times 4 \times 4)$ and the convergence tolerance used is 1%.

   - Time-step 1= 1.35×10^{-04} sec.
   - Time-step 2= 0.45×10^{-04} sec.

   It is found that both the time steps give approximately the same results. For the final study, the time-step of 0.45×10^{-04} is selected.

The comparison between the Jaumann stress rate and new incremental objective stress measures is shown in Figures (5.2-5.3). The figures show that both the stress measures predict the same level of maximum displacement and equivalent stress for the single-body elastic analysis.

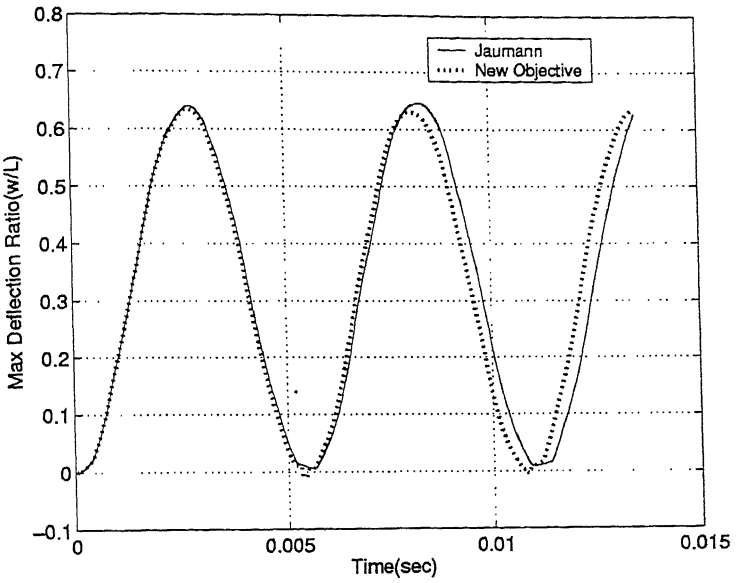

Figure 5.2: Dynamic response of the cantilever at $\Delta t = 0.45 \times 10^{-04}$ sec

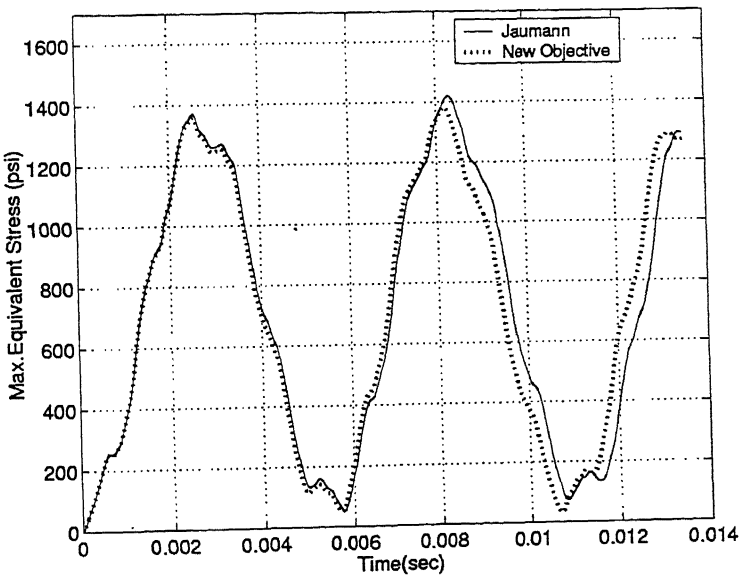

Figure 5.3: Maaximum equivalent stress response at $\Delta t = 0.45 \times 10{-}04$ sec

5.2 Large Deformation Elastic Contact-Impact Analysis.

5.2.1 Impact of Two Identical Bars

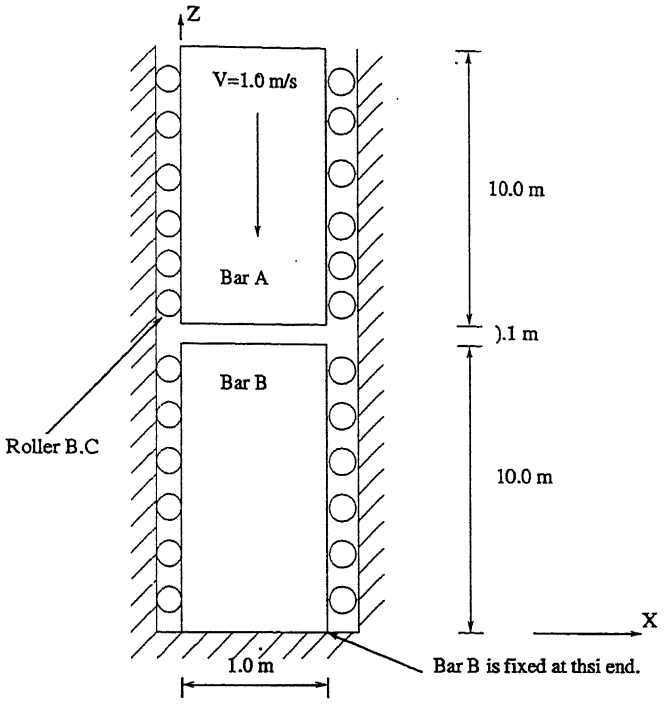

Figure 5.4: Impact of two identical bars

This problem is solved by Belytschko and Neal [44]. Figure (5.4) shows the initial configuration of the bars along with the boundary conditions. One of the bars is given an initial velocity so that it impacts with the second bar. The material properties are so chosen that the wave εpeed in each of the bar is 10.0 m/sec. Since $c = \sqrt{\frac{E}{\rho}}$, the material properties chosen are:

- Young's modulus E = 10 N/m^2
- Poission's ratio $\nu = 0.0$
- Density $\rho = 0.1$ Kg/m^3.

The geometric properties of each bar are as follows:

- Length of the bar L = 10.0 m
- Thickness = 1.0 m

- Width = 1.0 m

The initial velocity of the impacting bar i.e bar A is 1.0 m/sec. As Newmark's scheme is used to calculate the velocities and accelerations, it has to be made sure that the hitting body travels with zero acceleration before the impact. In order to achieve this the initial gap between the two bars has been kept at 0.1 m and the contact search length has been chosen as 0.11 m.

Mesh and Time – step Convergence Studies :

First a mesh convergence study is carried out to select an appropriate mesh. Next, time-step convergence study is carried out to select a proper time step.

1. **Mesh Convergence:** Following are the discretizations used for the mesh convergence study. The time step used is 0.1 sec and the convergence tolerance of 1% is used.

   - Discretization No. 1:
     - Number of elements: 10 $(10 \times 1 \times 1)$
     - Degrees of freedom: 132
   - Discretization No. 2:
     - Number of elements: 20 $(20 \times 1 \times 1)$
     - Degrees of freedom: 252

   The study shows that the second discretization gives better results. So it is chosen for further study.

2. **Time – step Convergence:** Following are the time-steps considered for the time-step convergence study. The discretization used is $(20 \times 1 \times 1)$ and the convergence tolerance used is 1%.

   - Time-step 1= 0.2 sec.
   - Time-step 2= 0.1 sec.

   The time-step convergence study shows that time-step 2 gives better results. So it is chosen for the further study.

Figures (5.5) and (5.6) give the velocity time histories at the interface of first bar ($Z = 10.1$), as well as second bar ($Z = 10.0$). Figures (5.7) and (5.8) give the comparison between the maximum equivalent stress in bodies A and B respectively. Both the stress measures predict almost the same values of maximum equivalent stress.

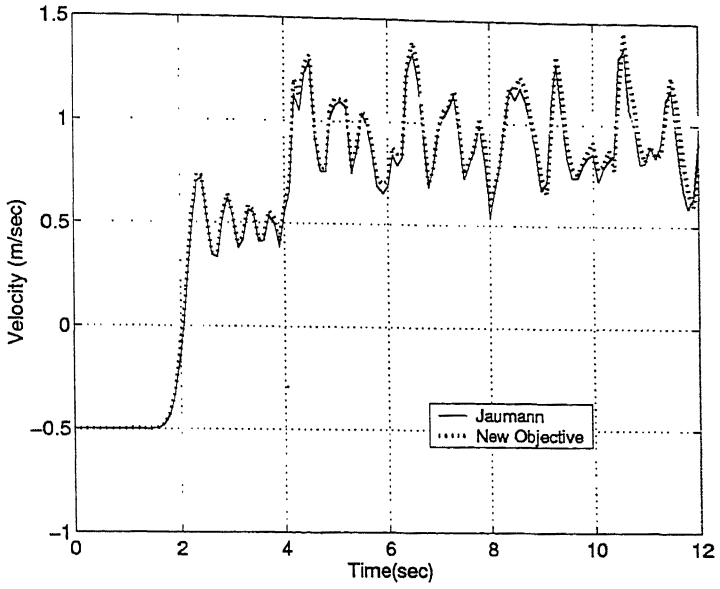

Figure 5.5: Velocity at interface of bar A

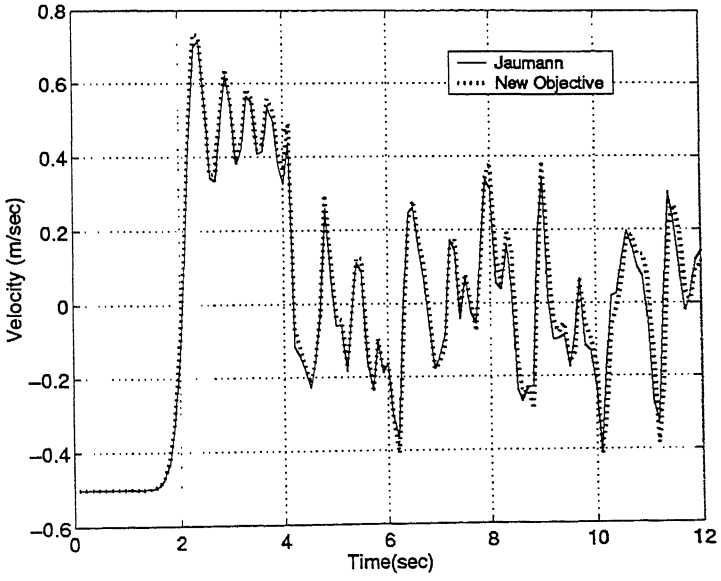

Figure 5.6: Velocity at interface of bar B

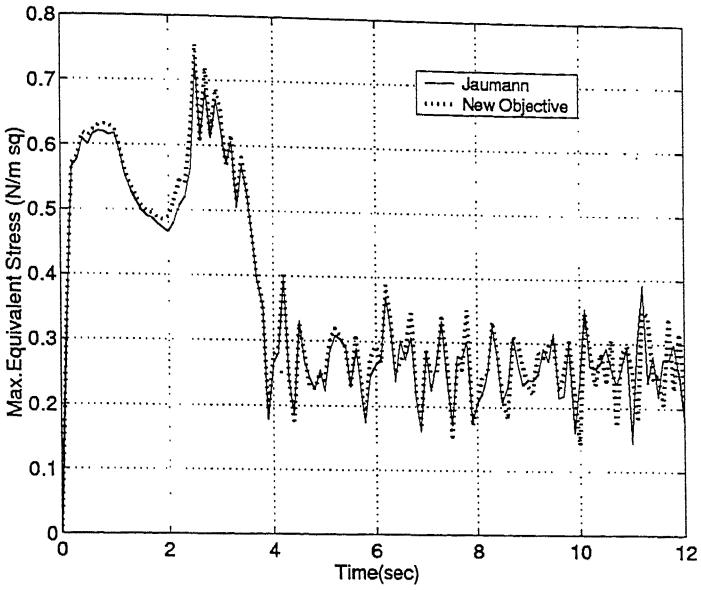

Figure 5.7: Maximum equivalent stress in bar A

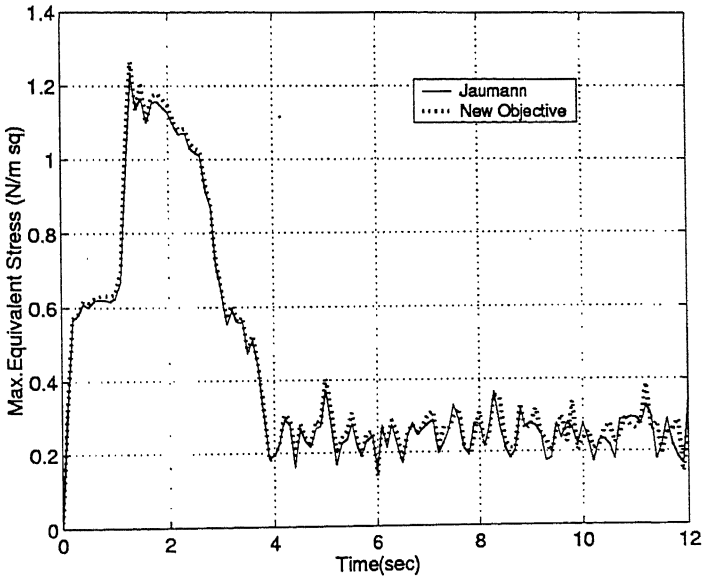

Figure 5.8: Maximum equivalent stress in bar B

5.2.2 Oblique Impact of Two Infinite Blocks

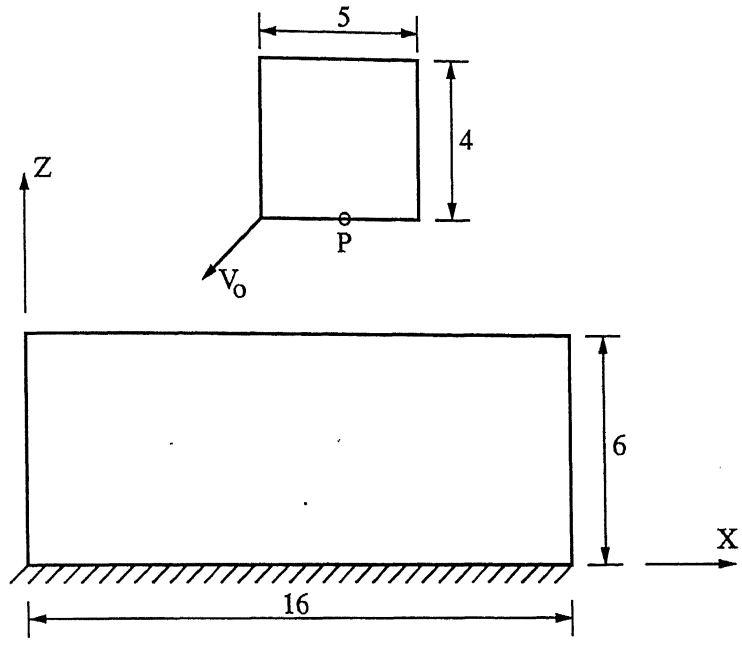

Figure 5.9: Oblique impact of two elastic blocks

The secondproblem used for comparison is the oblique impact of two infinite elastic blocks (plane strain problem) shown in Figure 5.9. This problem is reported in reference [49]. The top block is given a uniform initial velocity, $v_0 = (-10, 0, -10)$ units (in the coordinate system shown in figure). The geometric and material properties are:

- Hitting Block
  - length = 5 units
  - height = 4 units
- Target Block
  - length = 16 units
  - height = 6 units
- Young's modulus (E) = 1000 units, for both the blocks.
- Poisson's ratio (ν) = 0.0, for both the blocks.
- Density (ρ) = 0.1 units, for both the blocks.

Armero and Petocz [49] have solved this problem as a plane strain problem. Bhat [63] has solved the same problem, only for the frictionless case, using Jaumann stress rate measure and incremental Green-Lagrange strain measure, while Jayadeep [57] has solved the problem for both the friction and frictionless cases using Jaumann stress rate measure and incremental Green-Lagrange strain measure. In this work, however, new incremental objective stress and logarithmic strain measures are used and the results are compared to see the effect. Since the Poisson's ratio is zero, the plane strain and plane stress formulations will give the same results. In this work, the problem is solved with only one element in the Y-direction. To overcome the numerical difficulty arising due to low stiffness in Y-direction, the displacement along this direction is fixed at all nodes for both the bodies.

The following are the discretization and timestep considered:

- Discretization:
  - Number of elements in the hitting block = 20 ($5 \times 1 \times 4$)
  - Number of elements in the target block = 96 ($16 \times 1 \times 6$)
  - Number of d.o.f in the hitting block = 180
  - Number of d.o.f in the target block = 714
- Time-step = 0.01 units

There are two different cases. In the first case, there is no friction at contact interface and in the second case, friction coefficient (μ) between the hitting and target bodies is 0.4.

The X and Z displacements at point P are plotted against the time for both the Jaumann stress rate and new incremental objective stress measures in Figures (5.10) and (5.11). Both the displacements and time are measured from the instant of contact between the two blocks. Comparison of the maximum equivalent stress in bodies A and B is shown in Figures (5.12) and (5.13). The maximum equivalent stress predicted by the two stress measures differ at certain time-steps. No specific trend is observed.

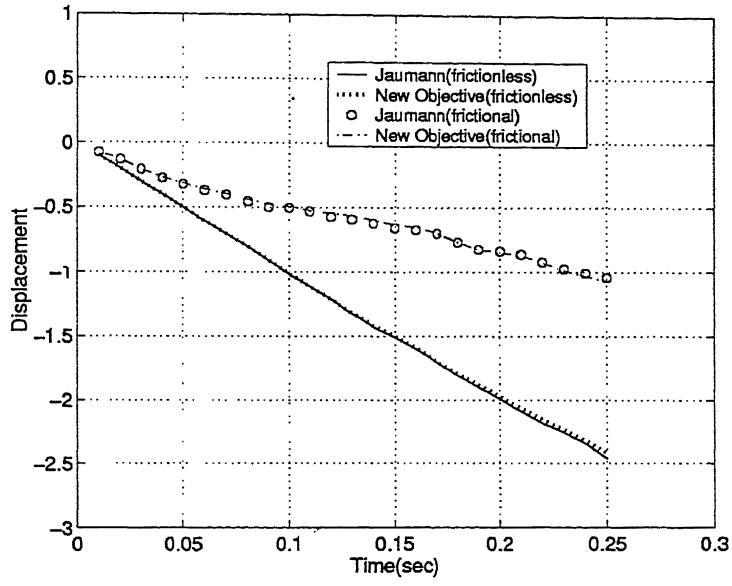

Figure 5.10: X-displacement of point P.

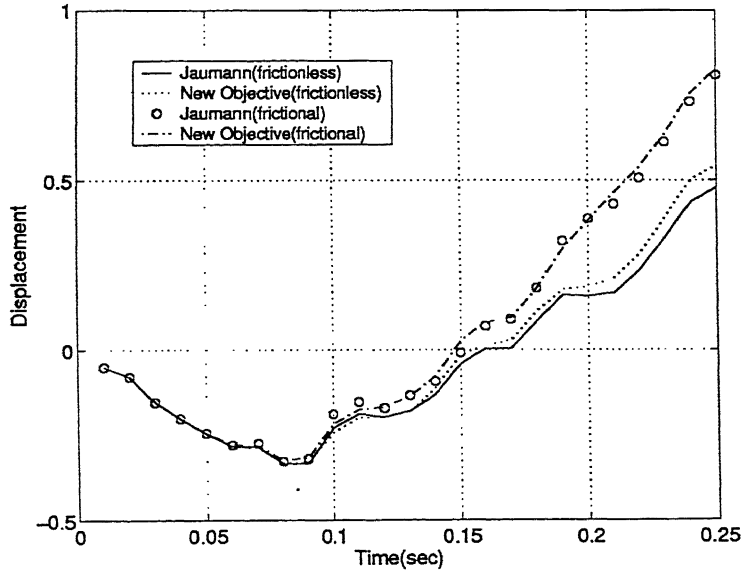

Figure 5.11: Z-displacement of point P.

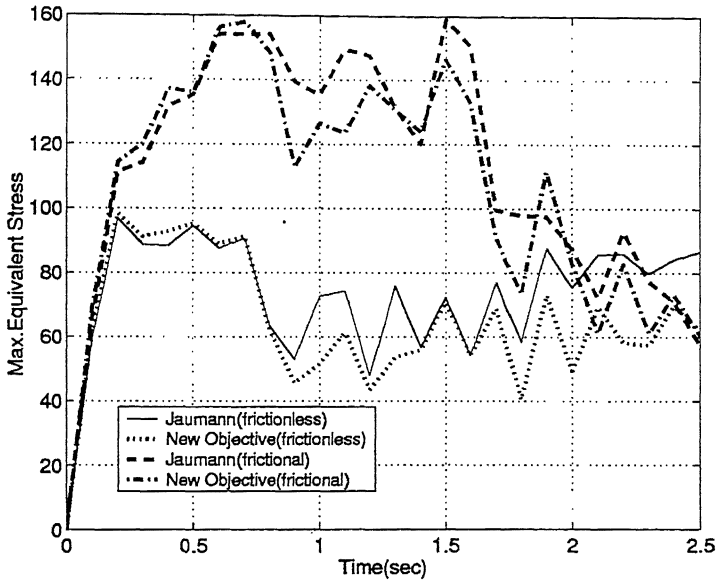

Figure 5.12: Maximum equivalent stress in block A

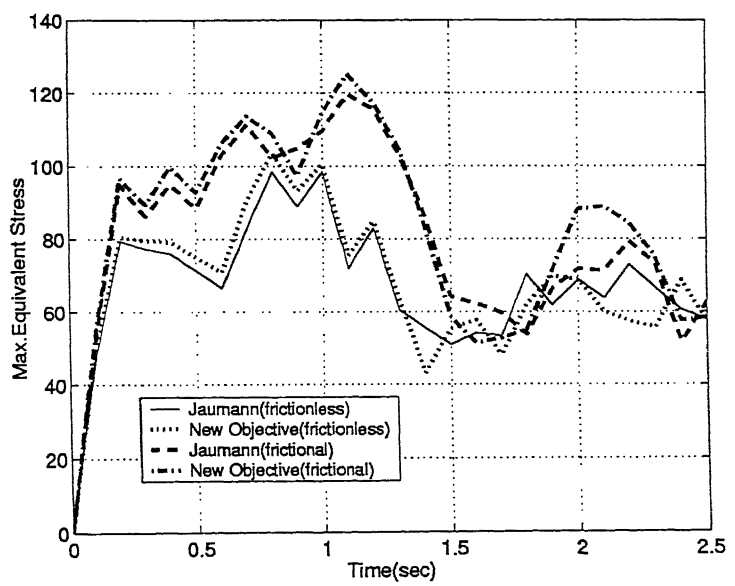

Figure 5.13: Maximum equivalent stress in block B

5.3 Large Deformation Dynamic Elasto-Plastic Single Body Analysis

5.3.1 Dynamic Elasto-Plastic Analysis of a Cube

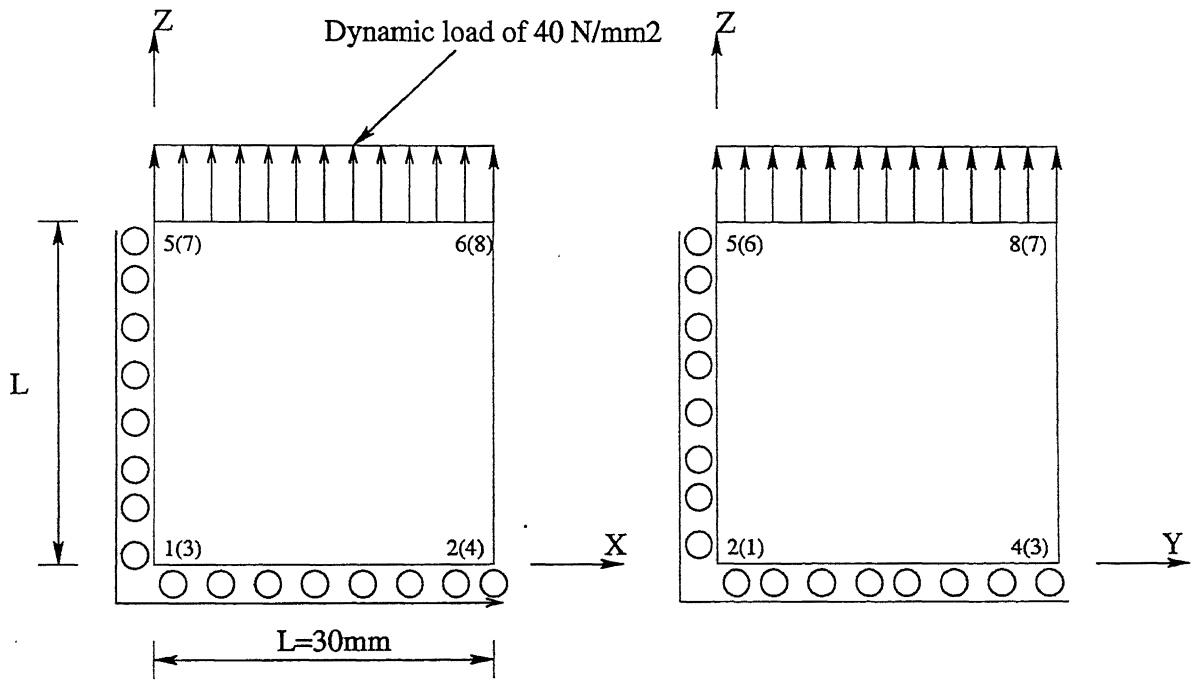

Figure 5.14: Cube: geometry and boundary conditions

The problem of a cube subjected to uniaxial step load and undergoing large deformation has been selected for single body elasto-plastic analysis. The geometry and boundary conditions are shown in Figure (5.14). The geometric and material properties are:

- Side of the cube (L) = 30mm
- Young's modulous (E) = 1114.58 N/mm^2
- Poisson's ratio (ν) = 0.36
- Density (ρ) = 2000×10^{-09} Kg/mm^3
- Hardening coefficient (K) = 87.42 N/mm^2
- Hadening exponent (n) = 0.909
- Initial yield stress ($^0\sigma_y$) = 44.58 N/mm^2

The discretization used is:

- Number of elements = 1 (1 × 1 × 1)
- Number of degree of freedom = 24

The convergence tolerence used is 1%..The equivalent stress is plotted against equivalent plastic strain in Figure (5.15) for both the Jaumann stress rate and new incremental objective stress measures. The actual hardening law

$$^{t}\sigma_{eq} = {}^{0}\sigma_{y} + K\,(\epsilon^{p}_{eq})^{n} \tag{5.1}$$

is also plotted in the same figure. The results show that the responses predicted by the two different stress measures are the same and match well with the actual hardening curve of the material. The unloading is also predicted correctly.

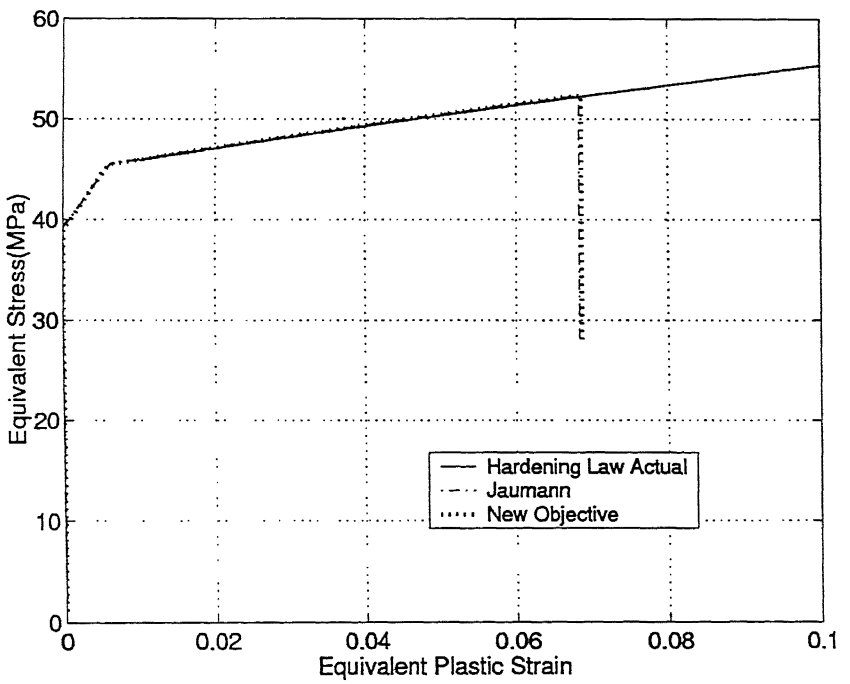

Figure 5.15: Elasto-plastic response of the cube

5.3.2 Dynamic Elasto-plastic Response of a Fixed Square Plate

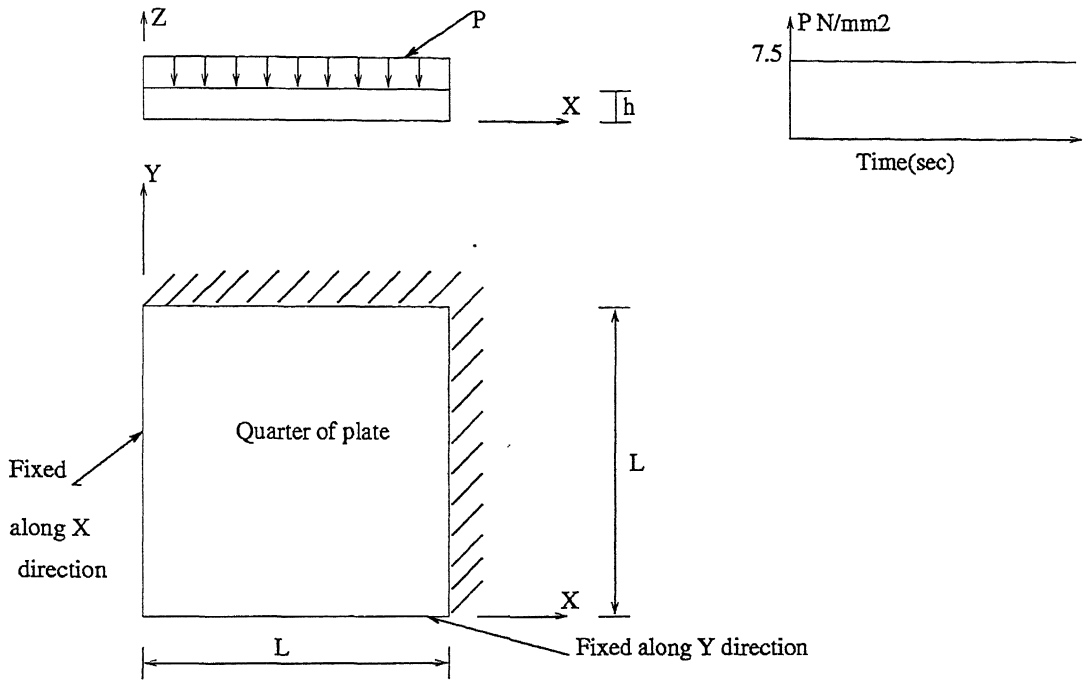

Figure 5.16: Plate: geometry and boundary conditions

The impact response of a square plate fixed at all its edges and charaterised by the elasto-plastic behaviour is obtained. Figure (5.16) shows the geometry and boundary conditions of the plate. Only one quarter of the plate has been modeled due to symmetry along X and Y axes. All specified quantities refer to the quarter plate model. The geometric and material data for the plate are:

- Side of the plate (L) = 125mm
- Thickness of the plate (h) = 25mm
- Young's modulous (E) = 1114.58 N/mm^2
- Poisson's ratio (ν) = 0.36
- Hardening coefficient (K) = 87.42 N/mm^2
- Hadening exponent (n) = 0.909
- Initial yield stress $({}^0\sigma_y) = 44.58\,\mathrm{N}/mm^2$
- Density of the plate material (ρ) = $2000 \times 10^{-09}\,\mathrm{Kg}/mm^3$

Mesh and Time – step Convergence Study

As stated earlier, mesh and time-step convergence studies are carried out to select an appropriate mesh and time step. The mesh and time steps used are given below.

1. **Mesh Convergence:** The time step used is $\Delta t = 0.3 \times 10^{-03} sec$ and the convergence tolerance used is 1%. The discretizations used are:

   - Discretization 1:
     - Number of elements = 200 $(10 \times 10 \times 2)$
     - Number of degrees of freedom = 1089
   - Discretization 2:
     - Number of elements = 1600 $(20 \times 20 \times 4)$
     - Number of degrees of freedom = 6615

   From the mesh convergence study, it is found that the second discretization gives better results. So it is chosen for the final comparison.

2. **Time Convergence:** The time steps used are stated below. The mesh used is $20 \times 20 \times 4$ and the convergence tolerance used is 1%.

   - Time-step 1: $0.6 \times 10^{-03} sec$
   - Time-step 2: $0.3 \times 10^{-03} sec$

   It is found that both the time steps give nearly the same results. For the final study, both the time steps are used.

The results obtained by using both the Jaumann stress rate and new incremental objective stress measures are shown in Figures (5.17-5.18). Use of Jaumann stress rate predicts a lower displacement response (Figure 5.17) but higher stress response (Figure 5.18) compared to that of the new incremental objective stress measure.

This can be explained as follows. It is well-known that the Jaumann stress rate is objective only when the rotation of the particle is small. When the particle rotation is large, it does not completely eliminate the change in Cauchy stress components due to rotation while calculating the incremental stress from the incremental strain. In the present problem, the particle rotation is large in most of the domain, especially at the point of maximum equivalent stress. This may be the reason for the higher prediction of the

maximum equivalent stress when the Jaumann stress rate measure is used. However in the previous problem (Section 5.3.1), there is no rotation, therefore, there is no discrepancey in the two responses.

To analyse the situation further, the variation of equivalent stress with equivalent plastic strain is plotted at a typical Gauss point (centre of the plate) for both the discretizations (Figures 5.19-5.20). The figures show that, even for a coarse mesh, the predictions of the new incremental objective stress measure match very well with the actual hardening curve of the material. On the other hand, the predictions of the Jaumann stress rate measure match the actual hardening curve only for the fine mesh. For a coarse mesh, the level of maximum equivalent stress predicted by the Jaumann stress rate measure is higher.

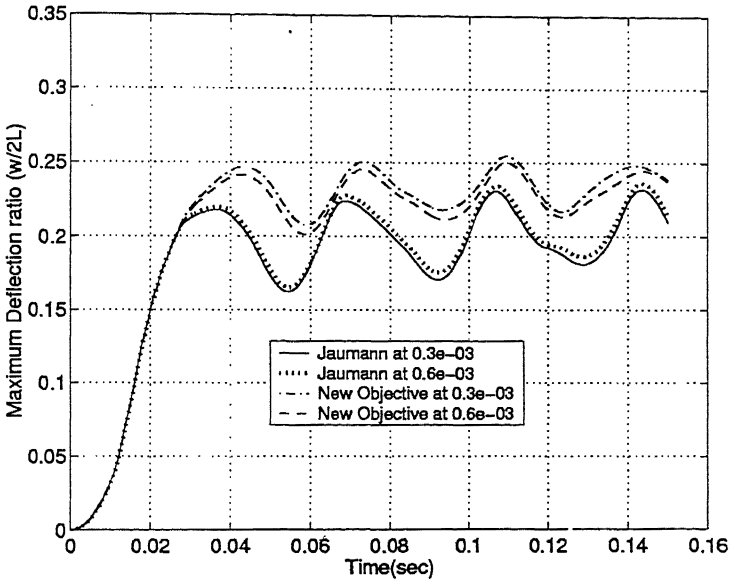

Figure 5.17: Maximum displacement response of the plate

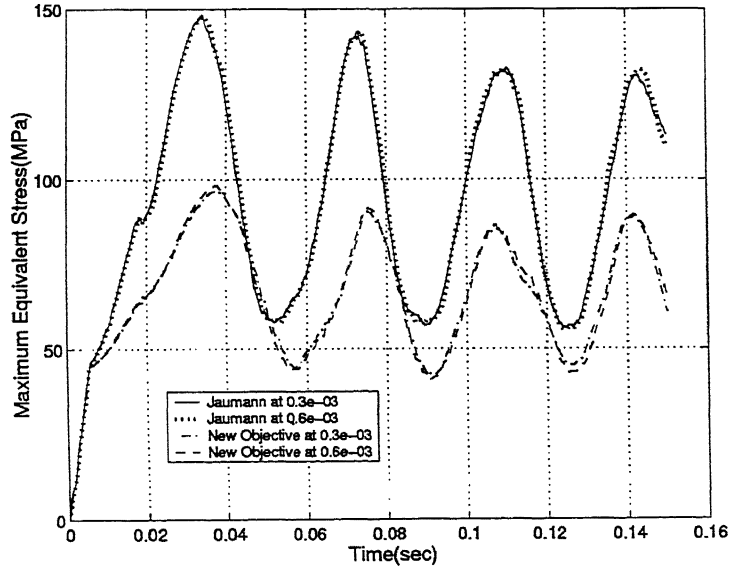

Figure 5.18: Maximum equivalent stress response of the plate

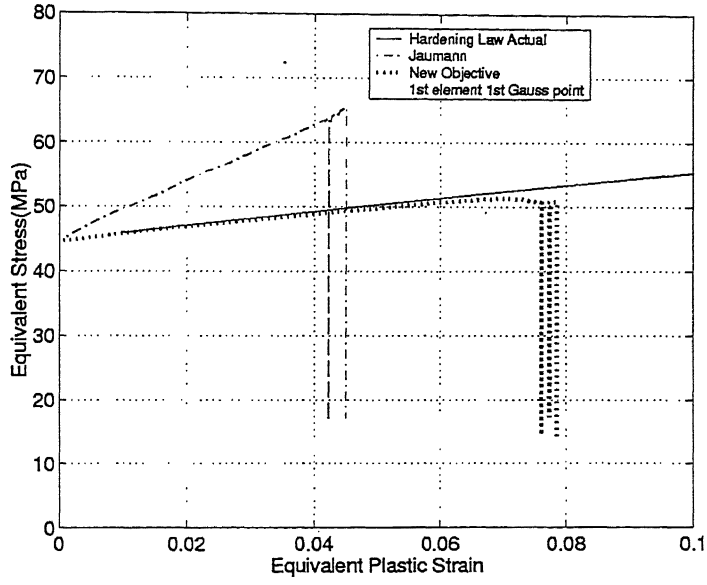

Figure 5.19: Variation of equivalent stress with equivalent plastic strain ($5 \times 5 \times 1$)

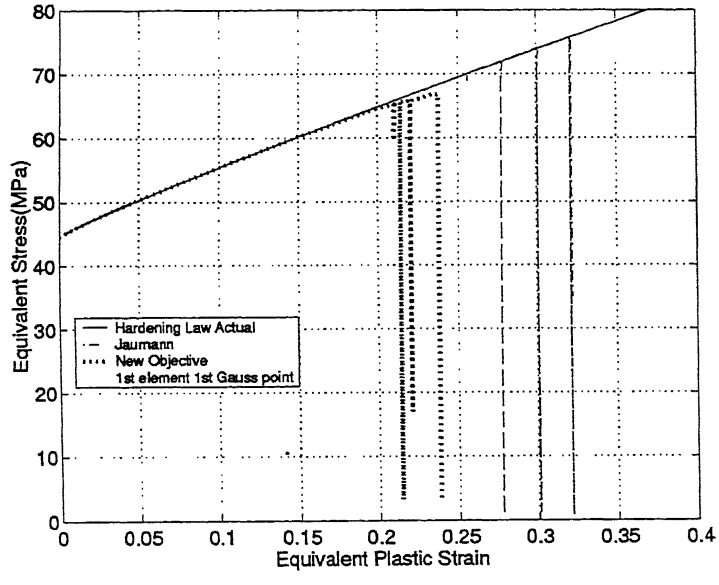

Figure 5.20: Variation of equivalent stress with equivalent plastic strain ($20 \times 20 \times 4$)

5.4 Large Deformation Elasto-Plastic Contact-Impact Analysis

5.4.1 Elasto-plastic Impact of a Sphere on a Plate

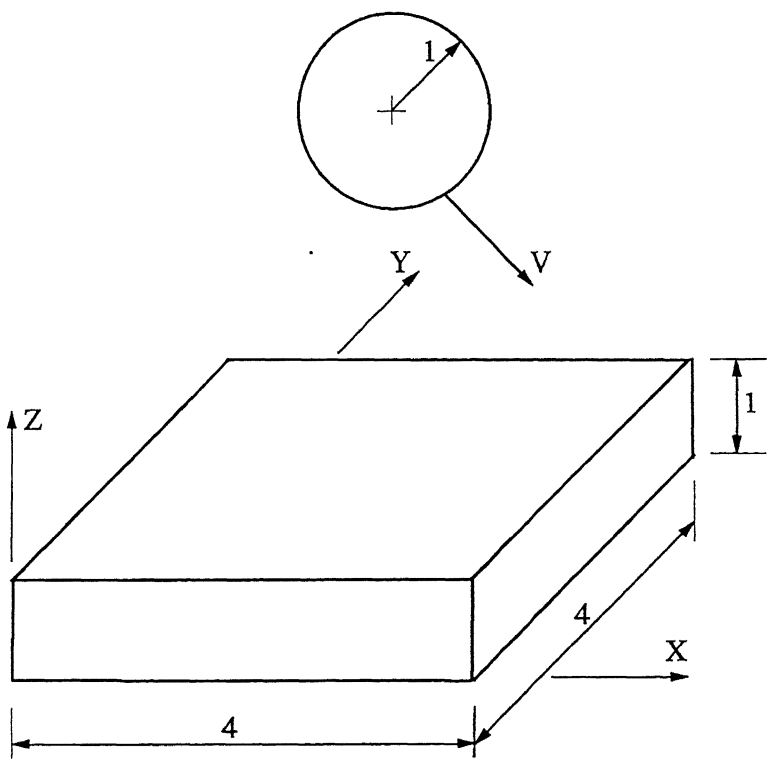

Figure 5.21: Impact of a sphere on plate

The problem of an impact of a sphere with a plate is selected for elasto-plastic contact-impact analysis (See Figure (5.21)). The sphere is given an initial velocity, V = (10,0,-10), in the coordinate system shown. The plate is fixed along the edges. The coefficient of friction used is $\mu = 0.2$.

The geometric details of the sphere and plate are shown in Figure (5.21). The material properties assumed for both the bodies are as follows:

- Young's modulus $(E) = 4 \times 10^5$ units
- Poisson's ratio $(\nu) = 0.3$
- Density $(\rho) = 4$ units
- Initial yield stress $((\sigma_y)_0) = 5000$ units

- Hardening coefficient $(K) = 40000$ units
- Hardening exponent $(n) = 0.4$

Time step used for the analysis is 0.002 units. The mesh details of the plate and sphere are as follows:

- Number of elements for sphere = 672 (See Figures (5.22) and (5.23))
- Number of elements for plate = 1024 ($16 \times 16 \times 4$)
- Number of d.o.f. for sphere = 2319
- Number of d.o.f. for plate = 4335

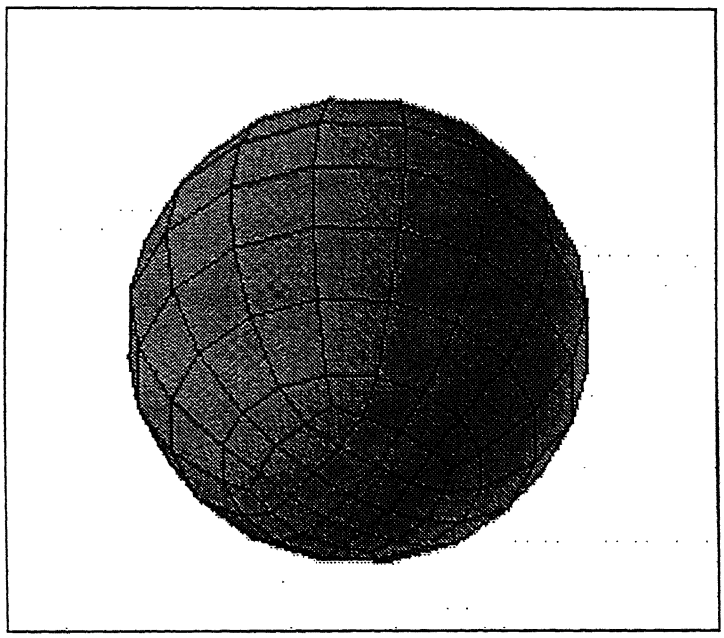

Figure 5.22: Finite element plot of sphere (Full view)

The X and Z displacements of the bottom node of the sphere are shown in Figures (5.24) and (5.25) for the frictionless case and in Figures (5.26) and (5.27) for the case of friction. It is observed that the displacement prediction of both the stress measures match well. Convergence difficulties were encountered for the case of friction for the new incremental objective stress measure after certain increment number.

The variation of maximum equivalent stress in both the sphere and plate for the frictionless case is shown in Figure (5.28). It is observed that, as in the case of single body

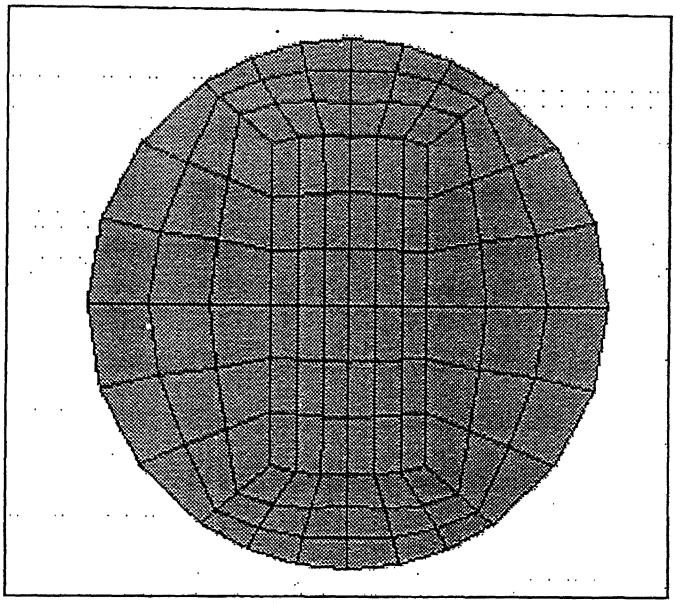

Figure 5.23: Finite element plot of sphere (Sectional view in X-Z plane)

analysis, the use of Jaumann stress rate measure predicts the higher value of maximum equivalent stress for both sphere and plate. The results for the frictional case are shown in Figure (5.29). Here also, the maximum equivalent stress predicted by the use of jaumann stress rate is higher.

The analysis was repeated for sphere and ball made of polycarbonate material with similar geometry and mesh details. The material properties of this material are given below:

- Young's modulus $(E) = 1.11458 \times 10^9$ N/m^2
- Poisson's ratio $(\nu) = 0.36$
- Density $(\rho) = 2000$ kg/m^3
- Initial yield stress $= 4.458 \times 10^7$ N/m^2
- Hardening coefficient $(K) = 8.742 \times 10^7$ N/m^2
- Hardening exponent $(n) = 0.909$

The velocity given to the sphere is (10,0,-10) m/s, in the coordinate system shown in Figure (5.21) and the coefficient of friction at the contact interface is 0.3, for the case of analysis with friction. The time step used in this analysis is 0.0003 seconds. The X and

Z displacements of the bottom node of the sphere for the frictionless case are shown in Figures (5.30) and (5.31). The results for the frictional cases are shown in Figures (5.32) and (5.33). The variation of maximum equivalent stress in both the sphere and plate is shown in Figure (5.34) for the frictionless case and in Figure (5.35) for the case of friction. Convergence difficulties were encountered in the frictional case, and therefore the analysis was done upto 0.0123 seconds for the case of Jaumann stress rate and 0.0081 seconds for the case of new incremental objective stress. As in the earlier cases, the use of Jaumann stress rate predicts the higher value of maximum equivalent stress.

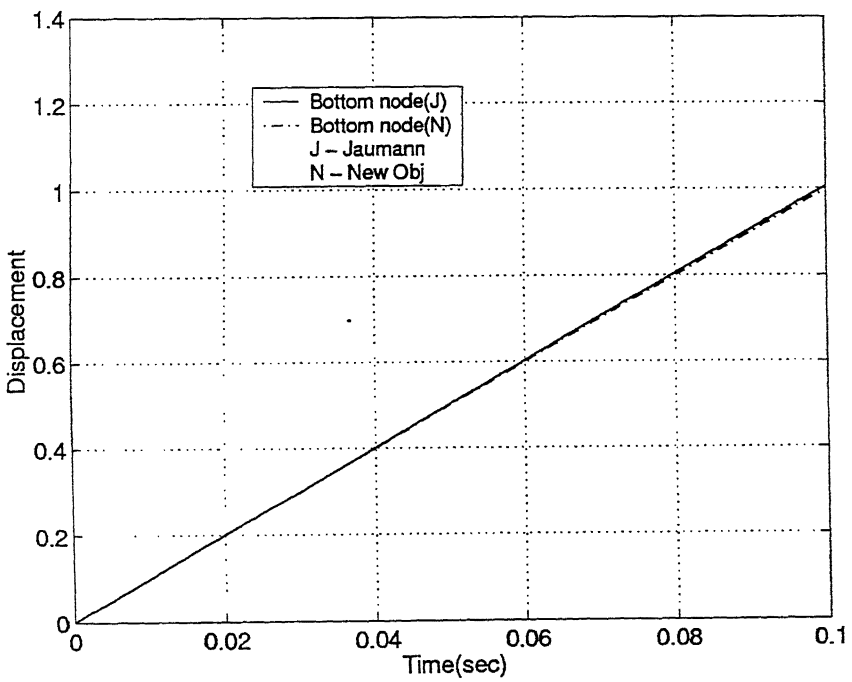

Figure 5.24: Displacement of the sphere along X-direction for frictionless case.

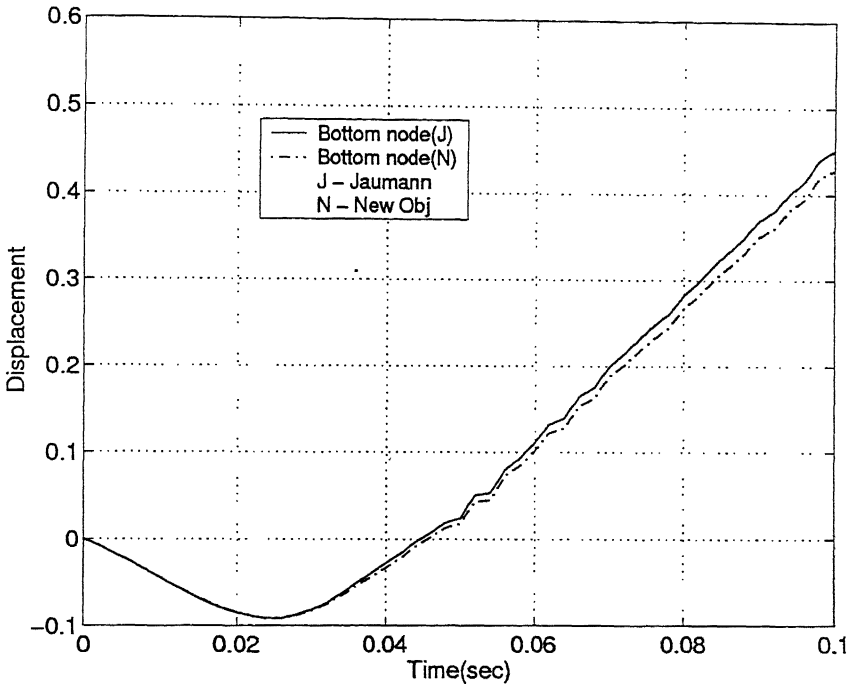

Figure 5.25: Displacement of the sphere along Z-direction for frictionless case.

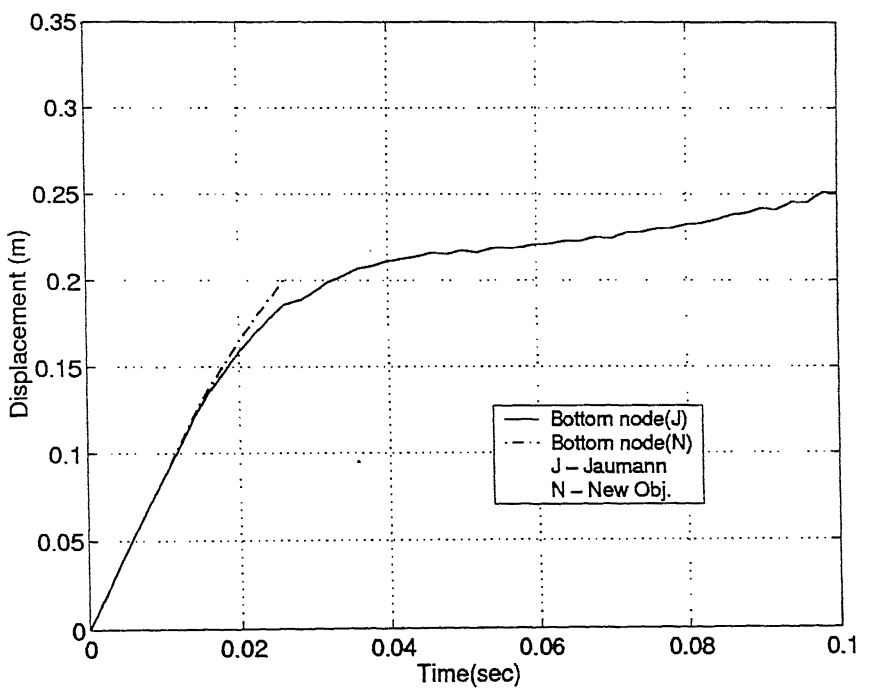

Figure 5.26: Displacement of the sphere along X-direction for frictional case.

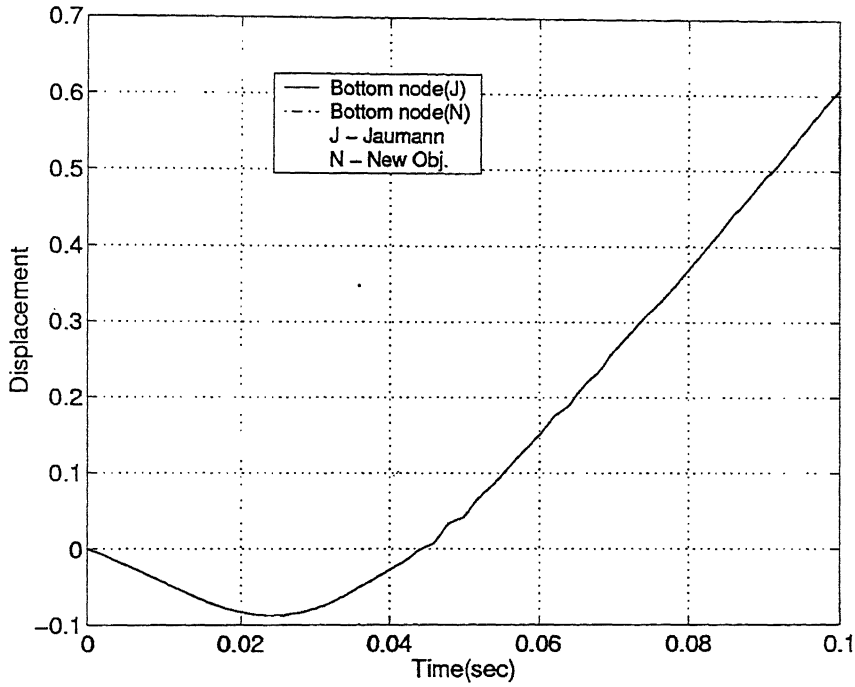

Figure 5.27: Displacement of the sphere along Z-direction for frictional case.

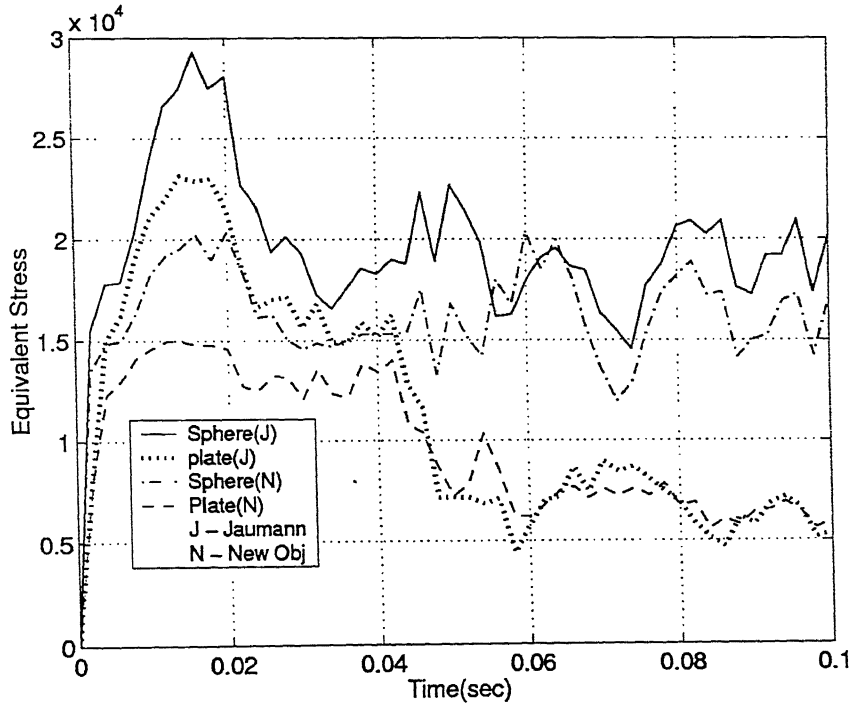

Figure 5.28: Maximum equivalent stress in sphere and plate for frictionless case

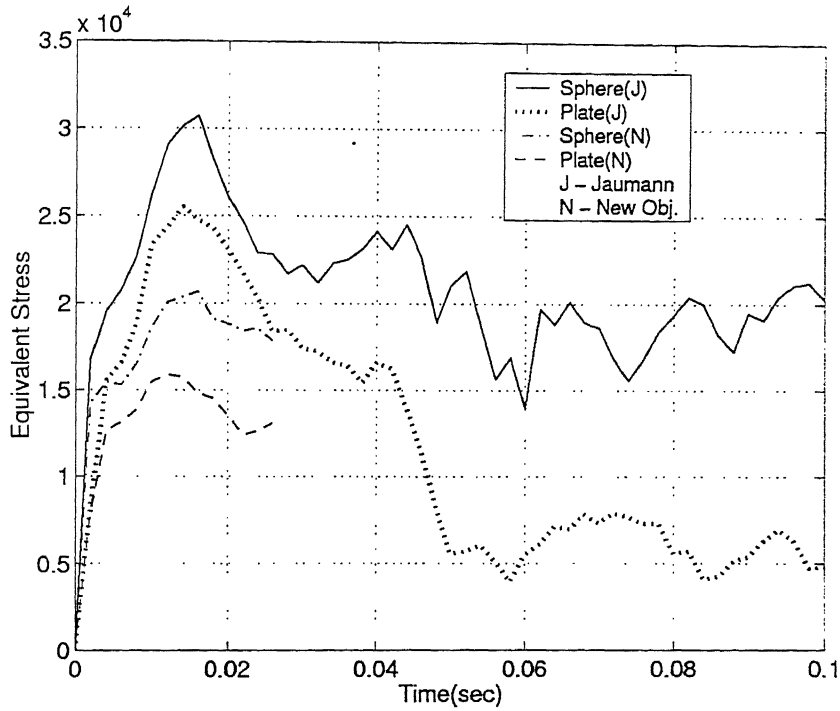

Figure 5.29: Maximum equivalent stress in sphere and plate for frictional case

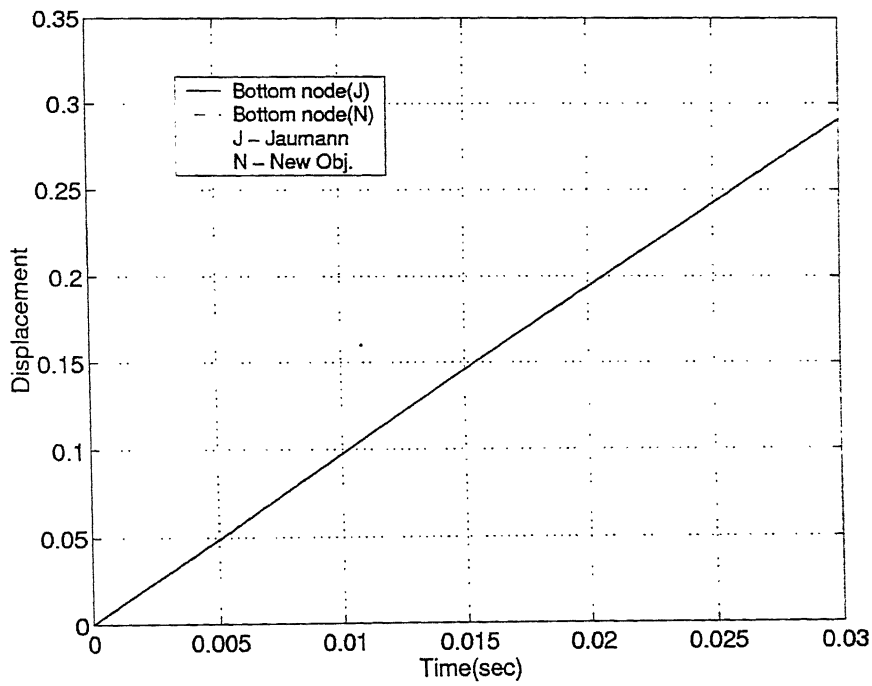

Figure 5.30: Displacement of the sphere along X-direction (polycarbonate material) frictionless case

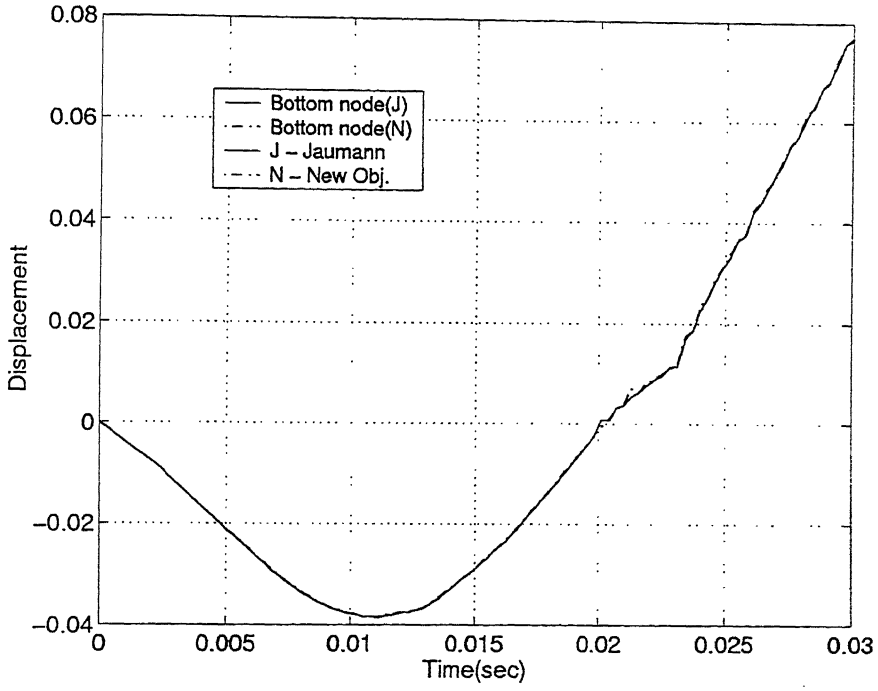

Figure 5.31: Displacement of the sphere along Z-direction (polycarbonate material) frictionless case

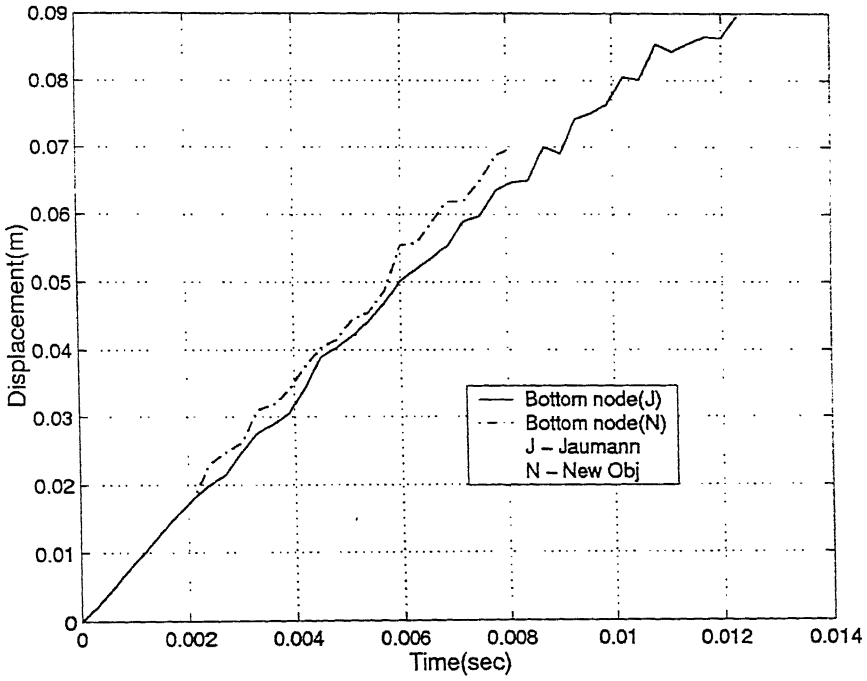

Figure 5.32: Displacement of the sphere along X-direction (polycarbonate material) frictional case

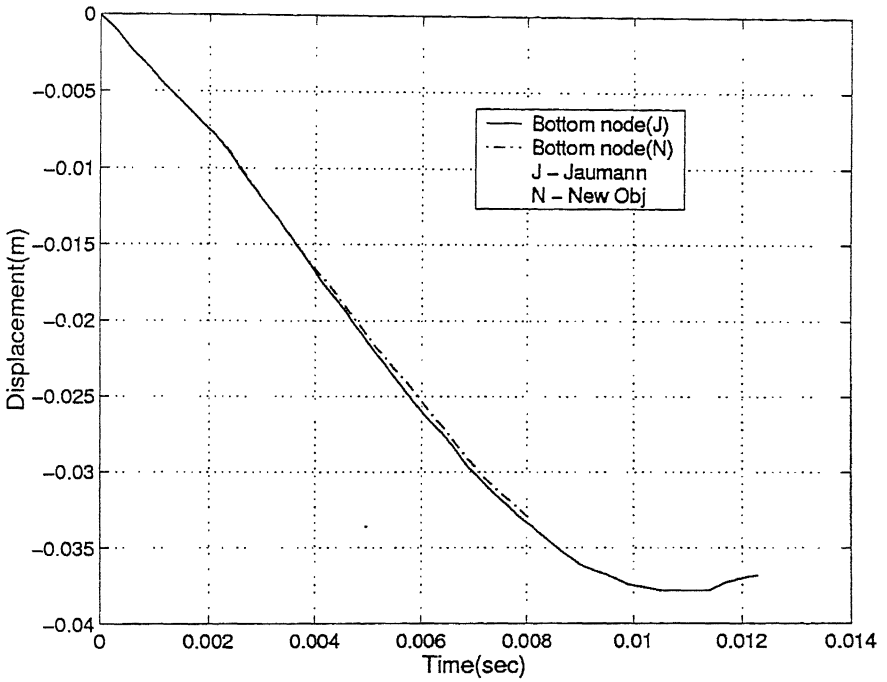

Figure 5.33: Displacement of the sphere along Z-direction (polycarbonate material) frictional case

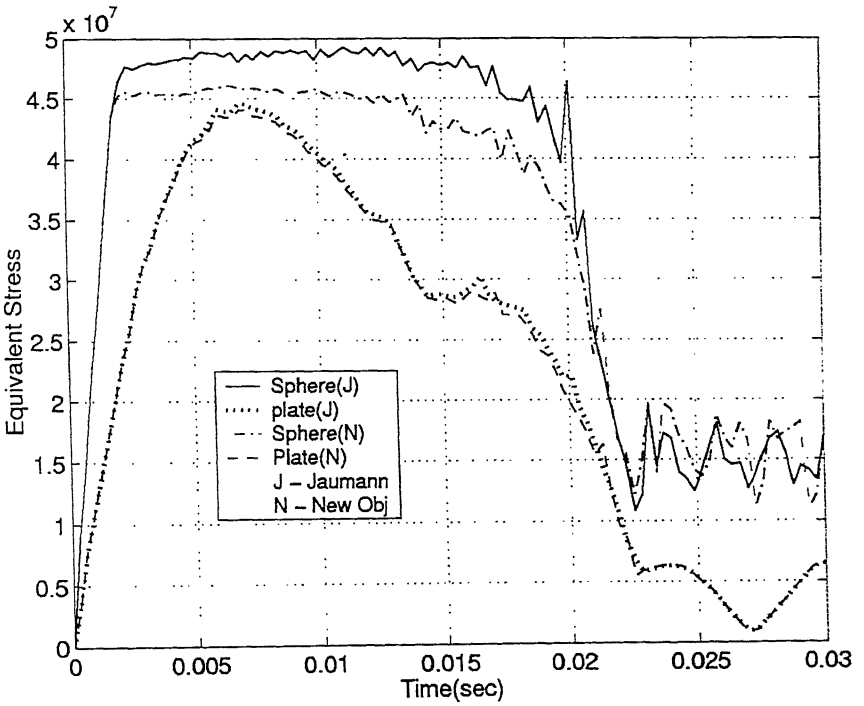

Figure 5.34: Maximum equivalent stress in sphere and plate (polycarbonate material) frictionless case

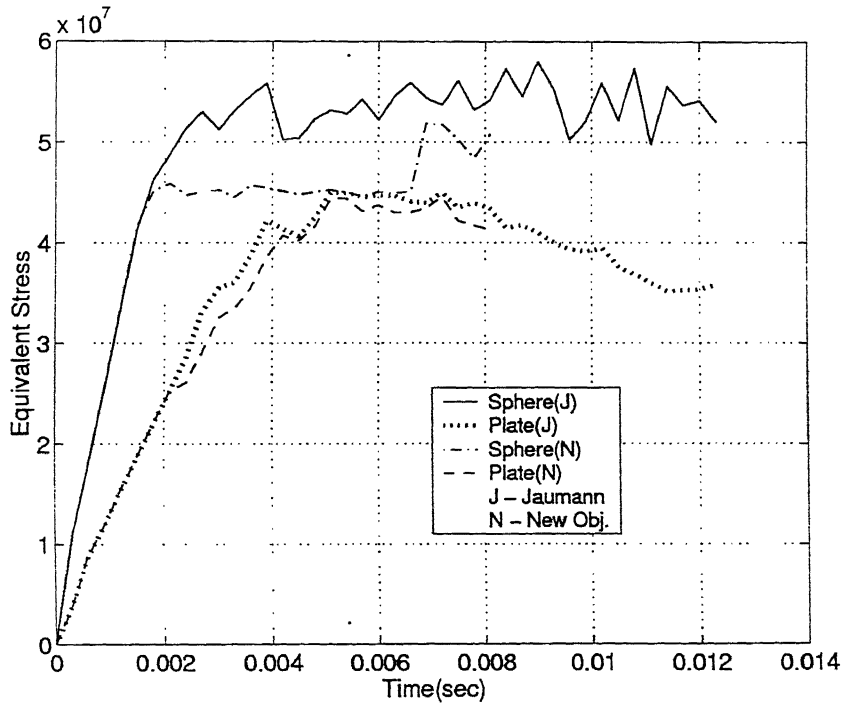

Figure 5.35: Maximum equivalent stress in sphere and plate (polycarbonate material) frictional case

Chapter 6

Conclusions and Scope for Future Work

6.1 Conclusions

The objective of the present work is to compare the realative performance of two objective stress measures namely the incremental Jaumann stress rate measure and the new incremental objective stress measure. The comparison is carried out for the following four cases:

1. Large deformation, dynamic, elastic, single body analysis.
2. Large deformation, elastic, contact-impact analysis.
3. Large deformation, dynamic, elasto-plastic, single body analysis.
4. Large deformation, elasto-plastic, contact-impact analysis.

The following conclusions can be drawn:

1. For single-body elastic analysis, both the stress measures give the identical results.
2. For elastic contact analysis, the maximum equivalent stress predicted by the two stress measures is somewhat different.
3. For single-body elasto-plastic analysis, the use of Jaumann stress rate measure predicts higher maximum equivalent stress compared to the new incremental objective stress measure. However, in problems involving no rotation, both the responses are identical.

4. For the case of elasto-plastic contact analysis also, the use of Jaumann stress rate predicts higher maximum equivalent stress compared to the new incremental objective stress measure.

6.2 Scope for Future Work

The desired future extensions of this work are the following:

1. Currently the programme has the provsion of Jaumann stress rate measure and new objective stress measure. Other stress measures along with appropriate strain measures can be incorporated and a comparitive study can be performed.

2. Advanced solution procedures such as the arc length method may be employed to handle snap-through and snap-back responses in structures, since such cases cannot be handeled by the Newton-Raphson technique.

3. Finite elements other than eight noded brick element can be incorporated.

4. Material damping effects can be included.

5. Option for using penalty function method for developing the contact stiffness matrix can be incorporated.

6. Other material models like kinematic and anisotropic hardening and hardening laws other than power law can be implemented.

7. Non-classical friction laws can be used for modelling the effect of friction.

8. Finally, it is highly desirable to have versatile pre and post processors, for the generation and interpretation of results in 3-D analysis.

References

[1] R. Hill. *The Mathematical Theory of Plasticity.* Oxford University Press, Oxford, 1950.

[2] L. E. Malvern. *Introduction to the Mechanics of a Continuous Medium.* Prentice Hall Inc., Englewood Cliffs, New Jersy, 1969.

[3] O. C. Zienkiewicz, X. K. Li, and S. Nakazawa. Dynamic transient analysis by a mixed iterative method. *Int. J. Numer. Methods Eng.*, 23:1343, 1986.

[4] K. J. Bathe. *Finite Element Procedures.* Prentice Hall of India, New Delhi, 1996.

[5] T. G. Hughes. A note on the stability of Newmarks's Algorithm in non-linear structural dynamics. *Int. J. Numer. Methods Eng.*, 5:386, 1975.

[6] J. H. Argyris. Elasto-plastic matrix displacement analysis of three dimensional continua. *J. Roy. Aero. Soc.*, 69:633, 1965.

[7] J. C. Nagtegaal and J. E. De Jong. Some computational aspects of elastic-plastic large strain analysis. *Int. J. Numer. Methods Eng.*, 17:15, 1981.

[8] M. A. Crisfield. *Non-linear Finite Element Analysis of Solids and Structures*, volume 1. John Wiley and Sons, Chichester, 1994.

[9] R. H. Dodds Jr. Numerical techniques for plasticity computations in finite element analysis. *Comput. Struct.*, 26:767, 1987.

[10] P. Jetteur. Implicit integration algorithm for elastoplasticity in plane stress analysis. *Eng. Comp.*, 3:251, 1986.

[11] S. Caddemi and J. B. Martin. Convergence of the Newton-Raphson algorithm in elastic-plastic incremental analysis. *Int. J. Numer. Methods Eng.*, 31:177, 1991.

[12] M. Ortiz and E.P. Popv. Accuracy and stability of integration algorithms for elasto-plastic constitutive relations. *Int. J. Numer. Methods Eng.* , 21:1561, 1985.

[13] A. S. Gendy and A. F. Saleeb. Mixed finite element modeling for the dynamics of beam assemblages undergoing large overall motions in space. *Int. J. Computational Engg. Science*, 2(2):309, 2001.

[14] J. Chakrabarty. *Theory of Plasticity.* McGraw Hill, New York, 1981.

[15] E. H. Lee. Elastic-plastic deformation at finite strains. *J. Appl. Mech.*, 36:1, 1969.

[16] I. Doghri. *Mechanics of Deformable Solids.* Springer, 2000.

[17] K. J. Bathe, E. Ramm, and E. L. Wilson. Finite element formulations for large deformation dynamic analysis. *Int. J. Numer. Methods Eng.*, 9:353, 1975.

[18] D. P. Mondkar and G. H. Powell. Finite element analysis of non-linear static and dynamic response. *Int. J. Numer. Methods Eng.*, 11:499, 1977.

[19] A. S. Gendy and A. F. Saleeb. Nonlinear dynamics for mixed shells with large rotation and elastoplasticity. *Int. J. Computational Engg. Science*, 1(1):1, 2000.

[20] H. Hertz. On the contact of elastic solids. *Jr. of Math.*, 92:156, 1881. (in German).

[21] K. L. Johnson. One hundred years of Hertz contact. In *Proceedings of Instn. of Mech. Engs.*, volume 196, page 363, 1982.

[22] N. I. Muskhelishvili. *Some basic Problems of Mathematical Theory of Elasticity.* Noordhoff, Groningen, 1953.

[23] G. M. L. Gladwell. *Contact problems in the Classical Theory of Elasticity.* Sijthoff & Noordhoff, Alphen aan den Rijn, 1980.

[24] S. Ohte. Finite element analysis of elastic contact problems. *Bulletin of JSME*, 16(95):797, 1973.

[25] R. Gaertner. Investigation of plane elastic contact allowing for friction. *Comput. Struct.*, 7:59, 1977.

[26] A. Francavilla and O. C. Zienkiewicz. A note on numerical computation of elastic contact problems. *Int. J. Num. Methods Eng.*, 9:913, 1975.

[27] T. D. Sachdeva and C. V. Ramakrishnan. A finite element analysis for the two-dimensional elastic contact problems with friction. *Int. J. Num. Methods Eng.*, 17:1257, 1981.

[28] J. J. Kalker and Y. van Randen. A minimum principle for frictionless elastic contact with application to non-Hertzian half-space contact problem. *Jr. Engg. Math.*, 6:193, 1972.

[29] N. D. Hung and G. de Saxce. Frictionless contact of elastic bodies by finite element method and mathematical programing technique. *Comput. Struct.*, 11:55, 1980.

[30] F. F. Mahmoud, A. K. Al-Saffer, and A. M. El-Hadi. Solution of the non-conformal unbounded contact problems by the incremental convex programming method. *Comput. Struct.*, 39(1/2):1, 1991.

[31] J. Bohm. A comparison of different contact algorithms with applications. *Comput. Struct.*, 26(1/2):207, 1987.

[32] N. G. Bourago. A survey on contact algorithms. In *Workshop "Grid Generation: Theory and Applications"*, Moscow, 2002.

[33] N. Kikuchi and J. T. Oden. *Contact Problems in Elasticity, A Study of Variational Inequality and Finite Element Methods.* SIAM, Philadelphia, 1988.

[34] K. J. Bathe and A. Chaudhary. A solution method for planar and axisymmetric contact problems. *Int. J. Numer. Methods Eng.*, 21:65, 1985.

[35] P. Wriggers and J. C. Simo. A note on tangent siffness for fully non-linear contact problem. *Comp. in App. Num. Meth.*, 1:199, 1985.

[36] H. Parisch. A consistent tangent stiffness matrix for three-dimensional non-linear contact analysis. *Int. J. Numer. Methods Eng.*, 28:1803, 1989.

[37] W. Chen and J. Yeh. Finite element analysis of finite deformation contact problems with friction. *Comput. Struct.*, 29(3):403, 1988.

[38] F. J. Gallego and J. J. Anza. A mixed finite element model for elastic contact problem. *Int. J. Numer. Methods Eng.*, 28:1249, 1989.

[39] Z. H. Zhong. *Finite Element Procedures for Contact-Impact Problems.* Oxford University Press, Oxford, 1993.

[40] G. Gilardi and I. Sharf. Literature survey of contact dynamics modelling. *Mechanism and Machine Theory*, 37(10):1213, 2002.

[41] J. H. Sung and B. M. Kwak. Large displacement dynamic analysis with frictional contact by linear complementarity formulation. *Comput. Struct.*, 80:977, 2002.

[42] E. Bittencourt and G. J. Creus. Finite element analysis of three-dimensional contact and impact in large deformation problems. *Comput. Struct.*, 69:219, 1998.

[43] T. C. Werner. Elasto-plastic impact of a cantilever beam using non-linear finite elements and event simulation. Master's thesis, Youngstown State University, 1998.

[44] T. Belytschko and M. O. Neal. Contact-impact pinball algorithm with penalty and Lagrangian methods. *Int. J. Numer. Methods Eng.*, 31:547, 1991.

[45] J. G. Malone and N. L. Johnson. A parallel finite element contact/impact algorithm for non-linear explicit transient analysis: Part I — search algorithm and contact mechanics. *Int. J. Numer. Methods Eng.*, 37:559, 1994.

[46] K. Brown, S. Attaway, S. Plimpton, and B. Hendrickson. Parallel strategies for crash and impact simulations. *Comput. Methods Appl. Mech. Engrg.*, 184:375, 2000.

[47] R. L. Taylor and P. Papadopoulos. On a finite element method for dynamic contact/impact problems. *Int. J. Numer. Methods Eng.*, 36:2123, 1993.

[48] T. A. Laursen and V. Chawla. Design of energy conserving algorithms for frictionless dynamic contact problems. *Int. J. Numer. Methods Eng.*, 40:863, 1997.

[49] F. Armero and E. Petocz. A new dissipative time-stepping algorithm for frictional contact problems: Formualtion and analysis. *Comput. Methods Appl. Mech. Engrg.*, 179:151, 1999.

[50] M. L. Ayari and V. E. Saouma. Static and dynamic contact/imapct problems using fictitious forces. *Int. J. Numer. Methods Eng.*, 32:623, 1991.

[51] J. C. Simo and T. A. Laursen. An augmented Lagrangian treatment of contact problems involving friction. *Comput. Struct.*, 42(1):116, 1992.

[52] C. Kane, E. A. Repetto, M. Ortiz, and J. E. Marsden. Finite element analysis of nonsmooth contact. *Comput. Methods Appl. Mech. Engrg.*, 180:1, 1999.

[53] K. Farahani, M. Mofid, and A. Vafai. A solution method for general contact-impact problems. *Comput. Methods Appl. Mech. Engrg.*, 187:69, 2000.

[54] J. K.Dienes. On the analysis of rotation and stress rate in deforming bodies. *Acta Mechanica*, 32:217, 1979

[55] D. R.Metzger, R. N.Dubey. Objective tensor rates and frame indifferent constitutive models. *Mechanics Research Communications*, 13(2):91, 1986.

[56] S. N. Varadhan. Dynamic large deformation elasto-plastic analysis of continua. Master's thesis, Department of Mechanical Engineering, IIT Kanpur, 2003.

[57] Jayadeep U.B. Finite element analysis of dynamic Elasto-Plastic contact problem with friction. Master's thesis, Department of Mechanical Engineering, IIT Kanpur, 2003.

[58] W. Jaunzemis *Continuum Mechanics* The MacMillian Company, New York, 1967.

[59] L. A.Segel *Mathematics Applied to Continuum Mechanics* Macmillian Publising Company, New York, 1977.

[60] D. R. J. Owens and E. Hinton *Finite Elements in Plasticity: Theory and Practice.* Swansea: Pineridge Press, (1980).

[61] P. M. Dixit, V. Sundararajan, N. N. Kishore and R. Patnaik Analysis of Bird Impact with the wind screen of the Light Combat Aircraft. Project Report, Department of Mechanical Engineering, IIT Kanpur, 1995.

[62] O. C.Zienkiewicz. *The Finite Element Method.* Tata McGraw-Hill, New Delhi,2001.

[63] Kuldeep Bhat. Finite element analysis of dynamic elasto-plastic contact problem. Master's thesis, Department of Mechanical Engineering, IIT Kanpur, 2002.